Insights into pulmonary hypertension pathogenesis and novel stem cell derived therapeutics

Nicholas Cober

Thesis submitted to the University of Ottawa
in partial fulfillment of the requirements for the
Doctorate in Philosophy (PhD) program in Cellular and Molecular Medicine

Department of Cellular and Molecular Medicine
Faculty of Medicine
University of Ottawa

Abstract

Pulmonary arterial hypertension (PAH) is a devastating lung disease characterized by arterial pruning, occlusive vascular remodeling, and inflammation contributing to increased pulmonary vascular resistance with resultant right heart failure. Endothelial cell (EC) injury and apoptosis are commonly considered triggers for PAH, the mechanisms leading from injury to complex arterial remodeling are incompletely understood. While current therapies can improving symptoms, with the exception of parenteral prostacyclin, they do not significantly prolong transplant free survival. As well, there are no therapies that can regenerate the damaged lung short of transplantation. In this project, I sought to both advance the understanding of disease pathogenesis and explore regenerative therapeutic options for PAH. To this end, I first employed single cell RNA sequencing (scRNA-seq) at multiple time points during the Sugen 5416 (SU) – chronic hypoxia (CH) model of PAH, to provide new insights into PAH pathogenesis both during onset and progression of disease. We also employed microCT analysis to visualize and quantify the arterial pruning associated with PH and found significant loss up to 65% of the healthy arteriolar volume in this model. Through scRNA-seq analysis performed at four timepoints spanning the onset and progression of disease, two disease-specific EC cell types emerged as key drivers of PAH pathogenesis. The first was the emergence of capillary ECs with a de-differentiated gene expression profile, which we termed dedifferentiated capillary (dCap) ECs, with enrichment for the *Cd74* gene. Interestingly, RNA velocity analysis suggested that these cells may be undergoing endothelial to mesenchymal transition during PAH development. At later times, a second arterial EC population became apparent, which we termed activated arterial ECs (aAECs), since it uniquely exhibited persistently elevated levels of differential gene

expression consistent with a migratory, invasive and proliferative state. Interestingly, the aAECs together with the smooth muscle (SM)-like pericytes, a population which was also greatly expanded in PAH, expressed *Tm4sf1*, a gene previously associated with a number of cancers and abnormal cell growth. Furthermore, by immunostaining, TM4SF1 was found to be spatially localized to sites of complex and occlusive arterial remodeling, associated with both endothelial cells and pericytes in these lesions, suggesting an important role for the aAECs and SM-like pericytes in arterial remodeling and PH progression. Together, these findings suggest that aAECs, dCap ECs, and SM-like pericytes are emerging cell populations responsible for lung arterial remodeling in PAH, which drives disease progression, and that TM4SF1 may be a novel therapeutic target for this disease. As a first step in trying to develop approaches to regenerate lung arterial bed that is lost in PAH, we investigated the potential role of endothelial colony forming cells (ECFCs) and mesenchymal stromal cell (MSC) derived extracellular vesicles (EVs) as novel therapeutics, on the premise that these stem/progenitor cells would stimulate lung regeneration by mainly paracrine mechanisms. Additionally, we used biomaterials to microencapsulate cells and EVs to improve their local delivery and retention. While ECFCs were found to be ineffective in treating the monocrotaline model on their own, they were poorly retained in the lung and microencapsulation of ECFCs led to enhanced lung delivery within the first 72 hours, with resultant hemodynamic improvements in this model of PAH. MSCs are well known to be immunomodulatory and proangiogenic, largely acting through paracrine mechanisms, including by the release of EVs. Yet, following intravenous administration, nano sized EVs are rapidly cleared from circulation, potentially limiting their therapeutic potential. I adapted our microencapsulation strategy for EVs, and demonstrated significantly greater retention of microgel-loaded EVs were within the lung, resulting in enhanced local cell uptake. Interestingly, the hydrogel used for microencapsulation induced a local immune response which made it unsuitable for testing any potential therapeutic benefits of MSC-EVs in this study. Nonetheless, this work demonstrated proof-of-principle for the utility of microencapsulation as a strategy to enhance EV lung delivery. Overall, this work has identified novel lung cell populations (aAECs, dCap ECs, SM-like pericytes) driving arterial remodeling associated with PH progression, demonstrated the potential of ECFCs as a regenerative cell for the treatment of PAH, and illustrated the utility of microencapsulation as a tool to enhance lung targeting of both cells and EVs.

Acknowledgments

First, thank you Dr. Stewart for the opportunity to join your lab. Thank you for the opportunity to start as a technician back in 2016, and your willingness and support in my transition to doctoral research. I've appreciated your mentorship and the supportive lab environment you have fostered. You've provided me many exciting opportunities to learn and challenged me to grow throughout this degree.

I started in the Stewart lab in 2016 as a research technician, and through my time in my PhD, numerous people have passed through. When I first joined the lab, I had the pleasure to work directly with Ketul, who is both an excellent supervisor and great mentor. I've appreciated all your advice and guidance over the years, even after you've started up your own lab! Katelynn, it was so much fun to work with you and discuss new ideas, it is hard to put in words how important the help you provided during all my animal studies was. Moe, Casey, Virgilio, and Rafael, you were all so welcoming when I joined, and I truly enjoyed all our discussions. Alvin and Jason, you were both so fun to work with, I enjoyed all our time travelling to conferences, scientific discussion, and support during experiments. Yupu and Anli, I don't think any of the animal studies would have been possible without your expertise, and I appreciated the opportunity to learn from you. Maria, Luci, Mahmoud, Yan, Yuan, Ken, Chyan-Jang, and Jia-Pey your help, guidance and support throughout the years was invaluable. Shirley, thanks for your advice over the years throughout the different projects. Dr. Courtman, your advice during lab meetings is always appreciated. Between questions from Dr. Stewart and yourself I never did give a short presentation! Saad, you were always willing to help and discuss new ideas. I've appreciated your support and mentorship throughout the years. Sam, Mfonsio, and so many other members of the cell manufacturing facility, we may not have worked together directly but lunch time discussions were always a pleasure. With major shifts in lab staff during the pandemic, it has been a pleasure to work alongside and train the next generation of technicians and students. Good luck to Elmira and Elham with your own doctoral studies; I wish you all the best.

To my wife, Janessa, you've been alongside me throughout the whole journey, and I couldn't have done it without you. Your love, encouragement, and guidance have been essential throughout the years and challenges of a PhD. Thank you for providing the support I needed to get through this degree. Danny, you are a bright, energetic, and thoughtful kid and it has been a joy to watch your grow. You certainly added to the challenges of a PhD but the joy you bring to our lives is unmatched. Charlotte, our newest addition, you may have come at the end of this journey, but we're excited to see where this new chapter takes us! Aspen, you will never read this, but you're the perfect dog for us and our walks in the woods together are the best mental reset I could have asked for. Pekoe, as a rabbit, you have made sharing an office space sometimes noisy and full of hay but always loaded with cuteness.

Mom and Dad, it's hard to believe we've made it all the way to the end of this degree. Thank you for your love, support, and guidance throughout the years; I'm very grateful for all the opportunities you provided me! To my in-laws, Karl and Grace, you are wonderful grandparents and have helped us in so many ways throughout this journey. Karl, your questions and scientific discussions always force me to think hard, and your curiosity is infectious. James, Fiona, Ryan, and Deanna, thank you for your motivation and encouragement throughout this degree.

Lastly, to my friends, you give me the opportunity to unwind, relax, and laugh. To the Ottawa crew, Carrie, Sarah, Tyler, Ally, Josh, Anneli, Stephanie, David, Michael, Maddie, and Kent, while people have moved back and then away again the dinners, drinks, celebrations, hikes, paddles, and camping trips are always a blast, and I'm lucky to have you all as friends. The Waterloo boys, Tyler, Christian, Sangwoo, and Zach, I'm so glad we still make time to get together and connect. The trips are always a highlight and you guys are the best. Finally, the Sefton lab boys, Alex and David, well we've been quite spread apart it has been great to stay connected. You've always been supportive of the process, and I've appreciated the support throughout the years.

Table of Contents

List of Tables

List of Figures

List of Abbreviations

aAEC	activated arterial endothelial cell
aCap	aerocytes
ANOVA	analysis of variance
BLI	bioluminescence imaging
BMPR2	bone morphogenetic protein type 2 receptor
CHD	congenital heart disease
dCap	de-differentiated capillary
DEG	differentially expressed genes
EC	endothelial cell
ECFC	endothelial colony forming cell
ECM	extracellular matrix
EDC	explant derived cardiac cell
EMT	epithelial to mesenchymal transition
EndoMT	endothelial to mesenchymal transition
EPC	endothelial progenitor cell
ERG	early response genes
EV	extracellular vesicle
FBS	fetal bovine serum
gCap	general capillary
GSEA	gene set enrichment analysis
HBSS	hank's balanced salt solution
HUVEC	human umbilical vein endothelial cell
i.p.	intra peritoneal
IPA	ingenuity pathway analysis
MCT	monocrotaline
microCT	micro computed tomography
MØ	macrophage
MSC	mesenchymal stromal cell
NES	normalized enrichment score
NK	natural killer cell
PAH	pulmonary arterial hypertension
PBS	phosphate buffered saline
PCA	principle component analysis
PDMS	dimethylpolysiloxane
RVH	right ventricular hypertrophy
RVSP	right ventricular systolic pressure
s.c.	subcutaneous
scRNA-seq	single cell RNA sequencing

SD	Sprague Dawley
SM-like	smooth muscle like
SMA	smooth muscle actin
SMC	smooth muscle cell
SU/CH	Sugen 5416 – chronic hypoxia
TF	transcription factor
TGFβ	transforming growth factor beta
TM4SF1	transmembrane 4 L6 family member 1
Treg	regulatory T cell
UMAP	uniform manifold approximation projection
UMI	unique molecular identifier
VEGFR2	vascular endothelial growth factor receptor 2

Contributors and funding agencies

This dissertation is written as a thesis by articles, and contains findings from the following manuscripts:

Chapter 1: Introduction: **Cober ND**, VandenBroek MM, Ormiston, ML, Stewart DJ. Evolving concepts in the pathobiology of pulmonary arterial hypertension. *Hypertension*. (2022). (*doi: 10.1161/HYPERTENSIONAHA.122.18261*).

Chapter 2: **Cober ND**, McCourt E, Godoy RS, Deng Y, Schlosser K, Situ A, Cook DP, Lemay SE, Klouda T, Yuan K, Bonnet S, Stewart DJ. Emergence of disease specific endothelial and stromal cell populations involved in arterial remodeling during development of pulmonary arterial hypertension. *bioRxiv* (2023). (*doi: 10.1101/2023.09.06.555321*). Submitted to *Circulation Research*.

Chapter 3: **Cober ND***, Chaudhary KR*, Deng Y, Lee CJ, Rowe K, Courtman DW, Stewart DJ. Single cell microencapsulation improves lung retention of endothelial colony forming cells after intravascular delivery and unmasks therapeutic benefit in severe pulmonary arterial hypertension. *bioRxiv* (2022). (*doi: 10.1101/2022.11.05.514522*). Submitted to *Pulmonary Circulation*.
*equal contributions

Chapter 4: **Cober ND**, Rowe K, Deng Y, Benavente-Babace A, Courtman DW, Godin M, Stewart DJ. Targeting extracellular vesicle delivery to the lungs by microgel encapsulation. *Journal of Extracellular Biology*. (2023). (*doi: 10.1002/jex2.94*).

Thanks to the following core service providers: StemCore laboratories at the Ottawa Hospital Research Institute (OHRI), in particular, Katayoun Sheikheleslamy for preparing and running samples for single cell RNA sequencing; the OHRI bioinformatics core, in particular Christopher Porter for processing single cell outputs through CellRanger and providing bioinformatics support.

Funding Sources

- Frederick Banting and Charles Best Canada Graduate Scholarship Doctoral Awards (Recipient: Nicholas Cober) 2019-2021
- Ontario Graduate Scholarship (Recipient: Nicholas Cober) 2018-2019
- Canadian Vascular Network Scholar Award (Recipient: Nicholas Cober) 2019 – 2021
- University of Ottawa Excellence Scholarship (Recipient: Nicholas Cober) 2018-2021

- Canadian Institutes of Health Research (CIHR) Foundation Grant (FDN – 143291; Recipient: Duncan J. Stewart)

Thesis Advisory Committee Members

- Dr. Darryl Davis
- Dr. Emilio Alarcon
- Dr. Robert Jankov

List of Publications

1. **Cober ND**, McCourt E, Godoy RS, Deng Y, Schlosser K, Situ A, Cook DP, Lemay SE, Klouda T, Yuan K, Bonnet S, Stewart DJ. Emergence of disease specific endothelial and stromal cell populations involved in arterial remodeling during development of pulmonary arterial hypertension. *bioRxiv* (2023). (*doi: 10.1101/2023.09.06.555321*). Submitted to Circulation Research.

2. Godoy RS*, **Cober ND***, Cook DP, McCourt E, Deng Y, Wang L, Schlosser K, Rowe K, Stewart DJ. Single cell transcriptomic atlas of lung microvascular regeneration after targeted endothelial cell ablation. *eLife* (2023). (*doi: https://doi.org/10.7554/eLife.80900).*
   **equal contributions*

3. **Cober ND,** Rowe K, Deng Y, Benavente-Babace A, Courtman DW, Godin M, Stewart DJ. Targeting extracellular vesicle delivery to the lungs by microgel encapsulation. *Journal of Extracellular Biology* (2023). (*doi: 10.1002/jex2.94).*

4. **Cober ND*,** Chaudhary KR*, Deng Y, Lee CJ, Rowe K, Courtman DW, Stewart DJ. Single cell microencapsulation improves lung retention of endothelial colony forming cells after intravascular delivery and unmasks therapeutic benefit in severe pulmonary arterial hypertension. *bioRxiv* (2022). (*doi: 10.1101/2022.11.05.514522).* Submitted to Pulmonary Circulation.
   **equal contributions*

5. **Cober ND,** VandenBroek MM, Ormiston, ML, Stewart DJ. Evolving concepts in the pathobiology of pulmonary arterial hypertension. *Hypertension*. (2022). *(doi: 10.1161/HYPERTENSIONAHA.122.18261)*.

6. **Cober ND,** Stewart DJ. Novel concepts in the endothelial pathobiology of pulmonary arterial hypertension. *Hypertension News* (2021). (*doi: 10.30824/2103-6)*. Part of ISSN: 2520-2782.

7. Evans CE, **Cober ND**, Dai Z, Stewart DJ, Zhao YY. Endothelial cells in the pathogenesis of pulmonary arterial hypertension. *Eur. Respir. J.* (2021). (*doi: 10.1183/13993003.03957-2020)*.

8. Chaudhary KR, Deng Y, Yang A, **Cober ND**, Stewart DJ. Penetrance of Severe Pulmonary Arterial Hypertension in Response to Vascular Endothelial Growth Factor Receptor 2 Blockade in a Genetically Prone Rat Model Is Reduced by Female Sex. *J Am Heart Assoc.* (2021). (*doi: 10.1161/JAHA.120.019488)*. Part of ISSN: 2047-9980.

9. Kanda P, Benavente-Babace A, Parent S, Connor M, Soucy N, Steeves A, Lu A, **Cober ND**, Courtman D, Variola F, Alarcon EI, Liang W, Stewart DJ, Godin M, Davis DR. Deterministic paracrine repair of injured myocardium using microfluidic-based cocooning of heart explant-derived cells. *Biomaterials*. (2020). (*doi: 10.1016/j.biomaterials.2020.120010).* PMID: 32259654.

Chapter 1: Introduction

Section 1.1 of this chapter has been previously published in the following review article:

Cober ND, VandenBroek MM, Ormiston ML, Stewart DJ. (2022). Evolving Concepts in Endothelial Pathobiology of Pulmonary Arterial Hypertension. *Hypertension*, 79: 1580 – 1590. doi: 10.1161/HYPERTENSIONAHA.122.18261.

Author Contributions:
Nicholas Cober: Developed review outline, wrote sections of the manuscripts, reviewed, and edited initial and revision versions.
Duncan Stewart: Developed review outline, wrote, and critically reviewed the manuscript.
Other authors: Content experts contributed to genetic and immune sections of the manuscript.

Acknowledgement: Figures 1.1, 1.2, and 1.3 were created with Biorender.com

1.1 Pulmonary Hypertension

Pulmonary hypertension (PH) is defined as an elevated mean pulmonary arterial pressure >20 mmHg. There are five distinct PH groups, which are classified based on the underlying aetiology and mechanism of pressure elevation. Pulmonary arterial hypertension (PAH) (or group 1 PH) is a disease affecting the pre-capillary pulmonary arterioles, and the diagnosis requires a pulmonary artery wedge pressure $\leq$15 mmHg and pulmonary vascular resistance (PVR) $\geq$3 Wood units, assessed by right heart catheterization.[1] PAH is characterised by endothelial injury and dysfunction, and proliferative arterial remodelling.[1] Of the subtypes of PAH, idiopathic (I)PAH is the most common, accounting for 30–50% of cases.[1] Heritable (H)PAH is diagnosed by the presence of a family history and/or a PAH causing mutation. Other subtypes include PAH associated with drug- and toxin exposure, connective tissue disease, HIV, portopulmonary hypertension or congenital heart disease (CHD).

PAH is a rare disease with an incidence of 2-2.4 cases per million adults in recent registries from France and the United States.[2] Despite the introduction of current therapies, PAH is still a devastating and progressive disease with a 3-year survival in the United States of 68% in the REVEAL registry.[2] Female sex is an important risk factor for PAH, with a 4:1 predominance of females to males according to the United States Pulmonary Hypertension Registry[3]; however, men with PAH demonstrate more rapid progression and have a worse prognosis, the so-called ‘estrogen paradox’*. PAH can affect people of all ages, including children, although more recent registry data has shown increased incidence in older individuals, possibly related to more awareness of the disease and widespread use of echocardiography. Mechanistic studies into

---

* While female sex is an important risk factor for PAH, the female sex hormone has been demonstrated to be protective in animal models.

the pathobiology of PAH have identified distinct disease phenotypes in pulmonary arterial (PA) endothelial cells (ECs), smooth muscle cells (SMCs) and adventitial fibroblasts, as well as various immune cell populations. Among this myriad of players, genetic and experimental evidence is converging on a critical role for the pulmonary endothelium as a central mediator of both disease initiation and progression,[4–7] which will be the main focus of this review.

1.1.1 The Genetics of PAH

Since the turn of the century, mutations in *BMPR2*, the gene encoding the bone morphogenetic protein (BMP) type-II receptor (BMPR-II), have been implicated in the development of PAH.[8] These heterozygous loss-of-function mutations account for 70% of HPAH cases, and 20% of seemingly idiopathic disease.[3,9] *BMPR2* mutations increase the odds of developing PAH from a prevalence of 10-15 per million to roughly 1 in 4 among mutation carriers.[3,10,11] Interestingly, disease penetrance in *BMPR2* mutation carriers is relatively low, with the Vanderbilt Pulmonary Hypertension Registry reporting an estimated penetrance of 14% in males and 42% in females.[11] Typically, mutation carriers that develop disease at an earlier age, have more severe hemodynamic abnormalities, and exhibit shorter survival times than the general PAH population.[12] Importantly, the reduction of BMPR-II expression has been found in PAH patients regardless of whether a mutation is present,[13,14] further highlighting the critical importance of this receptor to disease pathogenesis.

Although *BMPR2* is expressed across a range of cell types, there is substantial genetic evidence supporting that loss of endothelial *BMPR2* expression is of particular importance to disease initiation. In the lung vasculature, BMPR-II is predominantly expressed in the endothelium (Atkinson) and partners with the largely endothelial-restricted type-I receptor, Alk1, and co-receptor, endoglin, to form a receptor complex for circulating BMP9, BMP10 and heterodimers of the two ligands.[15,16] Importantly, the genomic assessment of PAH patient cohorts has identified mutations in the genes encoding Alk1 (*ACVRL1*), endoglin (*ENG*),[17] BMP9 (*GDF2*) and BMP10 (*BMP10*),[5,6] as well as downstream mediators of BMP signalling, *SMAD1*, *SMAD9*, and the common *SMAD4*[18] (**Figure 1.1**). The importance of impaired endothelial BMRP-II signalling is also supported by *in vivo* studies demonstrating spontaneous PH in mice bearing an endothelial-specific deletion of *Bmpr2*.[7] However, recent work has suggested that BMP9/10 signaling via the Alk1/BMPR-II receptor complex may also influence SMC phenotype and function.[19]

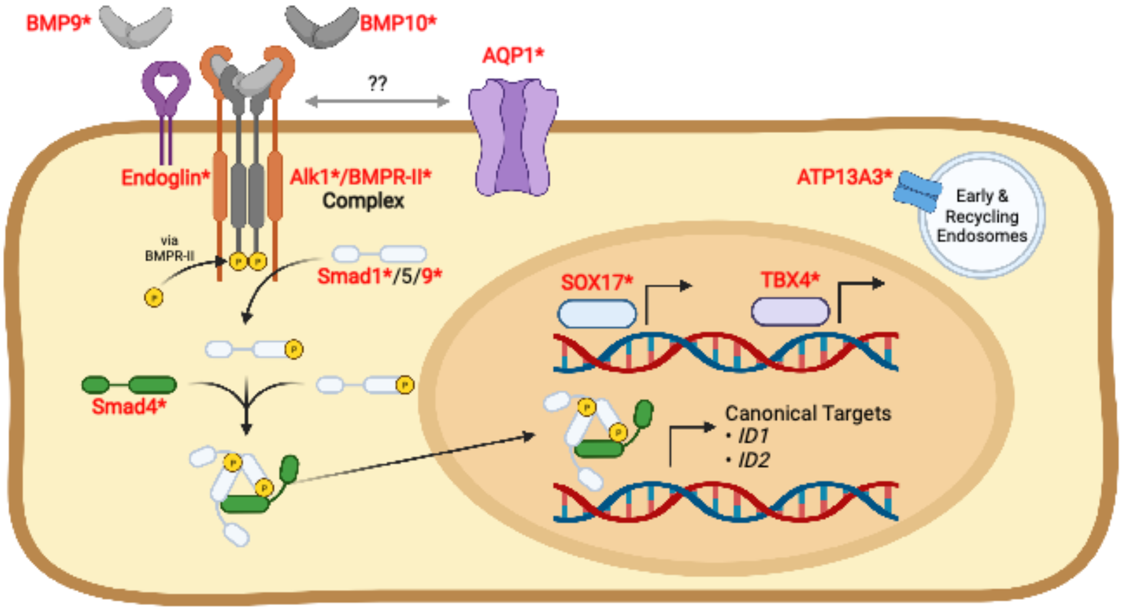

Figure 1.1: Disease-associated mutations in PAH underscore the importance of the pulmonary endothelium in disease development.
The genetic causes of PAH are centred around the BMPR-II signalling axis, with mutations (red text and asterisk) in the genes encoding BMPR-II, the type I receptor Alk1, the co-receptor Endoglin, BMP9 and BMP10, as well as the secondary messengers Smad1 and Smad9, and the

common Smad4 all present in the PAH population. Other mutations outside this canonical pathway have also been identified, including in the genes encoding the water channel *AQP1*, the potassium channel *KCNK3*, the transcription factors *SOX17* and *TBX4*, and the P-type ATPase *ATP13A3*. The high level of expression of these genes within the pulmonary endothelium emphasizes the critical role for this cell type in disease pathogenesis.

The therapeutic targeting of the BMP9/10 signaling axis is also complex. The enhancement of endothelial BMP signaling through the administration of exogenous recombinant BMP9 can prevent and reverse disease in rodent PH models.[4] However, the blockade of endogenous BMP9/10 signaling using an Alk1-Fc ligand trap has produced mixed results, with contrasting studies demonstrating either exacerbation[20] or inhibition[21] of PH progression. Ongoing work to reconcile these seemingly contradictory findings has demonstrated that BMP9 can act as a context dependent “angiogenic switch” that promotes endothelial quiescence and vascular stability in individuals with preserved BMPR-II levels, but induces pathological proliferation when the receptor is downregulated or lost, as it is in many PAH patients.[22] Endothelial BMPR-II loss is also linked to imbalanced signaling within the TGFβ superfamily, favouring SMADs 2/3 activation by the TGFβ/Activin/GDF arm of this family. Efforts to rebalance signaling using an Activin type-IIA Receptor (ActR-IIA) ligand trap targeting activin and growth and differentiation factor (GDF) ligands have shown efficacy in preclinical models of severe PAH[23] and provide a mechanistic basis for the ActR-IIA ligand trap, Sotatarcept, which has shown promising results in a phase 2 clinical study.[24]

Mutations in several genes outside the BMPR-II signalling axis are also significantly over-represented within the PAH patient population,[25] including the transcription factors *TBX4* and *SOX17*, the potassium channel *KCNK3*, the water channel *AQP1*, and the P-type ATPase

ATP13A3.[3,25–27] Importantly, *SOX17* is most abundantly expressed in ECs and shares a tissue expression pattern with *BMPR2* and the VEGF receptor *KDR*.[28] *AQP1* is also directly tied to endothelial *BMPR2* expression, as the loss of *BMPR2* in pulmonary microvascular ECs leads to reduced *AQP1* expression[29] and vice versa.[30]

1.1.3 Endothelial dysfunction in PAH

The term "endothelial dysfunction" was initially coined to describe the loss of endothelial derived vasodilator factors such as prostacyclin and nitric oxide (NO), with an increase in production of endothelial vasoconstrictors, such as endothelin-1.[31] This imbalance emerged as an important mechanism in PAH pathogenesis in the early 1990s and served as the basis for all currently approved PAH therapies, which were developed to target these three pathways. While availability of vasodilatory therapies has been a great advance in the management of this devastating disease with important hemodynamic and functional benefits for many patients, in general they have had more limited impact on slowing disease progression or extending the time to death or lung transplantation.[32,33] Over time, the concept of endothelial dysfunction has evolved to include other important roles of the endothelium in regulation of vascular functions, such as smooth muscle growth and medial hypertrophy, reduced anticoagulant function, metabolic abnormalities, reactive oxygen species production, increased expression of adhesion molecules, and the release of cytokines, chemokines, and growth factors.[34]

1.1.3.1 EC apoptosis in the initiation of PAH

While endothelial dysfunction is undoubtably an important contributor to PAH, it is believed that EC injury and apoptosis in vulnerable regions of the lung vasculature serves as a triggering event in disease pathogenesis.[35] The increased sensitivity of the PAH endothelium to apoptotic stimuli is linked to the genetics of disease, as both loss-of-function mutations in *BMPR2* and siRNA silencing of this gene enhance apoptosis and eliminate the anti-apoptotic effects of BMP9[4]. Interestingly, the two most common animal models of PAH, the monocrotaline (MCT) rat model and the SU5416 (SU)-chronic hypoxia (CH) rat, are also initiated by endothelial cell injury and apoptosis[36,37]. In the SU/CH model, administration of the VEGFR2 antagonist in combination with 2-3 weeks of CH induces lung arteriolar EC apoptosis in rats,[36] and to a limited extent in mice,[38] followed by the formation of complex occlusive lesions resembling the plexiform lesions observed in patients. Complex lesions can also be seen in the MCT model when it is combined with a left to right shunt[39] or left pneumonectomy[40] to induce increased pulmonary blood flow. Inhibition of apoptosis using nonspecific caspase inhibitors (i.e., Z-VAD) prevents the development of PH in both the SU/CH and MCT models.[35] Furthermore, a transgenic mouse model of Fas-induced EC apoptosis results in PH with dramatic pulmonary arteriopathy and perivascular inflammation,[41] supporting the critical role of EC apoptosis in the initiation and progression of complex arterial remodeling.

However, the precise mechanisms that link EC apoptosis to complex arterial remodeling and the development of PAH are not yet well elucidated. Endothelial injury and apoptosis can result in a variety of direct and indirect consequences, as summarized in **Table 1**. An immediate outcome of endothelial apoptosis could be the loss distal arteriolar integrity. The distal lung arteriolar bed is unique in that it lacks smooth muscle coverage and consists largely of an endothelial tube with scant matrix support and the occasional pericyte (**Figure 1.2**) and may therefore be dependent on survival signalling through VEGFR2 and BMPR-II to maintain EC homeostasis. The withdrawal of these signals via SU-mediated VEGF inhibition or *BMPR2* mutations could lead to distal arteriolar dropout, ultimately increasing PVR, causing pulmonary hypertension.

Table 1.1: Direct and indirect consequences of endothelial cell injury in PAH.

Direct Effects	Consequences
• **Loss of barrier function**	• Increased leakiness
• Increased coagulability	• Intravascular thrombosis
• Arteriolar drop out	• Loss of distal perfusion
• Increased immune cell trafficking	• Vascular inflammation
Indirect Effects	**Consequences**
• Endothelial dysfunction	• Vasoconstriction/SMC hyperplasia
• Reactive EC proliferation	• EC repair and vascular healing
• Emergence of apoptosis-resistant hyperproliferative cells	• Occlusive arterial remodeling

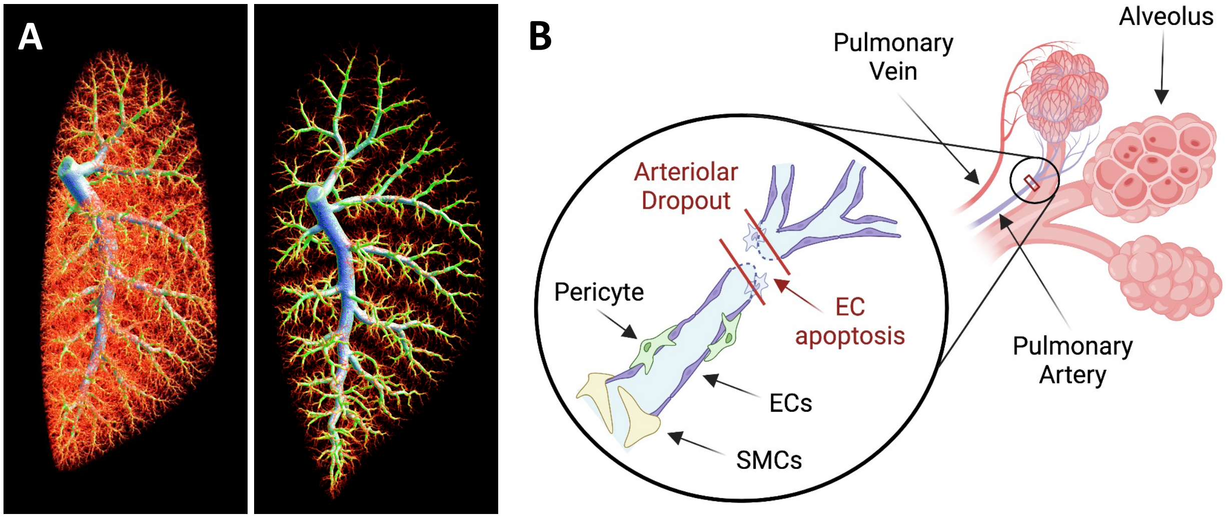

Figure 1.2: Vascular remodeling in PAH.

(A) High resolution micro-computerized tomography (HR-microCT) images of healthy (left) and SU/CH (right) rat lungs, demonstrating significant arteriolar dropout. (B) Proposed mechanism of endothelial cell injury resulting in dropout and loss of fragile pre-capillary arterioles.

While the histological examination of 2-dimensional lung sections is often used for quantifying arterial remodeling in late-stage PAH including medial hypertrophy, intimal hyperplasia and complex remodeling (i.e., plexiform lesions), this approach is not well suited for visualizing the early changes in complex 3-dimensional architecture of the distal arteriolar pulmonary circulation. Therefore, we have used high-resolution micro-computerized tomography (HR-MicroCT)[42] in animal models to quantify the extent of arteriolar volume loss in early stage disease and explore the potential contribution of this loss to the onset of PAH. HR-MicroCT has revealed >75% loss of distal arterioles in the SU/CH model of PAH as early as 4 weeks post SU (**Figure 1.2A**), coinciding with marked increases in pulmonary systolic arterial pressures, but preceding the appearance of overt occlusive arterial remodeling. Using fluorescence microangiography coupled with immunofluorescence staining, the abrupt cut-offs in pre-capillary arterioles could be localized to regions exhibiting a paucity of cells,[43] which is consistent with arteriolar dropout, rather than obliterative remodeling as the driver of early stage disease development (**Figure 1.2B**).

1.1.3.2 Role of hemodynamic stress in perpetuating of EC injury and progression of PAH

Surprisingly, EC apoptosis is not only seen during the first days or weeks following a single injection of SU, but may persist and even increase over a prolonged period, out to 11 weeks into this model,[4] well beyond the expected pharmacological effects of this compound. Recently, hemodynamic perturbation, in particular increased arteriolar shear stress, has been identified as a key driver for complex arterial remodeling in the rat SU/CH model of PAH,[44] which may sustain EC injury long after the initial triggering insult has worn off. Left pulmonary artery banding (LPAB) to reduce flow in the ipsilateral lung both prevented and reversed the formation of occlusive plexiform lesions when banding was performed either before or 5 weeks after the induction of PAH, respectively, suggesting that occlusive arteriopathy is a consequence, but not a cause, of the hemodynamic abnormalities responsible for early disease progression.

This work is also consistent with the well-described role for pathological intimal shear stress in PAH associated with congenital heart disease (CHD) and significant left to right shunting.[45] Indeed, the original description of plexiform lesions was made in patients with Eisenmenger's syndrome, a form of PAH in the CHD population that is pathologically indistinguishable from idiopathic or hereditary disease.[46] While early closure of left-right shunts can prevent or reverse the PAH in these patients, the disease becomes irreversible once systemic pulmonary arterial pressures are established, and the direction of shunting is reversed (Eisenmenger's physiology).[47] The mechanisms underlying the transition to irreversible arterial remodeling were recently explored in a CHD model induced by an aorto-caval anastomosis followed by administration of MCT.[48] Single lungs from the CHD model were transplanted into normal recipient rats at different timepoints post MCT administration to assess whether arterial remodeling would resolve after hemodynamic unloading. Complex arterial lesions were found to be completely reversible up to 3 weeks post MCT, whereas after this, lesions persisted or progressed despite the exposure to normal hemodynamics. The loss of reversibility coincided with the appearance of vascular cell senescence markers (p16, p21) and reversibility could be restored using a senolytic agent, strongly suggesting a role for cellular senescence in the transition to irreversible disease.[48]

1.1.4 Vascular cell proliferation in PAH – "wound healing gone awry"?

In addition to the induction of cellular senescence, failed endothelial regeneration in PAH is also thought to lead to the emergence of the hyperproliferative, cancer-like vascular cells that drive increased vascular resistance and late-stage disease progression by contributing to intimal hyperplasia, occlusive arterial remodelling, and plexiform lesion formation. The 'quasi malignancy' paradigm of severe pulmonary hypertension was first proposed in 2008[49] based on the remarkable similarities in cell growth dysregulation between the pulmonary ECs and SMCs of PAH patients and malignant cells from cancerous tissues. Importantly, both cancer and the complex arterial remodeling in PAH may arise as a result of chronic injury and failed 'wound' healing.[50] While PAH is largely restricted to the lung vasculature, it exhibits many of the classical hallmarks of cancer[51] with the exception of tissue invasion and metastasis. Unlike the exclusive hyperproliferation observed in other vascular cell types, such as SMCs, ECs exhibit contemporaneously both increased apoptosis and proliferation. The link between these two states may involve cellular senescence, which has been previously implicated in malignant transformation,[52] as a potential mechanism for the emergence of apoptosis-resistant and hyper-proliferative ECs in PAH.[53] As in cancer, there is increased expression of a wide range of proteins involved in growth regulation, including transcription factors (PIM1, NFAT, STAT3, FOXO1, YAP/TAZ, HIF1), survival factors (Survivin), adhesion molecules (ß-catenin) and regulators of DNA repair (PARP-1, BDR4).[54] PAH is also linked to a shift in cellular energetics, from oxidative metabolism to aerobic glycolysis. Although this cancer-like shift, known as the Warburg effect, has largely been examined in pulmonary vascular SMCs,[55] more recent work has shown similar changes in vascular ECs[56,57] and adventitial fibroblasts,[58] suggesting a more global shift in cellular metabolism and proliferation across cell types.

Much of the excitement for the cancer hypothesis of PAH comes from the possibility that therapeutic interventions designed to target key pathways for cancer could be repurposed for PAH. One of the first examples of this approach was the use of imatinib, a receptor tyrosine kinase inhibitor targeting PDGF receptors and BCR-ABL in chronic myelogenous leukemia, that showed promising results in randomized clinical trials of patients with PAH.[59] Although the development of imatinib stalled for a variety of reasons, both safety and commercial, the inhibition of PDGF signaling is still an important therapeutic target and a phase 2/3 trial with an inhaled imatinib is underway (ClinicalTrials.gov Identifier: NCT05036135). A number of other anti-neoplastic agents are also in development for PAH, including BRD4 and PARP-1 inhibitors (NCT03655704, NCT03782818), which have shown intriguing efficacy signals in preclinical animal models.[60,61] A search of Clinicaltrials.gov revealed 17 active studies using a wide range of antineoplastic drugs for PAH. The results of these ongoing clinical studies will be important in validating the cancer hypothesis of PAH and determining whether targeting growth dysregulation in the later stages of PAH will improve function and outcomes of patients.

1.1.5 Sex and the pulmonary vascular endothelium in PAH

The fact that PAH shows a strong female predominance suggests an important role for sex hormones in the pathogenesis of this disease. However, the link between female sex hormones and PAH is far from clear. While females are at a greater risk of developing PAH, male PAH patients tend to develop more severe disease and exhibit significantly shorter survival times post-diagnosis,[12,62] the so-called estrogen paradox. Similarly, postmenopausal women, who have substantially lower levels of estrogens, have been reported to have worse outcomes than those pre-menopause.[63] This "estrogen paradox" is recapitulated in many preclinical models of PAH, which show greater disease severity in male rats and important protective effects of estrogen.[64–67] While it has been difficult to show a direct association between estrogen and outcomes in PAH, a recent study found significantly higher levels of estradiol in men with PAH compared to a large male cohort of healthy controls, whereas levels of dehydroepiandrosterone (DHEA), a precursor in the synthesis of testosterone and estrogen, were lower.[68] Interestingly, exogenous DHAE was also found to be protective in the SU/CH model of severe PAH, largely by improving RV function.[69] There are also a number of preclinical and clinical studies that have implicated aberrant metabolism of estrogen in PAH. For example, high levels of 6α-OH-E1:2-OH, an estrogen metabolite generated by metabolism of estrone (E1) by CYP1B1, is related to PAH development in *BMPR2* mutation carriers[70] and CYP1B1 is upregulated in PAH.[71] In the SU/CH rat model, both CYP1A1 and the aryl hydrocarbon receptor (AhR), an activator of this enzyme, are upregulated, and pulmonary hemodynamics are ameliorated by inhibition of AhR.[72] Direct inhibition of CYP1A1 using tetramethoxystilbene (TMS) also reduced PH severity in a mouse SU/CH model.[71] Moreover, the McClean group showed that the aromatase inhibitor, anastrozole, which inhibits endogenous estrogen production, attenuated PH development, but only in female animals, in two rodent models.[73] In a small randomized clinical trial, anastrozole significantly reduced estradiol plasma levels in patients with PAH[74] and, while it failed to improve right ventricular function, a small improvement in walking distance was observed and a larger study is now underway (NCT03229499).

We studied the importance of female sex hormones to the penetrance of PAH in a unique colony of Sprague-Dawley rats that develop severe PAH in response to SU alone, without the need for hypoxia.[75] This model exhibits an ‘all or none’ bimodal response to SU, with ~70% of males and ~30% females developing a severe PAH phenotype. This distribution mimics the incomplete penetrance seen in *BMPR2* mutation carriers, although with reversed sex-dependence. Removal of female sex hormones by ovariectomy increased the penetrance of the PAH phenotype in female rats to levels equivalent to males, whereas exogenous estrogen administration eliminated PAH in both sexes in this model.[64] We proposed that the cyclical withdrawal of protective effects of estrogen at the end of the estrus cycle could create a window of vulnerability for the fragile lung distal arteriolar bed and a greater opportunity for injurious triggers to initiate EC apoptosis in women. In contrast, the more constant levels of sex hormones in men reduce this risk, but once PAH has been triggered, lower estrogen levels may contribute greater progression, providing an explanation for the estrogen paradox. However, this paradigm would not account for the higher estrogen levels in men with PAH compared with controls, as discussed above.[68] Therefore, there are still many questions that need answers about the role estrogens in both the initiation and progression of PAH.

1.1.6 Immune dysfunction in PAH

Immune dysfunction and chronic inflammation are also well-recognized features of PAH. Disease prevalence is significantly elevated in the setting of autoimmune conditions, such as autoimmune thyroid disease, scleroderma and lupus, and chronic viral infections, like HIV.[76,77] Even IPAH patients with no associated immune conditions exhibit signs of altered immune function, including elevated levels of circulating inflammatory cytokines,[78] pathological autoantibodies,[79] and ectopic lymphoid neogenesis.[80] Perivascular inflammation, defined by the accumulation of adventitial fibroblasts, altered macrophage polarization,[81] and the recruitment of monocytes/macrophage-derived fibrocytes, have also been linked to the progression of disease.[82] Here, we will focus more on the role of endothelial inflammation in vascular remodeling.

1.1.6.1 Elevated TGFβ signaling as a driver of endothelial inflammation and vascular remodeling

The inflammatory phenotype of PAH has been linked to the genetic underpinnings of the disease in the form of imbalanced signaling via the TGFβ/Activin/BMP superfamily (**Figure 1.3**). In PAH patients and animal models, impaired BMPR-II signaling via Smad1/5/9 (**Figure 1.1**) is often accompanied by elevated TGFβ and Activin signaling through Smad2/3.[23,83,84] Mice bearing a dominant negative form of *Tgfbr2*, the gene encoding the type-II TGF⍰ receptor (TGFBR-II), are protected in the chronic hypoxia model of PH[85] and approaches that block TGFβ or Activin signaling, using either small molecule inhibitors or ligand traps, prevent or reverse pulmonary hypertension in a variety of rodent models.[23,86,87] This link between BMPR-II loss, elevated TGFβ and pulmonary endothelial dysfunction was recently highlighted in rats bearing a phenotypically silent heterozygous deletion of *BMPR2*, which develop PH in response to endothelial inflammation induced by 5-lipoxygenase overexpression.[88] Neointimal remodeling in these animals is secondary to increased leukotriene B4 production and is marked by endothelial to mesenchymal transformation. Importantly, antagonizing TGFβ reversed this vasculopathy in *BMPR2* mutant rats, highlighting the central role for imbalanced TGFβ superfamily signaling in endothelial dysfunction and inflammatory vascular remodeling. As detailed above, rebalancing of the BMP-TGFβ/Activin pathways as a therapeutic strategy for PAH has received strong support from the recent PULSAR clinical trial of Sotatercept, which resulted in hemodynamic improvement, increased function and reduced levels of the biomarker, NT-proBNP.[24] A phase 3 clinical trial of Sotatercept is ongoing (NCT04576988).

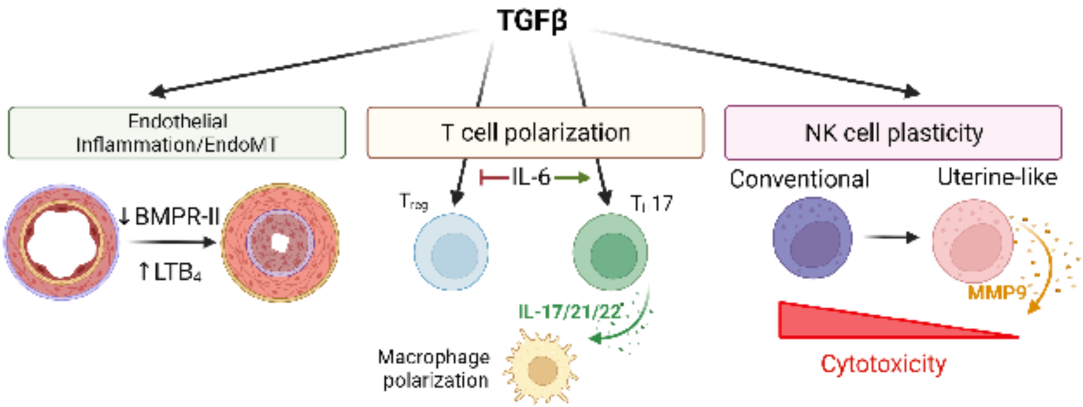

Figure 1.3: Proposed actions of elevated TGFβ signaling in PAH.
Elevated TGFβ, coupled with BMPR-II loss and inflammatory factors like leukotriene B_4 (LTB_4) can drive endothelial inflammation, proliferation and EndoMT. TGFβ can also perpetuate T_h17-driven immune responses in combination with IL-6 and drives the conversion of circulating NK cells to a poorly cytotoxic, uterine-like phenotype with the capacity to influence vascular remodeling.

TGFβ can also work in concert with inflammatory cytokines like IL-6 to divert the TGFβ-mediated differentiation of immunosuppressive regulatory T cells (T_{regs}) towards a proinflammatory T_h17 fate,[89,90] and can drive the conversion of innate lymphocytes, such as natural killer (NK) cells, towards a tissue-resident phenotype with a capacity to potentiate disordered vascularization.[91,92] Although an angiogenic role for NK cells in vascular remodeling was originally thought to be an exclusive feature of specialized uterine NK cells during pregnancy,[93] recent studies have identified a role for microenvironmental cues, like TGFβ and hypoxia, in the ectopic activation of a uterine NK program in the vascularization of solid tumors.[94,95] Importantly, NK cells from PAH patients exhibit signs of this angiogenic programming[96] and work in rodent models has identified spontaneous PAH in mice lacking NK cells or NK cell activating receptors,[97] a role for NK cells in the mechanism of action of experimental PAH therapies,[98,99] and a potential contribution of NK cell deficiency to right ventricular remodeling and failure in SU/CH rats.[100] Given the established links between PAH and cancer, as well as the recent appreciation for the potential contribution of senescent cells to disease pathogenesis, immunotherapies that target altered endothelial-immune interactions and enhance the anti-cancer and anti-senescent actions of NK cells may also merit investigation.

1.1.7 The past, present and future of PAH research

While great strides have been made in deciphering the complex pathobiology of PAH, especially over the last few decades, there is still much more that needs to be done. The pulmonary vascular endothelium has emerged as a critical driver in the initiation and progression of PAH; however, there are many paradoxes that are not well understood. While EC apoptosis is generally accepted as a central trigger for the development of this disease, it is also well established that EC hyper-proliferation and apoptosis resistance is a major mechanism in complex vascular remodeling. Female sex and sex hormones certainly have important influences, but it is still not clear by what mechanisms or even whether estrogens are beneficial or deleterious (or both depending on the context). The discovery of the genetic basis for hereditary PAH has been a major advance, particularly the most common mutations in *Bmpr2*, but there is still some uncertainty regarding the role of BMP9, the major agonist, in either protecting or promoting underlining vascular changes in this disease. In the brief review, we have tried to succinctly summarize some new insights into the endothelial pathobiology of PAH and some of its complexities. However, our understanding is increasing exponentially as the PAH research community grows and new technologies become available. For example, the recent development of technologies that can probe molecular correlates of PAH at a single cell level[101] will allow for a more holistic view of cell-cell interactions in health and disease.[102–104] These technologies will no doubt expand our understanding of interactions between the pulmonary endothelium and other vascular cell types, as well as endothelial-immune interactions, and hopefully provide the answers to some of the questions raised in this review. Future work will rely heavily on these advanced technologies, both in the discovery of new disease mechanisms and the assessment and translation of novel therapeutics.

1.2 Rodent models of PAH

Animal models are an essential tool to investigate PAH. While no model fully recapitulates the human disease, they provide both an opportunity to learn about disease progression and to test novel therapeutics. There are many available animal models of PAH, each with different utility depending on the research questions to be addressed.

1.2.1 Sugen – chronic hypoxia model

Initially developed in the early 2000's, the rat Sugen (SU) – chronic hypoxia (SU/CH) model combines a single subcutaneous injection of the vascular endothelial growth factor receptor 2 (VEGFR2) antagonist, SU5416, with exposure to hypoxia (10% oxygen) for three weeks to produce a severe model of PAH.[36] Subsequently, the SU/CH model was shown to be progressive upon return to normoxia, and able to recapitulate the formation complex plexiform lesions that are considered a hallmark of the human disease.[105] Interestingly, applying this same strategy to mice does not produce the same result; while weekly doses of SU led to elevated RVSP while animals were in CH, this effect was lost after removal to normoxia.[106] Thus, there are species specific differences in the response to SU/CH, where rats produce a more roboust model of PH then mice. Although these models require the use of hypoxia chambers to control oxygen levels, they are well tolerated with low mortality and the rat SU/CH is widely considered a gold standard because it produces lung vascular pathology that is similar to the human disease.

1.2.2 Monocrotaline model

Monocrotaline (MCT) is a plant derived pyrrolizidine alkaloid (PA). MCT is activated in the liver dependent on cytochrome P-450, producing reactive pyrrole metabolite dehydromonocrotaline (MCTP) which is an endothelial toxin.[37] In rats, a single intraperitoneal injection of MCT leads to a severe and progressive model of PAH within several weeks.[107] While the MCT model produces some of the expected pulmonary vascular remodelling, elevated pulmonary artery pressures, and right heart hypertrophy, this model on its own does not recapitulate the complex vascular lesions associated with the human disease.[108] However, it can be combined with a second hit from chronic hypoxia (CH),[109] left pneumonectomy,[40] or aortocaval shunt[110] to produce a more severe disease including these hallmark features; yet, the technical skills required for these complex surgical models limit their widespread utility. Additionally, the MCT model is often characterized by marked inflammation in the lungs, and accompanying off target damage to the liver, kidney, and heart.[107] Interestingly, attempts to produce an MCT mouse model have been unsuccessful, which may relate to a difference in the mouse's metabolism of MCT. However, a single dose of MCT produced symptoms in line with acute lung injury in mice within 7-10 days.[37] The single hit MCT model is commonly used to test therapeutic agents due to its relatively short development, yet its mechanisms of onset and off-target effects make it an imperfect model for studying some aspects of PH progression.

1.2.3 Chronic hypoxia model

Chronic hypoxia (CH) is used to induce a model of PH in mice and rats. Typically, animals are placed in hypoxic chambers at 10% oxygen for at 3-5 weeks.[111] The CH model produces some of the features of PH, primarily pulmonary artery muscularization due to, smooth muscle cell hypertrophy and proliferation, and right ventricular remodelling, but these changes are reversible upon return to normoxia.[112] Interestingly, the CH model produces more severe effects in rats then in mice, whereas mice develop a very mild PH phenotype.[111] CH model provides an opportunity to study some aspects of PH, and it is useful to study PH induced by hypoxia (i.e. group 3 PH), but it is not a model of PAH (group 1 PH) and does not reproduce the characteristic pathological features of PAH making it a poor model for this human disease.

1.2.4 Genetic models of pulmonary hypertension

Transgenic animal models provide the opportunity to address the role of specific genes in the development of PAH. These genetic manipulations are commonly performed in mice, and often coupled with the CH model as a second hit in an attempt to reproduce the development of PAH.[113] The most widely studied genetic manipulations are *BMPR2* knockouts, since mutations in *BMPR2* are strongly implicated in hereditary PAH.[8] The series of *BMPR2* related animal models are well summarized in the review by Boucherat et al., demonstrating a second hit is still required for more complete penetrance of PH.[108] Additionally, a number of other genes implicated in PH have been studied using transgenic models including ALK1, ENG (endoglin), CAV-1 (caveolin-1), PPAR-γ, IL-6, and Kcnk-3, demonstrating roles for these genes in PH progression.[108] In particular the prolyl-4 hydroxlyase-2 (PHD2) knockout mouse model[114] and the IL-6 overexpression model[115] have best reproduced the complex arteriopathy of PAH. These transgenic models can provide valuable insights into genetic factors associated with PH and serve as validation for role of suspected genetic mutations. Yet, they need to be used in concert with other general models to truly appreciate the intricacies of PAH progression.

1.3 Single cell transcriptomics

In recent years, new technological advances have made it possible to perform transcriptomic analyses at a single cell level. While traditional bulk RNA sequencing methodologies still provide important insights into transcriptomic changes at the tissue level, these methodologies lack the resolution to interrogate the cellular heterogeneity within an organ or biological system.[116] The advances made using single cell RNA sequencing (scRNA-seq) have aided in our understanding of the complexity of organs, and tissues at the single cell level during both healthy and disease conditions.[117] Commercially available equipment is now readily accessible from many companies, including 10x Genomics, to streamline the sample preparation and analysis process. Availability and access to local core facilities, such as StemCore laboratories and the OHRI bioinformatics core, allow researchers to rapidly adopt and apply these methods to their studies. Additionally, spatial transcriptomic technologies represent another tool that can provide important anatomical information about the spatial localization of various cell populations identified by single cell transcriptomics analyses to gain even deeper insights into disease.

1.3.1 Pulmonary hypertension and single cell transcriptomics

Single cell transcriptomics has aided in our understanding of both lung biology and pulmonary disease etiology. Whole lung cell atlases have been developed,[118] as well as, atlases of specific cell types, including endothelial cells.[102,119] Furthermore, combining single cell transcriptomic data with high resolution spatial biological interrogation, has given us new insights into the unique capillary populations within the lung: notably the alveolar capillary (aCap) ECs, or aerocytes, which represent the structural vascular component of the air-blood barrier involved in gas exchange, and the general capillary or gCap ECs, which are less specialized but play an important role in repair following microvascular injury.[101,120] Single cell transcriptomics has also been applied to the study of PAH to gain new insights into the disease; however, most of these studies have focused on end stage disease. One study comparing the MCT and SU/CH models with healthy controls used computational approaches to identify new potential druggable targets.[104] Another study has suggested a role for proinflammatory ECs in PH associated remodeling.[121] This approach has also been applied to human disease, but is often limited by the availability of donor tissue, for example in isolated pulmonary arteries from control and PAH lung donors, a skewed cellular communication within PAH arteries was demonstrated, which is implicated in arterial muscularization.[122] While these studies all provide valuable insights into PAH, they have yet to take advantage of consecutive sampling during disease progression to better understand pathogenesis, an approach we have successfully employed in a mouse model of endothelial ablation and regeneration.[120]

1.4 Regenerative medicine, stem cells and extracellular vesicles

Over the last several decades, regenerative medicine has been pushing the boundaries of what may be possible for the treatment of chronic diseases and severe organ or tissue damage. Advances in the fields of stem cell biology, tissue engineering, extracellular vesicles (EVs) and biomaterials have expanded the opportunities to directly repair and regenerate damaged organs, in particular for cardiovascular disease. In part this work will focus on the application of stem cells and stem cell derived EVs with the use of biomaterials to enhance their potential as a therapy for PAH since stem and progenitor cells and their derived EVs have potential regenerative properties through stimulating angiogenic responses, or immunomodulation.

1.4.1 Endothelial Progenitor Cells

The term endothelial progenitor cells (EPCs) refers to a highly heterogeneous collection of highly pro-angiogenic cells, only some of which have the potential to differentiate into endothelial cells and form new blood vessels.[123] EPCs can be isolated from the circulating blood through culture of mononuclear cells on a suitable matrix (i.e., fibronectin or collagen) in the presence of endothelial growth factors and have been typically classified as 'early' or 'late-' EPCs based on the timing of their appearance during *in vitro* culture. Early-EPCs appear with the first week of culture and retain many characteristics of mononuclear cells with variable endothelial gene expression. However, they are highly pro-angiogenic mononuclear cells whose therapeutic potential is primarily through paracrine mechanisms.[124] Late EPCs appear only after 2 weeks of culture and are highly proliferative cells with a strong endothelial phenotype, sometimes referred to as endothelial colony forming cells (ECFCs).[125,126] Both EPC sub-types have been used to treat a variety of disease models including PAH. Previous work from our lab has demonstrated the regenerative efficacy of early EPCs to both prevent and reverse severe PAH, which can be enhanced by eNOS-transfection.[127] Late EPCs or ECFCs have been used to treat ischemic hind limbs models, demonstrating their angiogenic potential;[128] however, attempts to treat PAH with ECFCs have not been successful.[98,129]

1.4.2 Mesenchymal Stromal Cells

The therapeutic potential of mesenchymal stromal cells (MSCs) has been studied for a wide array of diseases. MSCs are multipotent adult progenitor cells, which have tri-lineage potential to form cartilage, bone, and adipose tissue.[130] These cells have been identified, isolated, and cultured from multiple sources including bone marrow, adipose tissue, and umbilical cords with source dependent differences in their therapeutic potential.[131,132] In addition to their differentiation potential, MSCs are known to contribute to angiogenic remodeling and vascular repair. Their major role in regeneration is hypothesized to be through paracrine mechanisms, such as immune modulation.[133] Due to their highly angiogenic, immune-modulatory nature, MSCs have been judiciously studied in pre-clinical models, and have begun clinical translational for cardiovascular disease. Through systematic review and meta-analysis of these trials, there is evidence of modest therapeutic improvements for cardiovascular diseases such as myocardial infarction.[134] Furthermore, MSCs have been assessed for treatment of PAH with some evidence of reduced inflammation and improved right ventricular systolic pressure.[135] We are interested in the application of MSC-EVs as a cell free therapeutic by harnessing the paracrine mediated effects of the EVs. MSC derived EVs have been used to treat many cardiovascular diseases in pre-clinic models of myocardial infarction,[136] stroke,[137] and ischemic hind limb injury.[138] Additionally, MSC derived EVs were also demonstrated to have potential therapeutic implications as observed in a mouse model of chronic hypoxic-induced PH,[139] and in rat models of PAH.[140]

1.4.3 Extracellular vesicles

In recent years there has been growing interest in the role of EVs in disease progression and regeneration. EVs are small membrane-bound particles which are released by cells and play an important role in cell-cell communication. EVs include apoptotic bodies, microvesicles and exosomes which are stratified based on size from largest to smallest, respectively, but each has unique biogenesis.[141] Apoptotic bodies are produced by membrane blebbing from cells undergoing apoptosis and represent a broad range in EV sizes. Microvesicles are also produced through outward membrane blebbing (ectocytosis) and can range greatly in size from 20-1000nm. In contrast, exosomes are produced through the endosomal system and released by exocytosis, representing the smallest fraction of EVs.[141] These EVs can contain microRNA, mRNA, and proteins derived from their cell of origin, and reflective of the current cell state. Yet, the overlap in size ranges makes physical separation based on unique biogenesis currently not feasible. The International Society of EV's recent position paper suggested new terminology can be based on size (composition, or cell of origin) rather than biogenesis to avoid confusion, e.g., small EVs (sEV), less than 150nm in size to replace the previous designation of exosomes.[142] EVs can be isolated from cell conditioned media and are shown to play a role in mediating the paracrine activities of therapeutic cells. Endothelial colony forming cell (ECFC) derived EVs were protective in kidney ischemia reperfusion injury,[143] and MSC derived-EVs have been used as a therapy for bronchopulmonary dysplasia[144] and PAH.[140] Clearly, stem cell derived EVs can play an important role in tissue regeneration.

1.4.4 Extracellular vesicles biodistribution

A challenge when delivering nano-sized particles, such as sEVs, is their rapid distribution throughout the systemic circulation; the primary outcome is rapid clearance in the liver, kidney, spleen, or less so the lungs.[145,146] Pharmcokinetic studies have demonstrated that EVs are cleared from the circulation within minutes of delivery.[147] Interestingly, there appears to be differences in EV accumulation based on the cell source, isolation conditions, and disease state. While many cell sources result in EV accumulation within the liver and spleen,[148] breast cancer derived EVs were found to rapidly redistribute to the liver and lungs, with certain cell lines yielding increased EV accumulation in the lungs.[149] Pretreatment to modify the surface glycosylation of mouse liver derived EVs was used to promote EV targeting to organs other than the liver.[150] Vinas et al. demonstrated the difference in EV biodistribution during disease state, showing increased EV accumulation in the kidney following ischemia reperfusion injury compared to a sham surgery.[151] Clearly, there are a number of factors to consider when attempting to deliver EVs to injured lungs, including biomaterials which our lab has previously studied for delivery of cell therapy products.[152]

1.5 Biomaterials and cell therapy

Biomaterials integrate well with the field of stem cell biology offering a wide range of possibilities to develop synergistic interactions between cells and materials, thereby recapitulating aspects of the native extra-cellular matrix (ECM) of these cells. Both naturally derived hydrogels and synthetic polymers can be used as biomaterials for 2D or 3D cell culture.[153] Additionally, biomaterials can be used as a vehicle for transplantation of cells, this could include bulk or micro encapsulation strategies.[153] Previously, our lab has utilized an agarose hydrogel to singly encapsulate MSCs as a method of improving their survival and retention post transplantation in a mouse hind limb.[152] Agarose is a naturally derived thermally gelling polymer. Using ultra low gelling agarose, a liquid suspension can be maintained above 30°C, which rapidly gels when cooled to form a hydrogel.[154] The thermal gelation makes agarose useful for encapsulation of cells and subsequent transplantation experiments.[152] Yet, other biomaterials or combinations may offer improved microgel properties for controlled cell or EV release *in vivo*. Collagen is one of the most abundant natural ECM proteins and provides many sites for cellular adhesion.[155] Alternatively, gelatin is hydrolyzed collagen and can be exposed to a wider array of temperatures than collagen, while still being suitable for cell adhesion and maintains the ability to form a hydrogel. To a limited extent agarose-gelatin combinations have been shown as a cell friendly, degradable matrix *in vitro* for human umbilical vein endothelial cells (HUVECs), and fibroblasts.[156]

1.5.1 Microencapsulation

The original microencapsulation method in our lab uses a vortex to create an emulsion of hydrogel + cell droplets while suspended in oil.[152] This simple 'vortex-emulsion' method produces a heterogeneous population of microgels but is rapid and yields sufficient quantities of cell or EV-loaded microgels for *in vivo* experiments. Technologies have been developed that provide more control over the encapsulation process producing a more homogenous microgel product, including air-jet encapsulation,[156] and microfluidics encapsulation.[157] Of particular interest, microfluidics encapsulation uses pressure driven flow through microfluidic channels to cause droplet formation of an aqueous phase within an oil phase producing uniform microgel droplets.[158,159] Both, vortex-emulsion and microfluidic encapsulation strategies are viable options to produce encapsulated cell or EV products.

1.5.2 Microencapsulation and cell therapy

Microencapsulation has been demonstrated to enhance the efficacy of some cell therapies, by increasing cell retention. Agarose encapsulated explant derived cardiac cells (EDCs) have been used to increase the retention of the EDCs within the heart and provide enhanced therapeutic effects over EDCs in suspension.[160,161] Alternatively, a conformal alginate coating to microencapsulate MSCs has demonstrated increased retention, and paracrine secretions of microencapsulated MSCs compared to non-encapsulated or bulk encapsulated MSCs.[157] We plan to apply principles learned from such studies for EV microencapsulation. Recently, bulk alginate encapsulated EVs were used as a treatment for myocardial infarction in a rat model, demonstrating the biomaterial potential to enhance local EV retention.[162] In this work, we will further assess the value of microencapsulation to provide an efficient delivery vehicle for stem cells or EVs to the lung.

1.6 Objectives and Hypotheses

While we have gained significant insights into the pathogenesis of PAH, aiding in the refinement of treatment approaches; the exact steps in progression remain poorly defined. Furthermore, while regenerative stem cell and EVs treatments have shown some evidence of therapeutic potential in pre-clinical models of PAH, improvements in the delivery of therapeutics may enhance these benefits. Thus, the overall objective of this work is to both characterize the progression and pathogenesis of PAH using animal models and refine therapeutic strategies to treat and regenerate this disease.

Manuscript 1*: Emergence of disease specific endothelial and stromal cell populations involved in arterial remodeling during development of pulmonary arterial hypertension*

Despite advances in our understanding, the pathogenesis and progression of PAH remains incompletely understood. Recent advances in scRNA-seq have provided opportunities to understand disease heterogeneity at a single cell level. While several studies have employed this technology in PAH,[104,121] their focus has largely been on the end stage of disease.

Objective: We sought to use scRNA-seq to study serial timepoints during the development of the SU/CH model of PAH, to gain deeper insights into mechanisms responsible for the onset (early timepoints) and progression (later timepoints) of disease.

Hypothesis: We hypothesize that early transcriptomic changes in vascular and inflammatory cells during SU/CH progression will provide new insights into the mechanisms of initiation of PAH whereas later changes, particularly in arteriolar EC and stromal cell populations, would reveal mechanisms underlying to arterial remodeling and progression of disease, as well as providing novel therapeutic targets.

Manuscript 2*: Single-cell microencapsulation improves lung retention of endothelial colony forming cells after intravascular delivery and unmasks therapeutic benefit in severe pulmonary arterial hypertension*

Objective: To evaluate the ability of encapsulation of ECFCs into microgels to increase their retention and engraftment within the lungs, improve regeneration of damaged vasculature and reduce the PH severity.

Hypothesis: We hypothesize that ECFC-loaded microgels will have significantly increased retention within the lung, as measured by bioluminescent imaging and histology, and lead to increased therapeutic efficacy in disease models of PAH, as assessed by improvements in right ventricular systolic pressure (RVSP) and right ventricular hypertrophy (RVH), and regeneration of lung arterial vasculature.

Manuscript 3: *Targeting extracellular vesicles to the lungs by microencapsulation*

sEVs derived from MSCs and EPCs have been demonstrated to have therapeutic potential as a "cell free" therapeutic. However, large numbers of these EVs may be necessary when administering them systemically since the vast majority of EVs are cleared by the liver and spleen with limited local uptake by other organs.[146] By incorporating EVs into microgels, the EVs can be retained within the lungs, and with proper microgel design, they will be released into the local environment to facilitate tissue repair, specifically in the context of PAH.

Objective: To investigate the therapeutic potential of MSC derived small EVs, and explore microencapsulation as a novel delivery method for enhancing local retention in the lung.

Hypothesis: We hypothesize that EV-loaded microgels will increase EV retention locally within the lungs, and improve their efficacy for the treatment of PAH, specifically by inducing regeneration of damaged lung arterial vasculature.

Chapter 2: Emergence of disease-specific endothelial and stromal cell populations responsible for arterial remodeling during development of pulmonary arterial hypertension

Nicholas D Cober[1,2], Emma McCourt[1], Rafael Soares Godoy[1], Yupu Deng[1], Ken Schlosser[1], Anu Situ[1], David P Cook[2], Sarah-Eve Lemay[3], Timothy Klouda[4], Ke Yuan[4], Sébastien Bonnet[3], and Duncan J Stewart[1,2,*]

[1] Ottawa Hospital Research Institute, Sinclair Centre for Regenerative Medicine Program, Ottawa, ON, Canada
[2] University of Ottawa, Faculty of Medicine, Department of Cellular and Molecular Medicine, Ottawa, ON, Canada
[3] Institut Universitaire de Cardiologie et de Pneumologie de Quebec. Research Center Laval University, Quebec City, QC, Canada
[4] Division of Pulmonary Medicine, Boston Children's Hospital, Harvard Medical School, Boston, MA, USA

ORCIDs:
NDC: 0000-0001-8061-806X
DJS: 0000-0002-9113-8691

***Corresponding author:** Duncan J Stewart, djstewart@ohri.ca.
Executive Vice-President Research, The Ottawa Hospital; CEO & Scientific Director,
Ottawa Hospital Research Institute; The Evelyne & Rowell Laishley Chair and
Professor, Department of Medicine, University of Ottawa
501 Smyth Road, Box/C.P. 511, Ottawa, ON, K1H 8L6
613-739-6686

Author Contributions

NDC has contributed to all aspects of this work including conception, experimental design, performing the experiments, data analysis and preparation of this manuscript. EM contributed to data analysis and figure preparation. RSG assisted with collection of the first experiment of single cell samples and preliminary analysis. YD was instrumental in preparation and collection of the lung samples for microCT analysis and in all animal studies. KS performed the IPA analysis. AS performed the RNA velocity analysis and contributed to figure preparation. DPC assisted with single cell transcriptomic analysis and provided valuable support in initial experimental design. SEL performed immunofluorescent staining on all human samples and contributed to figure preparation. TK performed immunofluorescent staining on fresh frozen rat sections. KY collected images on rat lung sections, assisted with figure preparation and data interpretation, and manuscript review. SB provided access to human PAH samples, contributed expertise to interpretation of results, and manuscript review. DJS was involved in the conception, experimental design, data analysis and interpretation, figure design, and drafting the manuscript. DJS is accountable for all aspects of this work.

2.1 Abstract

Pulmonary arterial hypertension (PAH) is a severe and lethal pulmonary vascular disease characterized by arteriolar pruning and occlusive vascular remodeling leading to increased pulmonary vascular resistance and eventually right heart failure. While endothelial cell (EC) injury and apoptosis are known triggers for this disease, the mechanisms by which they lead to complex arterial remodeling remain obscure. We employed multiplexed single-cell RNA sequencing (scRNA-seq) at multiple timepoints during the onset and progression of disease in a model of severe PAH to identify mechanisms involved in the development of occlusive arterial lesions. There was significant loss of arterial volume as early as 1-week by microCT, preceding any evidence of occlusive arteriopathy, consistent with early arteriolar dropout. Maximal arterial pruning was seen by 5 to 8 weeks, with signs of progressive occlusive remodeling. Analysis of the scRNA-seq data resolved 44 lung cell populations, with widespread early transcriptomic changes at 1 week affecting endothelial, stromal and immune cell populations. Notably, this included emergence of a relatively dedifferentiated (dD) EC population that was enriched for *Cd74* expression compared to general capillary (gCap) ECs which were primed to undergo endothelial-mesenchymal transition, as evidenced by RNA velocity analysis. However, at late timepoints (5 and 8 weeks), activated arterial ECs (aAECs) were the only cell population exhibiting persistent differential gene expression. This was characterized by a growth regulated state, including high expression of *Tm4sf1*, a gene implicated in cancer cell growth, which was also expressed by a smooth muscle (SM)-like pericyte cluster. Both these populations were localized to regions of arterial remodeling in the rat model and PAH patients, with aAECs contributing to intimal occlusive lesions and SM-like pericytes forming bands of medial muscularization. Together these findings implicate disease-specific vascular cells in PAH progression and suggest that TM4SF1 may be a novel therapeutic target for arterial remodeling.

Keywords: Pulmonary arterial hypertension; Endothelial cells; Pericytes; Vascular remodeling

2.2 Introduction

Pulmonary arterial hypertension (PAH) is a severe and lethal disease defined hemodynamically by a mean pulmonary artery pressure > 20mmHg, pulmonary wedge pressure $\leq$ 15mmHg and pulmonary vascular resistance $\geq$ 3 woods units.[1] While the pathobiology of PAH is incompletely understood, endothelial cell (EC) dysfunction has long been recognized to contribute to increased vascular tone and remodeling.[163] More recently, EC injury and apoptosis has been recognized as a central trigger for initiation of disease,[164] and underlying mutations in BMPR2, which represent the most common cause of hereditary PAH,[8] have been shown to increase susceptibility of ECs to injury and apoptosis.[165] However, it is still uncertain how EC apoptosis leads to loss of vasculature and the development of complex arterial remodeling, i.e. plexiform lesions,[164] which is a hallmark feature of advanced PAH. It has been reported that perturbed pulmonary hemodynamics are necessary for the development of occlusive arterial remodeling,[44] possibly as a result of increased intimal shear stress within the lung arteriolar bed which could contribute to ongoing endothelial injury.

We have suggested that there are distinct phases during the development of PAH;[164] the first representing the initial response to the triggering injury, which is followed by the progressive damage and loss of precapillary arterioles progressing to complex arterial remodeling at later stages of disease, largely driven by hemodynamic consequences of arteriolar pruning. Single-cell transcriptomics is a powerful tool that can elucidate the transcriptional changes underlying the onset and progression of disease at the resolution of individual cells, thereby providing new insights into the mechanisms driving the functional and structural vascular abnormalities of

PAH. Single-cell RNA sequencing (scRNA-seq) has been widely employed to better characterize lung cell populations under homeostatic conditions,[102,103] and in various disease states.[118,166] Several studies have recently employed scRNA-seq to characterize the advanced stage in several PAH experimental models.[104,121,122,167] However, all of these studies have been limited by primarily focusing on established disease, whereas the mechanisms leading to the development of PAH may be quite different in the early stages. Multiplexed scRNA-seq analysis can increase the number of samples analyzed at one time, making it feasible to study multiple timepoints with increased biological replicates by reducing costs.[168]

Therefore, we sought to employ multiplexed scRNA-seq to map out the temporal changes in transcriptomic profiles and cell populations during the full course of PAH onset and progression in the SU5416-Chronic Hypoxia (SU/CH) rat model, focusing mainly on the vascular cell populations. We were able to identify two main phases of disease progression characterized in the early stages (i.e., 1 week post SU) by widespread changes in endothelial, stromal, and immune cell populations, and the emergence of a dedifferentiated capillary (dCap) cluster, which may be undergoing endothelial to mesenchymal transition (EndoMT) based on RNA velocity analysis. At later stages of disease (i.e., 5 and 8 weeks), there was a remarkable normalization of global transcriptional activity in most lung cell populations, with the notable exception of the activated arterial ECs (aAECs), which would be most affected by perturbed lung hemodynamics, and these continued to exhibit persistent and robust changes in gene expression. Interestingly, these cells were highly localized to regions of complex arteriolar remodeling, along with the smooth muscle (SM)-like pericytes, both expressing *Tm4sf1*, a marker previously implicated in cancer biology.

2.3 Methods

2.3.1 Sugen – chronic hypoxia model of PAH

All animal experiments were approved by the University of Ottawa Animal Care Committee and conducted according to the guidelines from the Canadian Council for Animal Care. Male Sprague Dawley (SD) rats (6-10 weeks old) were administered with a single dose of Sugen 5416 (SU) (20mg/kg, Tocris) delivered in CMC vehicle (as previously described)[36] or DMSO and placed in hypoxia chambers (10% O_2, Biospherix) for three weeks, followed by 5 weeks of normoxia. Animals at baseline, 1, 3, 5, and 8-weeks (**Figure 2.1A**) were anaesthetized by an i.p. injection of ketamine (100 mg/kg) and xyalzine (10 mg/kg) and right ventricular systolic pressure (RVSP) was measured as previously described.[169] Lungs were either isolated for tissue digestion (described below) or formalin fixed and paraffin embedded for subsequent histological analysis. The heart was excised and right ventricular hypertrophy (RVH) was assessed by the ratio of right ventricle (RV) to the left ventricle plus septum (LV+S), as previously described.[169]

2.3.2 Sample preparation for micro-computed tomography (microCT)

Lungs were prepared for microCT, as previously described.[42] In brief, animals were thoroughly perfused with heparinized saline (LEO Pharma Inc.) through the jugular vein with a closed chest and mechanical ventilation, using pressure matching the measured RVSP. Subsequently, chests were opened, and an additional perfusion of heparinized saline cleared residual blood from the lungs. Barium – gelatin mix (E-Z-EM Canada Inc; Sigma-Aldrich) was perfused until consistent pressure matching RVSP was obtained. Lungs were cooled to 4°C and inflated with formalin through the trachea. Lung samples were stored at 4°C in formalin for 2 days, washed with PBS, and stored in ethanol until images were acquired with desktop microCT (SkyScan 1272, Bruker microCT). Image analysis was performed with CTAn software (Bruker microCT), and CTVox software (Bruker microCT).

2.3.3 H&E staining and vascular occlusion scoring

Hematoxylin and eosin (H&E) staining was performed on paraffin sections. Sections (5µm thick) were deparaffinized and rehydrated as previously described using a series of xylene, ethanol, and water washes. Sections were stained with hematoxylin for up to 8 min and washed with water. Then incubated in Scott's solution for 2 min, washed and soaked in eosin stain for 3 min. Slides were washed in water, and then dehydrated in a reverse series of ethanol and xylene rinses. Slides were mounted with Cytoseal XYL media (Thomas Scientific) and left to dry overnight. Slides were scanned with Panoramic Desk (3D Histech, Budapest, Hungary) and analyzed with CaseViewer (3D Histech).

2.3.4 Lung digestion and single cell preparation

Lung digestion was performed in a similar manner as previously described.[120] In brief, animals were perfused with 20ml of 0.9% saline containing 25U/ml heparin (LEO Pharm Inc.) through the right ventricle, to drain the blood from the lungs. Lung tissue was isolated, minced with scissors and placed in Hank's Balanced Salt Solution (HBSS, Gibco) on ice. Enzymatic digestion was performed with 2500U Collagenase (Worthington), 30U Neutral Protease (Worthington), and 165U DNase I (Sigma Aldrich) in HBSS, samples were loaded into gentleMACS C tubes (Milltenyi Biotec), and placed on the OctoMACS dissociators (Milltenyi Biotec) using program 37C_LDK_m_1 for ~30min. Samples were immediately placed on ice, filtered through 70µm cell strainers (Falcon), and washed with phosphate buffered saline (PBS, Gibco) with 2mM EDTA (ThermoFischer Scientific) and 0.5% bovine serum albumin (BSA, Wisent) (PEB). Dissociated cell samples were spun at 400g for 5min at 4°C and washed again. Samples were incubated in 1x red blood cell lysis (eBioscience) for 3min, diluted with PEB, and filtered again through 70µm cell strainers (Milltenyi Biotec). Cells were washed, as above and counted with Trypan Blue (ThermoFisher Scientific) on a Cell Drop BF (DeNovix).

2.3.5 Multiplex single cell sample processing

Individual biological samples were barcoded using the MULTI-seq protocol described by McGinnis et al.[168] In brief, single cells were incubated with 1:1 molar ratio of anchor: unique barcode oligonucleotide sequence for 10 min at room temperature with gentle mixing. Followed by addition of the co-anchor to stabilize barcodes within membranes which was incubated for 5min on ice. Barcoded cells were washed in PBS, counted as above, and pooled at an equal ratio of cells per biological replicates. Samples with viability > 80% were sent for further processing. Pooled samples were processed using 10x Genomics Chromium (10x Genomics).

2.3.6 Processing of single cell RNA sequencing libraries

RNA library construction was performed using 10x Genomics Single Cell 3’ RNA sequencing kit as previously described.[120] This experiment was performed with unique biological replicates on different dates, and data was later merged. Libraries were created and sequenced with NextSeq500 (Illumina) for an estimated 37554 cells with 21879 mean reads per cell, 2372 median UMI per cell, and 1118 median genes per cell (first experiment) and 35546 cells with 22322 mean reads per cell, 3152 median UMI per cell, and 1370 median genes per cell (experiment repeat). CellRanger (10x Genomics, version 6.1.2) was used to process raw sequencing reads using the Ensembl104 rat transcriptome annotations with additional inclusion of Pecam.

2.3.7 Quality control and single cell data analysis

Filtered feature barcode matrices were imported into R package Seurat (https://github.com/satijalab/seurat) for subsequent analysis.[170] Quality control was performed within Seurat to remove cells with >30% mitochondrial transcripts and cells with low complexity (<200 detected genes). Barcodes were demultiplexed using a manual threshold method outlined within the deMULTIplex R package (https://github.com/chris-mcginnis-ucsf/MULTI-seq).[168] Cells with multiple barcodes (doublets) or with no identifiable barcodes were removed from analysis. An additional round of doublet removal was performed with scDblFinder (https://github.com/plger/scDblFinder).[171] A total of 23,122 cells from experiment 1 and 26,611 cells from experiment 2 were retained. Data was merged into a single Seurat object for downstream analysis. To ensure that clustering would not be impacted by batch effects or biological variability we used the integration method implemented by Seurat v3. We integrated based on biological replicates using the SCT method to regress out cell cycle and mitochondrial associated genes prior to calculation of principal component analysis (PCA) and uniform manifold approximation projection (UMAP). Cell clusters were characterized by assessment of cell-specific genes and comparison with cell classification tool Single Cell Net.[172] Cell prioritization was performed with the R package Augur (https://github.com/neurorestore/Augur) to identify populations that were most affected by PAH.[173]

Clusters corresponding to endothelial, stromal, immune, and epithelial cells were identified by *Cldn5, Col1a1, Ptprc, and Epcam*. These populations were re-clustered using the same normalization and integration approach to refine cluster identification and for subsequent analysis. Contaminating clusters were removed representing small populations with mixed canonical markers (eg. *Ptprc*+ cluster within the endothelial subset) likely representative of residual doublets not identified during previous steps.

2.3.8 Differential gene expression and gene set enrichment analysis

Differential gene expression analysis was performed using the R package *muscat* (https://github.com/HelenaLC/muscat) to account for the available biological replicates,[174] using standard workflow. Significant genes were identified with an adjusted p value <0.05 and a detection rate of at least 5% within the tested conditions. Gene set enrichment analysis was performed using R package *fgsea* (version 1.20.0) on the fold change ranked list of genes for a given condition tested. Gene sets were queried and annotated which comprised all GO terms, KEGG pathways, Reactome pathways, and the MSigDB Hallmark gene sets, which were acquired from the Molecular Signatures Database (v6).[175,176] Significantly affected gene sets were filtered on an adjusted p-value of <0.05. The normalized enrichment score (NES) indicated the degree of up or down regulation of a given gene set. Volcano plots of DEGs were generated with r package EnhancedVolcano (version 1.12.0).

2.3.9 Ingenuity pathway analysis

Pathway enrichment analysis was performed assessing only DEGs using Ingenuity Pathway Analysis (IPA) web-based software application (Qiagen). Standard workflows were followed within the core analysis function to identify gene sets of disease or biofunctions from the IPA library that were significantly enriched based on the input DEGs.[177]

2.3.10 Transcription factor analysis

Transcription factor (TF) activity was predicted from available transcriptomic data using deCoupleR (version 2.0.1).[178] We employed the weighted mean method using our gene expression data to infer TF activity and their targets from the DoRothEA curated network.[179]

2.3.11 RNA velocity and trajectory inference analysis

We used scVelo[180] as an input for CellRank[181] to evaluate RNA velocity profiles of the combined vascular cells (ECs and stromal cells). We employed scVelo's dynamical model to infer macrostates as an input for CellRank, which then performed RNA velocity and trajectory inferences.

2.3.12 Immunofluorescent staining

OCT prepared lung sections were removed from -80°C freezer and thawed to room temperature and fixed in 4% paraformaldehyde solution for 20 minutes. Sections were washed three times in 1x PBS (15 minutes per wash) and then blocked with 5% goat serum in 0.5% Triton X-100/PBS (PBS-Tx) for one hour at room temperature. After blocking, samples were incubated in primary antibodies overnight at 4°C. The next morning samples were washed in PBS-Tx (3x, 15 minutes per wash) and incubated with secondary antibodies overnight at 4°C. The following morning samples were washed in PBS-Tx and prepared for confocal microscopy with mounting media containing DAPI. All images were captured using a laser scanning Zeiss 880 confocal microscope with Fast Airyscan (Zeiss) and processed with Aivia software. Primary antibodies with their respective concentrations were as follows Griffonia Simplicifolia Lectin I (GSL I) Isolectin B4 (1:25, Vector Laboratories, #FL-1201), mouse monoclonal anti-3G5 IgM (1:10, from Ke Yuan lab), FITC anti- αSmooth Muscle Actin mouse monoclonal antibody (1:300, Sigma Aldrich, #F3777), and rabbit anti-TM4SF1 antibody (1:25, Invitrogen, #PA5-21119).

2.3.13 Human sample preparation

PAH patient and control lung samples (n = 7 for both) were available from the Quebec Respiratory Health Network tissue bank (www.rsr-qc.ca). Paraffin sections (5µm thick) were deparaffinized and rehydrated as previously described using a series of xylene, ethanol, and water washes. Heat mediated antigen retrieval was performed by pressure cooking in citric acid-based antigen unmasking solution. Sections were washed in PBS with 0.1% Tween-20 (PBS-T) and blocked in 5% goat serum (Cedarlane #CL1200-500) in PBS-T for 1h at room temperature. Primary antibodies were incubated overnight at 4°C using TM4SF1 (ThermoFisher Scientific #PA5-21119, 1:200) and CD31 (Dako #M0823, 1:100) antibodies. The following day samples were washed 4x in PBS-T and incubated with secondary antibodies anti-Rabbit alexa fluor 488 (ThermoFisher Scientific #A11008, 1:500) and anti-mouse alexa fluor 594 (ThermoFisher Scientific #A11005, 1:500) for 1h at room temperature. Samples were washed in PBS-T, mounted using DAPI (4',6-diamidino-2-phenylindol) Fluoromount G mounting medium (Electron Microscopy Science) and imaged with an Axio Observer microscope (Zeiss).

2.3.14 Statistical analysis

Data are presented as means +/- SEM. Non single cell statistical analyses were performed with GraphPad Prism v9 (GraphPad Software). Analysis of variance (ANOVA) was performed with multiple comparisons using Tukey correction used to identify statistically significant differences. P-values <0.05 were considered significant. For scRNA-seq experiments we used four animals per time point and statistical analysis was performed in line with recommendations for each analytical package used.

2.4 Results

2.4.1 Characterization of functional and structural vascular changes in the SU/CH PAH model

The SU/CH model exhibits many of the hemodynamic and pathological changes characteristic of human PAH, including complex arterial remodeling leading to the development of occlusive arterial lesions.[107] To better define the stages in the development of PH, we evaluated animals at serial timepoints after the administration of SU and initiation of CH (**Figure 2.1A**). Significant elevation of RVSP was observed as early as 1-week (47mmHg; $p = 0.056$), plateauing at >100mmHg by 5-weeks (**Figure 2.1B**). Right ventricular hypertrophy (RVH) was increased by 3-weeks, persisting to 8 weeks (Fulton index >60%; **Figure 2.1C**). In small arterioles (<50µm), there was evidence of severe arteriolar remodeling (>50% lumen loss) by 5 and 8 weeks, compared to healthy lungs (**Figure 2.1D**). MicroCT analysis revealed a progressive loss of pulmonary arterial vasculature during PH progression, (**Figure 2.1E – H; Sup Figure 2.1**). The loss of the functional arterial bed primarily affected vessels <150µm in diameter, with evidence of significant arterial pruning as early as 1-week (**Figure 2.1F**), corresponding to the initial increase in arterial pressures, reaching a maximal loss of 65% at 5-weeks in vessels <200µm in diameter (**Figure 2.1G**). RVSP and lung arterial volume were negatively correlated (**Figure 2.1H**). Therefore, the rat SU/CH model is well suited to explore the cellular and molecular mechanisms during the development of PAH.

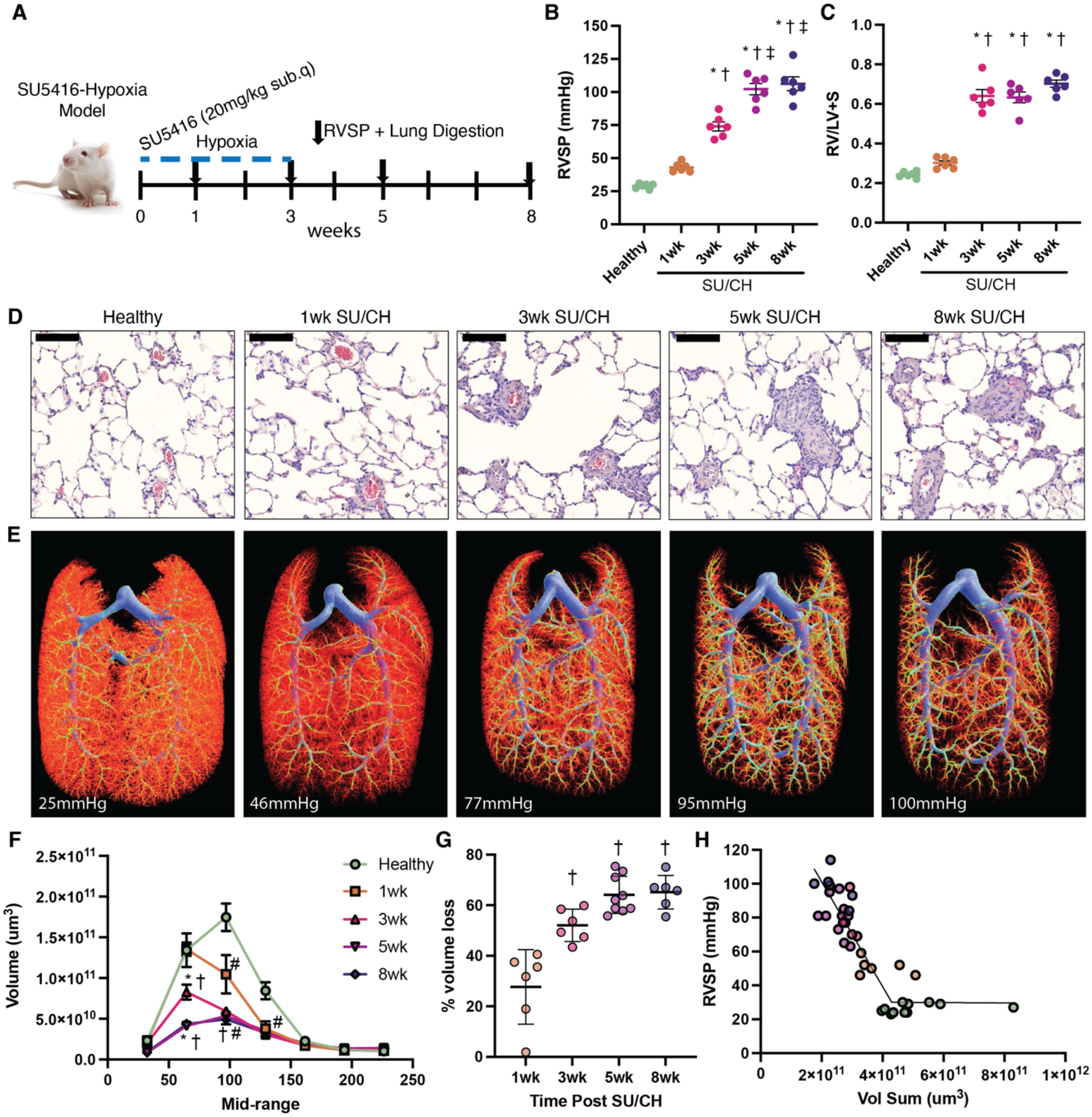

Figure 2.1: Characterization of Sugen-Chronic Hypoxia (SU/CH) model of PAH.

A) Timeline of the SU/CH model and relevant end of study sampling. B) Right ventricular systolic pressure (RVSP). C) Right ventricular hypertrophy (RV/LV+S). D) Representative H&E histological images showing progression of arterial remodeling associated during development of pulmonary hypertension (PH). E) Representative image of micro computed tomography (MicroCT) of lung arterial angiograms during the development of PH. F) Summary of quantitative analysis of arterial volumes by MicroCT showing the greatest reduction in arterioles under 150µm in diameter. G) Percent volume loss relative to healthy control in arteries under 200µm in diameter. H) Relationship between arterial volume (<500µm diameter) and RVSP during PH development. Data represented as mean ± SEM, n = 6 – 12. * $p < 0.05$ for

3-, 5-, 8- weeks SU/CH vs control, † $p < 0.05$ for 3-, 5-, 8- weeks vs 1-week, ‡ $p < 0.05$ for 5-, 8- weeks vs 3-weeks, # $p < 0.05$ for 0.01 for all timepoints vs control. Scale bar represents 100μm.

2.4.2 Transcriptomic changes in global lung cell populations in PAH

Multiplexed single cell analysis was performed on lung samples from healthy controls, and 1-, 3-, 5-, 8-weeks post SU/CH initiation, incorporating four biological replicates per timepoint. Poor quality cells and those lacking a sample barcode or containing multiple barcodes were removed (**Sup Figure 2.2**). Additional doublet removal was performed with scDblFinder,[171] and independent experiments (23122 cells Expt1 and 26611 cells Expt2) were merged, integrated, and aligned (**Sup Figure 2.3A, B**). Broad cell type annotations (endothelial, stromal, myeloid, lymphoid, and epithelial) were assigned to resulting clusters based on the expression of canonical markers and each were then subclustered for high resolution analysis (**Sup Figure 2.3C**). This resulted in the designation of 44 unique lung clusters (**Figure 2.2A**). Global UMAPs of all lung cell populations at each time point are presented in **Sup Figure 2.4**. At 1-week, transcriptomic changes were clearly evident in many cell populations, involving all lineages, but most evident in endothelial and myeloid cells (**Figure 2.2B, left)**. Surprisingly, at 5 weeks there was a remarkable and somewhat paradoxical 'normalization' of global transcriptional profiles, at a timepoint when the hemodynamic and vascular changes of PAH were reaching their peak (**Figure 2.2B, right**). Augur[173] was used to identify cell populations most affected by SU/CH at 1- and 5-weeks relative to control cells. At 1 week, many cell clusters showed marked transcriptional changes, with the activated arterial (aA) ECs and a smooth muscle (SM)-like, *Acta2* positive pericyte populations demonstrating the most substantial changes from control conditions (**Figure 2.2C**). In contrast, at 5 weeks, there was an overall resolution of transcriptional changes with the notable exception of the aAECs (**Figure 2.2D**). Similarly, at early timepoints high numbers of differentially expressed genes (DEG) were observed across many different cell populations (**Figure 2.2E**), with the greatest increases seen in immune cells, particularly transitional monocytes (>400 DEGs), and various endothelial populations at 1 week. However, again there was a progressive decrease in the number of DEGs over time, with the exception of aAECs, which continued exhibit ~150 DEGs for up to 8 weeks. Expansion in relative cell numbers was seen in several populations including the arterial and aAEC clusters, and lymphatic ECs clusters, as well as some monocyte (alveolar, interstitial, and transitional macrophages), neutrophil and NKT cell clusters (**Sup Figures 2.5-2.8**). However, SM-like *Acta2*$^+$ pericytes exhibited the most robust relative increase in cell number beginning at 3 weeks post SU/CH coinciding with the advent of arterial remodeling (**Sup Figure 2.5**). For the remainder of this study, we focus mainly on the endothelial and stromal populations, which showed the most marked overall changes in the global analyses. However, relevant details of cell annotation and transcriptomic changes for myeloid, lymphoid, and epithelial cells are provided in **Sup Figures 2.9-2.11**.

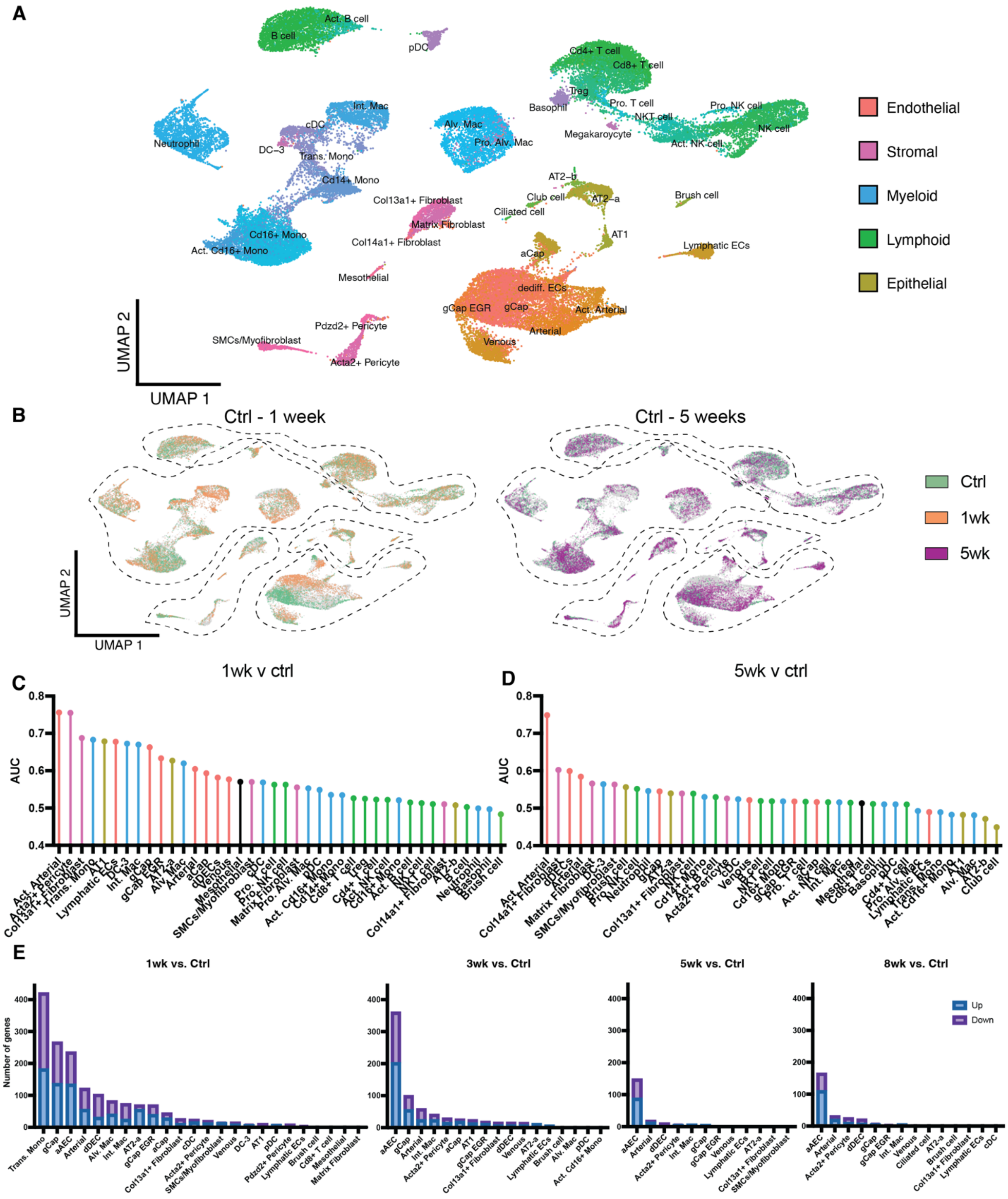

Figure 2.2: Multiplexed single cell transcriptomic atlas of lung cells during PAH progression. A) 44 unique lung clusters were identified and integrated into the global uniform manifold approximation and projection (UMAP). B) Global UMAPs colored by timepoint with control (green) compared with 1-week (orange) and 5-weeks (purple). Cell prioritization was performed using a machine learning algorithm to identify clusters that were most affected between 1-

week and control (C) and 5-weeks and control (D). At 1-week major transcriptomic changes indicated by an increase in area under the curve (AUC) were seen in many populations with the greatest increases in activated arterial ECs (aAECs) and *Acta2*+ pericytes. However, at 5-weeks there was a general reduction in transcriptomic changes, with the exception of the aAEC population E) Number of all non-zero differentially expressed genes (DEGs) in lung cell populations at 1-, 3-, 5-, and 8- weeks post SU compared with control (healthy). High numbers of DEGs were seen in transitional macrophages and many EC clusters at 1-week, but only aAECs displayed a persistently high numbers of DEGs at later timepoints. Single cell data was obtained from n = 4 animals per timepoint, multiplexed using unique barcodes, pooled and subjected to library construction using 10x-Genomics.

2.4.3 Emergence of disease specific endothelial populations during PAH progression

Sub-clustering of endothelial cells produced 8 distinct cell clusters encompassing all expected populations including arterial, venous, lymphatic, general capillary (gCap) and aerocytes (aCap) ECs **(Figure 2.3A)**, as identified based on expression profile of commonly used markers [102,119,182] such as, *Dll4*, *Slc6a2*, *Mmrn1*, *Aplnr*, *Apln*, among many others (**Figure 2.3B and C**). Interestingly, arterial ECs consisted of two distinct populations, a ‘classical’ arterial cluster and the ‘activated’ aAEC cluster, which is further characterized below. Similarly, the gCap EC population was made up of two clusters; a typical gCap EC population and another cluster characterized by expression of early response genes (ERG), such as *Fos* and *Egr*, as was previously described.[120] Of interest, the gCap-EGR cluster shared expression of some of these early response genes with the venous ECs (**Figure 2.3C**), suggesting possible zonation changes across the capillary-venous axis.[119] Finally, a novel EC population (cluster 1) was identified, termed ‘de-differentiated’ ECs (dDECs) that exhibited an atypical endothelial gene expression profile with some of their top distinguishing genes related to nonendothelial lineages. Again, this cluster is further characterized below.

Using proliferative markers, including *Mki67*, *Cdca8*, and *Birc5*, evidence of proliferation was seen in cells mainly located in a distinct 'proliferative' node (**Figure 2.3D**), representing cells from several clusters, in particular dDECs and aAECs (**Figure 2.3A**). Endothelial UMAPs for each timepoint show the major transcriptomic changes between healthy (control) and early stages (1 and 3 weeks), or the later stages (5 and 8 weeks) of PAH progression (**Figure 2.3E**). Phenotypic changes were most evident in the gCap at weeks 1 and 3 but returned to the baseline distribution at weeks 5 and 8. This was accompanied by the marked expansion in clusters 1 and 4 (dDECs and aAECs, respectfully) at 1 week which persisted to week 8. The fold-change relative to control in each EC cluster, proportional to the total EC population, is shown in **Figure 2.3F**. There was an early and sustained increase in the dDECs and aAEC populations, with later expansion in arterial and lymphatic ECs. Again, this supports an important role for the aAECs and dDECs as disease-specific endothelial populations during the onset and progression of PAH.

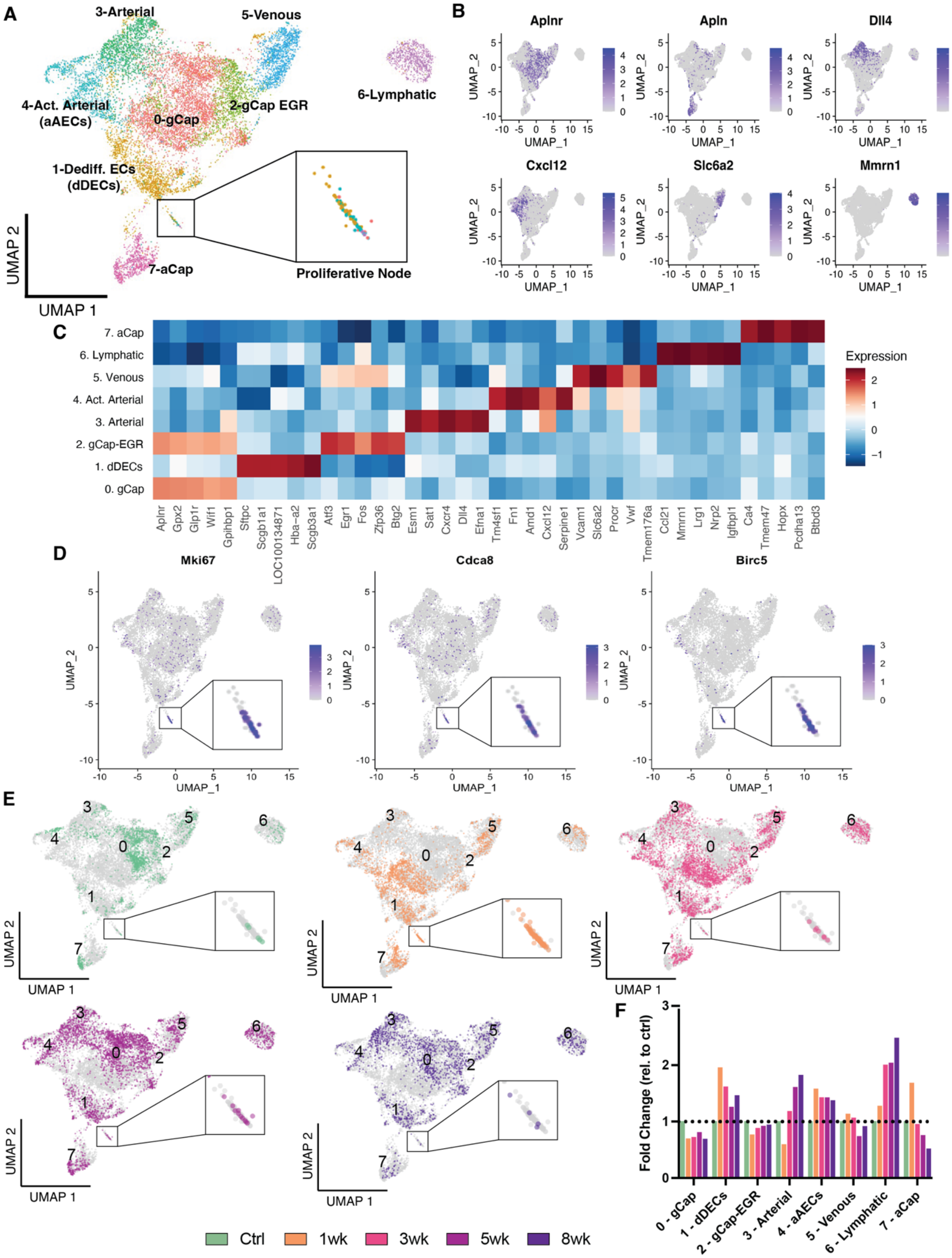

Figure 2.3: Changes in endothelial cell populations during PAH progression.
A) Uniform manifold approximation and projection (UMAP) representation of all endothelial populations at all sampled timepoints showing 8 distinct cell types and a proliferative cell node

enlarged in the box. B) Feature plots highlighting genes typically associated with distinct endothelial cell (EC) populations including: *Aplnr* (gCap), *Apln* (aCap), *Dll4* (arterial), *Cxcl12* ('activated' arterial [aAECs] and arterial), *Slc6a2* (venous) and *Mmrn1* (lymphatic). C) Heatmap showing the top 5 differentially expressed genes distinguishing each EC population. D) Feature plots showing the distribution of proliferation-related genes, *MKi67*, *Cdca8* and *Birc5*, largely within the proliferative node, highlighted and enlarged in the box. E) UMAP of cells present at each timepoint demonstrating transcriptomic shifts compared to control at 1-, 3-, 5- and 8-weeks. F) Fold change of each EC populations relative to their control levels. Early and persistent increases were seen in the relative size aAECs and 'dedifferentiated' (dD) ECs, whereas as arterial and lymphatic ECs showed a later expansion.

2.4.4 Differential gene expression analysis in activated arterial and dedifferentiated EC populations

To better understand the distinct transcriptomic profiles within these populations, we compared changes in gene expression (including all timepoints) between arterial ECs and aAECs and between gCap and dDECs since these populations were closely related on the UMAP (**Figure 2.4A and B**, respectively). aAECs were characterized by reduced expression of typical arterial genes,[102] including the notch ligands (*Dll4* and *Notch1*), gap junction proteins (i.e., *Gja5*), signaling molecules (*Efnb2* and *Efna1*), and chemokine receptors (i.e., *Cxcr4*) (**Figure 2.4A**). Moreover, they showed increased expression of the transitional extracellular matrix (ECM) proteins, such as fibronectin (*Fn1*), Matrix gla protein (*Mgp*) and elastin (*Eln*), and signaling molecule stromal derived factor 1 (*Cxcl12*), all consistent with an activated endothelial phenotype. Of particular interest, transmembrane 4L6 family 1 (*Tm4sf1*), has been strongly implicated in cancer cell growth,[183] The differences in gene expression between gCap and dDECs were consistent with a de-differentiated state of dDECs with decreases in endothelial tight junction genes, VE-cadherin (*Cdh5*) and claudin 5 (*Cldn5*), as well as typical gCap markers such as plasmalemma vesicle associated protein (*Plvap*) and apelin receptor (*Aplnr*) (**Figure 2.4B**). Interestingly, numerous genes associated with ribosomal proteins (*Rpl*) were upregulated in dDECs, which is a feature of a hyper-transcriptomic state characteristic of progenitor cells,[184] together with genes associated with antigen presentation and inflammation (*Cd74*, *RT1-Da*), and tumor protein, translationally-controlled 1 (*Tpt1*) (**Figure 2.4B**), an oncogene and proinflammatory factor previously implicated in PAH.[13,185] The relative expression in selected genes between all EC populations are depicted in **Figure 2.4C**, showing the relative overexpression of genes associated with an activated endothelial state in aAECs, in particular *Tm4sf1*, whereas dDECs exhibited a predominance of genes associated with antigen presentation, while displaying lower expression of typical EC tight junction genes. By ingenuity pathway analysis (IPA), aAECs were enriched for biofunctions associated with cell proliferation, protein synthesis, invasion and inflammation consistent relative to classic arterial, consistent with a ‘cancer-like’ phenotype, together with reduced expression of gene sets associated with angiogenesis and vascular development (**Figure 2.4D**). In contrast, dDECs showed enrichment of gene sets for inflammation, protein synthesis, cardiovascular disease and cell death/apoptosis compared to gCap ECs (**Figure 2.4D and E**), consistent with a role vascular disease.

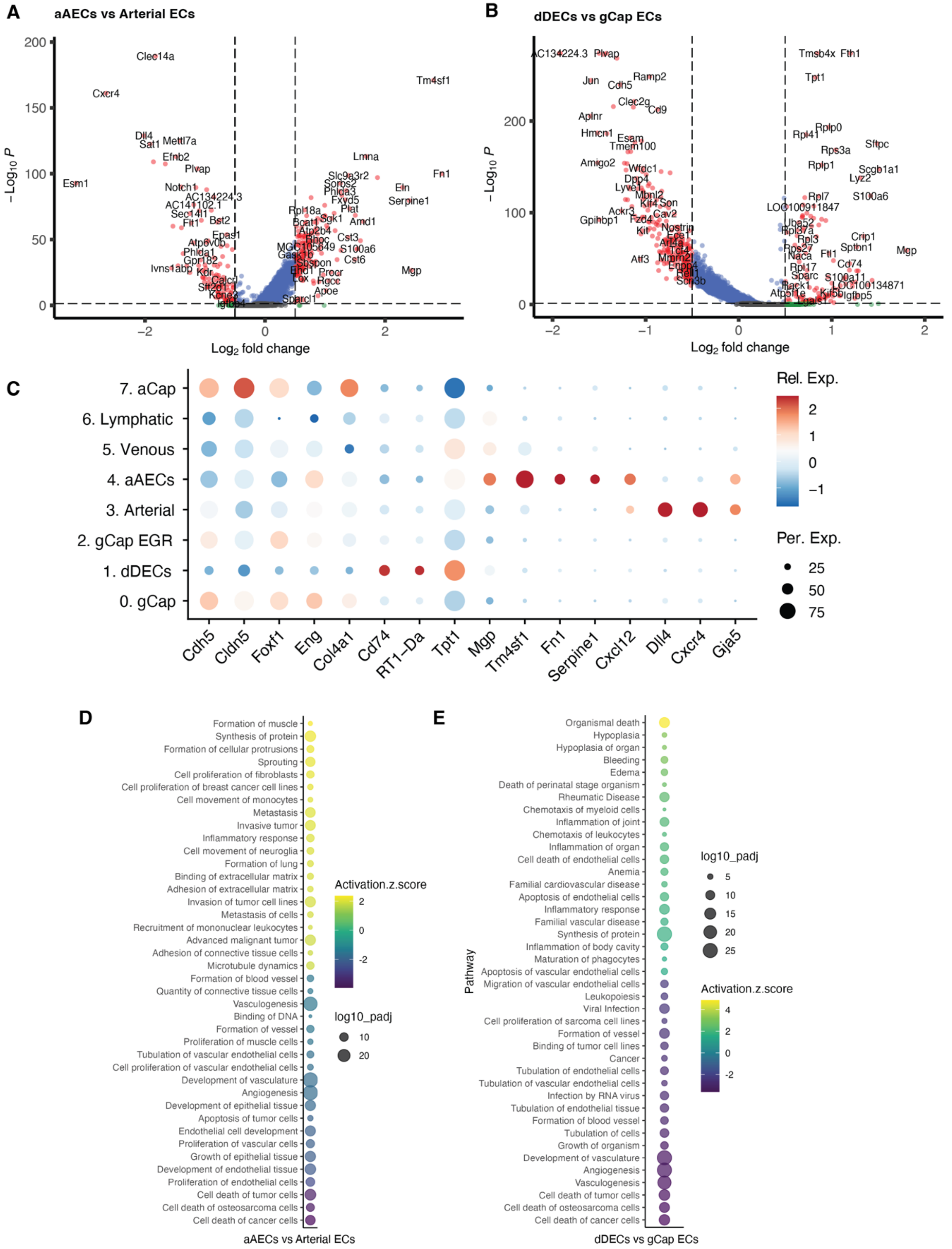

Figure 2.4: Transcriptomic signature of disease-specific activated arterial and dedifferentiated EC populations.

Volcano plots for all differential expressed genes between A) aAECs and arterial ECs and B) dDECs and gCap ECs including all timepoints. C) Dot plot showing relative expression of genes of interest between all EC clusters. dDECs exhibited the lowest expression of *Cldn5* and *Cdh5*, and the highest expression of *Cd74*, *RT1Da* and *Tpt1*, whereas aAECs showed the highest expression of *Tm4sf1*, among other genes associated with an activated phenotype and low expression of typical arterial genes (*Dll4* and *Cxcl4*). D) Ingenunity pathway analysis (IPA) comparing aAECs and arterial ECs showing the top 15 significantly up and down regulated gene sets. aAECs exhibited upregulation of gene sets associated with cancer cell proliferation, migration and invasion, with downregulation of gene sets for angiogenesis, vascular development and apoptosis. E) IPA comparing dD and gCap ECs showing the top 15 significantly up and down regulated gene sets, demonstrating upregulation of gene sets in dDECs associated with inflammation and apoptosis and downregulation of gene sets associated with vascular development and angiogenesis.

2.4.5 Changes in stromal cells in response to PAH

Next, we re-clustered all stromal cell populations (fibroblasts, pericytes, smooth muscle cells) into 6 unique populations, including matrix fibroblasts, *Col13a1*+ fibroblasts, *Col14a1*+ fibroblasts, *Acta2+* pericytes, *Pdzd2*+ pericytes, and smooth muscle cells (SMCs)/myofibroblasts (**Figure 2.5A**). Fibroblasts were identified based on *Pdgfra* and *Tcf21* expression, and differential expression of *Col13a1* and *Col14a1*; while pericytes were identified by expression of *Pdgrb*, *Csgp4,* and *Mcam* (**Figure 2.5B and C**).[166,186] Pericytes were further distinguished into ‘classical’ pericytes uniquely expressing *Pdzd2*, *Postn*, *Gucy1b1* and ‘SM-like’ pericytes based on expression of contractile markers (*Acta2, Des*) (**Figure 52.B and C**), as previously described by Hurskainen et al.[166] SMCs and myofibroblasts were observed in a mixed population expressing *Acta2* and *Dcn*. Interestingly, both pericyte populations showed marked expansion during PAH progression, consistent with a possible contribution to arteriolar remodeling, in PAH whereas there was little change in the global proportion of other stromal cell populations (**Figure 2.5D and E**).

We then compared transcriptomic profiles of ‘classical’ and SM-like pericytes (at all timepoints). The SM-like pericytes exhibited high expression of genes associated contractile function including, *Acta2*, *Des*, *Myh11*, and *Mustn1*, as well as reduced expression of some typical pericyte genes, including *Postn, Gucy1a1, Pdzd2* and *Vtn* compared to classical pericytes (**Figure 2.5F and G**). Like aAECs, SM-like pericytes were somewhat enriched in *Tm4sf1* (**Figure 2.5G)**, consistent with a proliferative and invasive phenotype. Gene set enrichment analysis (GSEA) comparing SM-like pericytes to classical pericytes showed that SM-like pericytes exhibited robust enrichment of gene sets associated with contraction, muscle differentiation and translation, while gene sets associated with GTPase activity, lipid processing and organ development were decreased (**Figure 2.5H**). Therefore, these data are consistent with the SM-like pericytes possibly contributing to arteriolar remodeling and distal muscularization in PAH.

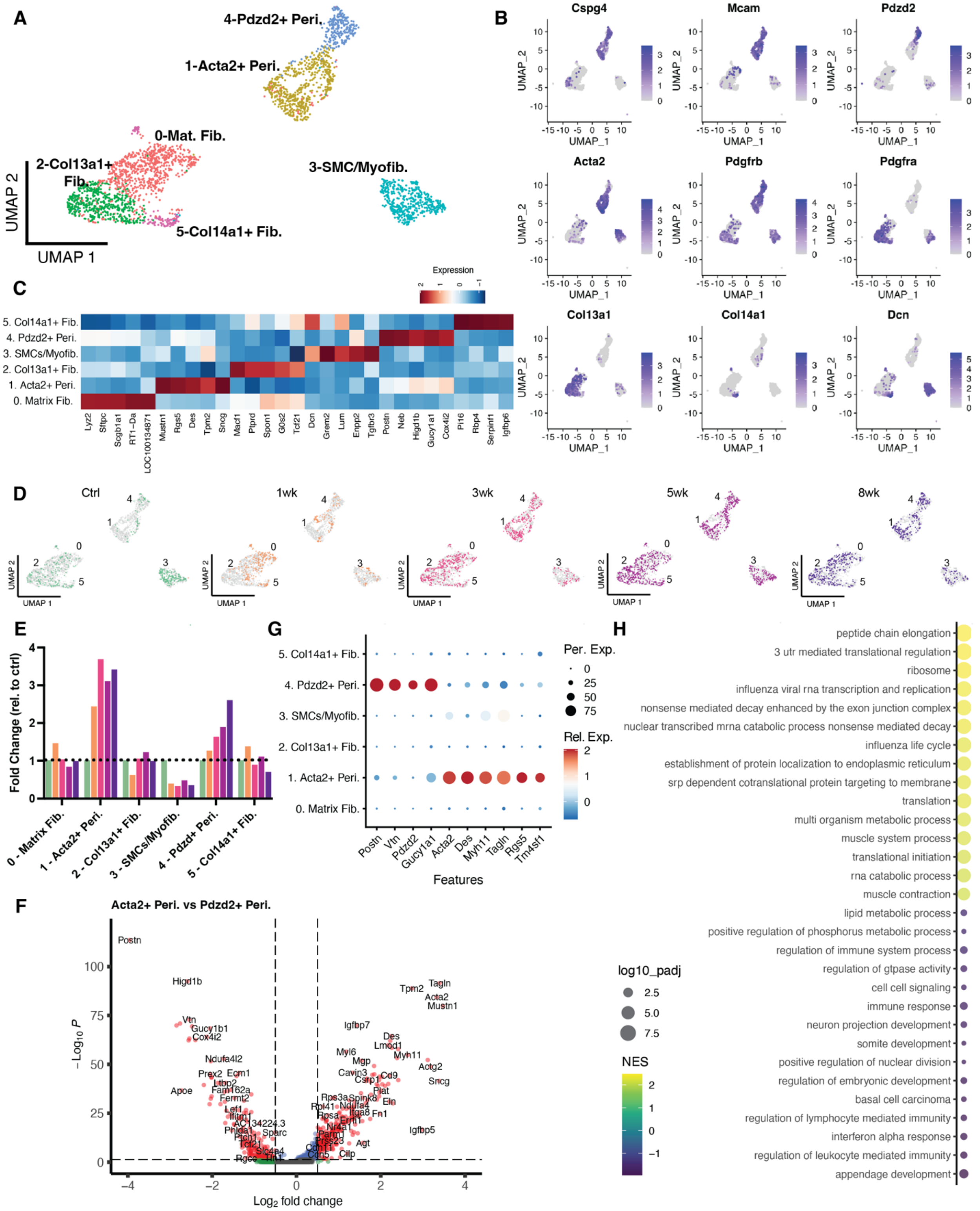

Figure 2.5: Stromal cell populations during PAH progression.

A) Uniform manifold approximation and projection (UMAP) representation of all stromal populations at all sampled timepoints showing 6 distinct cell types. B) Feature plots highlighting genes typical of distinct stromal populations including: pericytes (*Cspg4, Mcam, Pdgfrb*);

fibroblasts (*Pdgfra, Col13a1, Col14a1*); smooth muscle cells (*Acta2*); and myofibroblasts (*Dcn*). C) Heatmap of top 5 differentially expressed genes distinguishing each stromal population. D) UMAP portraying the presence of cells from each stromal population at each timepoint, showing a marked expansion of the pericyte populations by 3-weeks. E) Fold change of each stromal population relative to their respective controls demonstrating a marked relative increase in the 'smooth muscle' (SM)-like *Acta2*+ pericytes and less so the 'classical' pericyte population during PAH progression. F) Volcano plot of all differentially expressed genes (DEGs) between SM-like pericytes and classical pericytes. G) Dot plot showing relative expression of genes of interest between different pericyte populations. H) Gene set enrichment analysis with the top 15 up and down regulated gene sets between SM-like pericytes and classical pericytes.

2.4.6 Temporal profile of endothelial transcriptomic changes in aAECs during PAH progression

By performing scRNA-seq at multiple timepoints in the SU/CH model, we were able to discern changes in gene expression profiles during the development of the PAH phenotype. Volcano plots prtray DEGs within the aAEC cluster between control animals and SU/CH rats at weeks 1 or 5 (**Figure 2.6A and B**, respectively). A heatmap showing the top 20 up or down regulated genes for the aAEC cluster at each timepoint revealed three distinct profiles (**Figure 2.6C)**. The first was represented by an early increase in gene expression peaking at 1 week, with a partial normalization by 5 to 8 weeks. These were largely cell-cycle associated genes, including *Birc5*, *Cdc20*, *Cdkn2c*, *Cdkn3*, and *Cdk1* (**Figure 2.6C)**. Interestingly, a similar pattern of gene expression was observed in the dDECs at 1 week, consistent with the increase in EC proliferation observed in both populations (**Figure 2.3D, E**). A second pattern was unique to aAECs and was represented by genes that showed a sustained increase in expression compared to control at all timepoints and this included a number of genes which have previously been implicated in PAH such as, *Ramp1*,[187] *Trpv4*,[188] *Jag1*,[189] and *Pdgfa*[190]. Finally, a third pattern was made up of genes strongly expressed at baseline by both classical arterial ECs and aAECs, largely involved in angiogenesis and vascular development, such as *Dll4*, *Notch1*, *Efna1*, and *Erg1*, which were selectively downregulated in aAECs during PH development (**Figure 2.6C**). Not unexpectedly, *Cyp1a1* and *Cyp1b1*, which mediate drug metabolism,[191] were upregulated in all EC populations after treatment with SU, with the exception of lymphatic ECs (**Figure 2.6C**). Ingenuity pathway analysis (IPA) of changes in gene expression in aAECs between control and PAH timepoints confirmed the upregulation of gene sets associated with increased cell proliferation and cancer-like cell growth in aAECs, with downregulation of gene sets associated with angiogenesis, vasculogenesis and cell death (**Figure 2.6D**). Together, these results point to aAECs as a unique lung EC population exhibiting a transcriptional signature consistent with a growth dysregulated state, associated with decreased reparative and angiogenic capacity, and likely playing an important role in arterial remodeling in PAH.

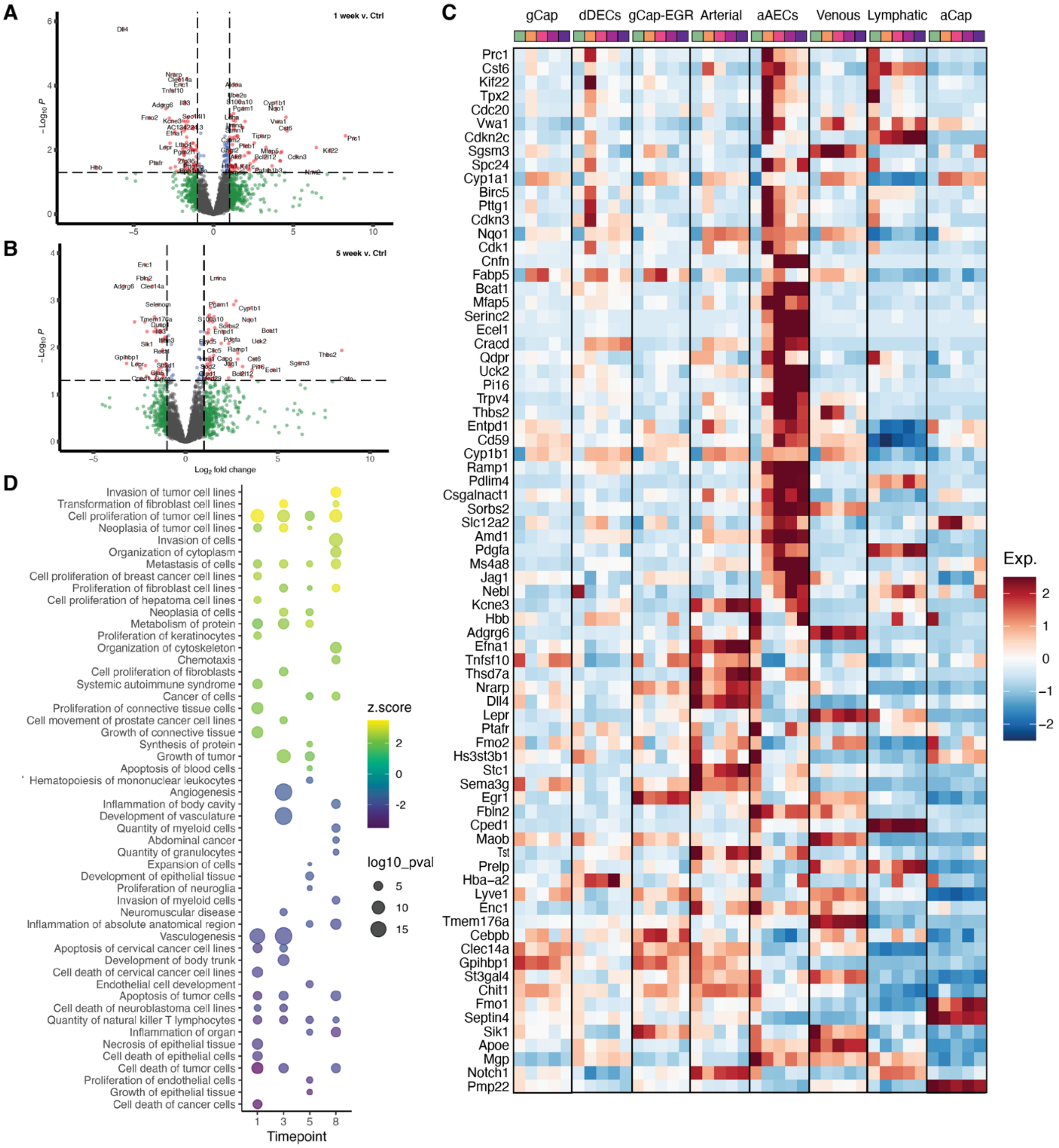

Figure 2.6: Endothelial transcriptomic changes during onset and progression of PAH. Volcano plots showing all DEGs for aAECs vs control at 1-week (A) and 5-weeks (B). C) Heatmap showing the top 20 up and downregulated DEGs for aAECs at each timepoint relative to control. Three transcriptional patterns can be discerned: i) peak increase at 1-week with partial normalization at later timepoints, ii) persistent elevation at all timepoints and iii) transient or sustained reduction in gene expression. D) Ingenuity pathway analysis (IPA) for aAECs comparing each timepoint to the control, showing the top up or downregulated disease or biofunction gene sets for each timepoint.

2.4.7 Spatial localization of Tm4sf1-expressing activated arterial ECs

Both the aAECs and SM-like (*Acta2*$^{+}$) pericytes exhibited expression of *Tm4sf1*, raising the possibility that this surface protein may be used as a marker of these populations. Therefore, we examined *Tm4sf1* expression across all 44 lung cell populations, and found that *Tm4sf1* was largely restricted to arterial and venous ECs, as well as pericytes and mesothelial cells, with by far the greatest expression in aAECs (**Figure 2.7A**). We then used immunofluorescent staining for TM4SF1, and co-staining using isolectin B4 (ECs), 3G5 (pericytes) or smooth muscle actin (SMA; smooth muscle cells), to identify the anatomic location of these cell populations in the healthy and diseased lungs. In control lung samples, TM4SF1 expression was localized mainly to 3G5^{+} pericytes surrounding alveolar capillaries, with sparse staining of ECs (**Figure 2.7B**). However, at 5 weeks post SU/CH, there was abundant TM4SF1 staining largely associated with ECs, identified by isolectin B4, localized mainly to severely remodeled arterioles with accumulation of TM4SF1^{+} ECs seen within the vascular lumen, consistent with a direct role for the aAECs in occlusive arteriopathy (**Figure 2.7C**). Interestingly, in the diseased lung, 3G5 staining was tightly associated with SMA^{+} bands of neomuscularization, suggesting a role for the SM-like pericytes in distal arteriolar medial remodeling. Notably, TM4SF1 staining was reduced in these SMA positive regions, possible indicating that as SM-like pericytes differentiate further towards a mature smooth muscle phenotype, they may lose the expression of this ‘progenitor’ cell marker. We also assessed the spatial distribution of TM4SF1 expression in human lung samples from control and PAH patients (**Figure 2.7D**). In the control samples, TM4SF1 staining could be seen surrounding small arterioles, but was not associated with ECs (CD31 staining). In contrast, in PAH samples there was abundant TM4SF1 staining, localized to the perivascular region but also adjacent to the intima, and clearly associated with ECs, with a relative paucity of staining in the intervening SMC layer (**Figure 2.7D**). Together these results confirm that TM4SF1 positive ECs are associated with complex arterial remodeling in PAH, together with SMA$^+$ pericytes, consistent with a pathological role of aAECs and SM-like pericytes in this disease.

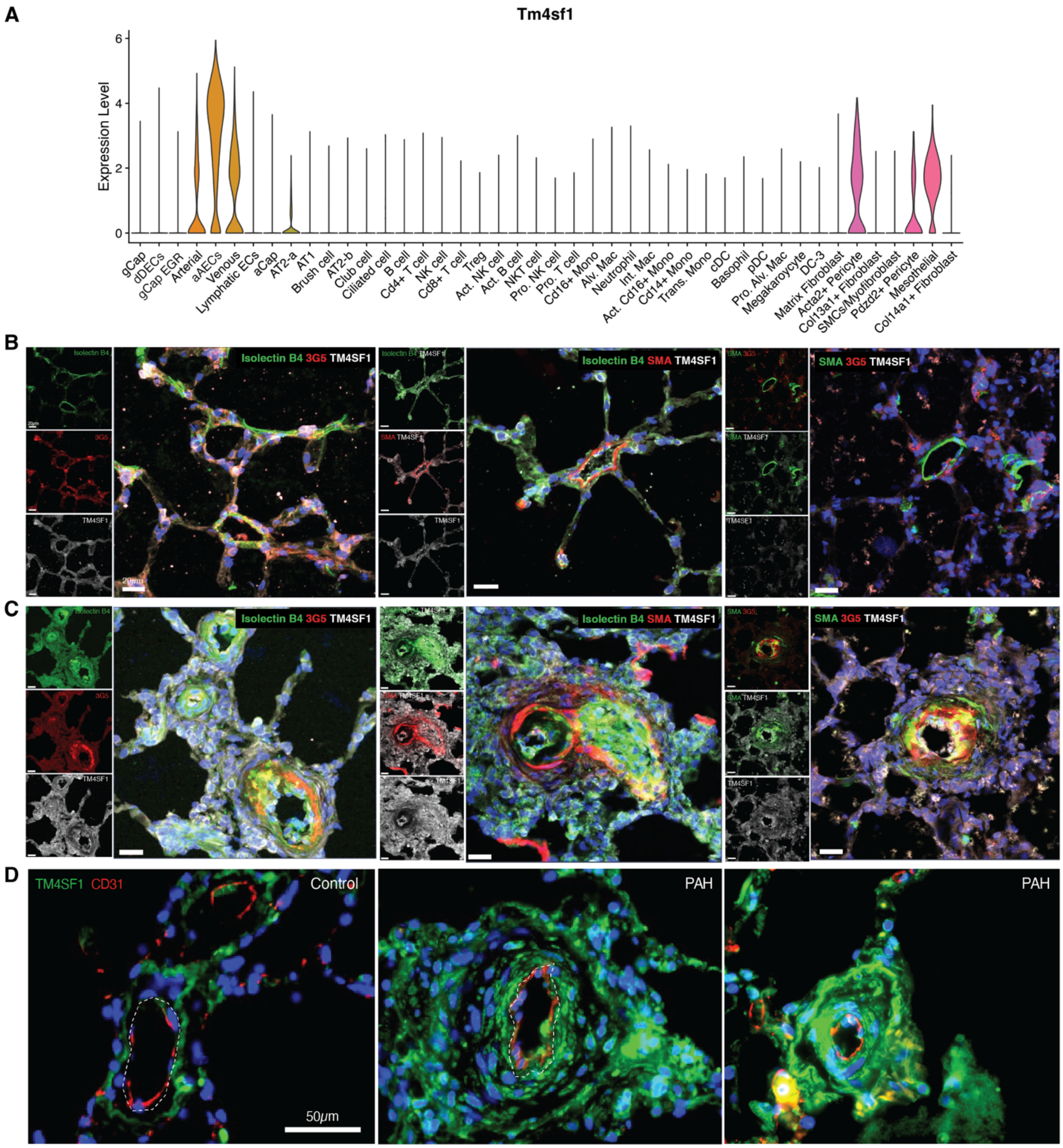

Figure 2.7: Tm4sf1 as a marker for aAEC and SM-like pericytes in arterial remodeling.
A) Violin plots showing *Tm4sf1* the highest expression in aAECs, with lower levels in arterial and venous ECs, SM-like pericytes and mesothelial cells. Immunofluorescent staining for TM4SF1 (white), isolectin B4 (ECs, green), 3G5 (pericytes, red) or SMA (smooth muscle cells, red) in healthy lungs (B) or at 5-weeks in the SU/CH severe PAH model (C). D) Immunofluorescent staining of lung sections from control subjects and PAH patients for TM4SF1 (green), co-stained for ECs (CD31, red). Scale bar represents 20μm (B and C) and 50μm (D). n = 3 biological replicates for the SU/CH immunofluorescent samples, n = 7 for the human PAH patient, and control immunofluorescent samples.

2.4.8 RNA velocity of endothelial and stromal cells during SU/CH progression

Endothelial to mesenchymal transition (EndMT) has been previously implicated in PAH.[192] To explore a potential role of cell fate transitions in the development of PAH we employed RNA velocity analysis, using scVelo dynamical modelling,[180] specifically addressing population dynamics within the EC and stromal clusters based on their importance in arterial remodeling. Notably, RNA velocity analysis demonstrated vectors originating in the arterial and aAEC populations passing through the dDECs cluster and directed to fibroblast populations (**Figure 2.8A**), consistent with the possibility of EndMT contributing to vascular stromal cells in this PAH model. Velocity vectors were also observed from the classical (*Pdzd2*$^+$) pericytes towards the SM-like (*Acta2*$^+$) pericytes, consistent with pericyte differentiation towards a smooth-muscle cell fate as a mechanism of distal muscularization. There were also vectors from the gCap-EGR cluster leading to the venous ECs, again supporting the possibility of zonation of this cluster towards the venous side of the alveolar capillary. The possibility of EndMT was further supported by a latent time analysis which provides an estimate of a cell's internal clock, from progenitor fates (approaching 0) to terminally differentiated cells (approaching 1). This model identified aCap and gCap ECs, *Col13a1*$^+$ fibroblasts, and classical (*Pdzd2*$^+$) pericytes as being close to 'terminal' states, while aAECs, dDECs, and SM-like pericytes were closer to a progenitor state (**Figure 2.8A'**). We then inferred transcription factor (TF) activities from gene expression data for the EC clusters using deCoupleR.[178] The location of dDECs (EC cluster 1) in the endothelial UMAP is shown in **Figure 2.8B**. TFs classically associated with EMT[193] including *Zeb1*, *Zeb2*, *Snai2* had predicted activity in dDEC cluster, as well as some other EC populations, whereas *Twist1* was seen mainly in gCap-EGR ECs (**Figure 2.8C**). The top 40 most variable TFs are presented in **Figure 2.8D**. Importantly, dDECs exhibited very low expression of the endothelial-restricted transcription factor, ETS-related gene (*Erg*), a principal determinant of EC identity,[194] as well as the Friend Leukemia Integration 1 Transcription Factor (*Fli1*), another member of the ETs family, which are both downregulated in EndMT.[195] As well, dDECs exhibited elevated activity associated with *Nr2f2*[196] and *Zeb2,*[193] both which have been implicated in EndMT, further supporting a potential role for this relatively de-differentiated EC population in EndMT during PAH progression (**Figure 2.8D, insert**). Interestingly, gCap-EGR and venous ECs shared a number of TFs (**Figure 2.8D**), further supporting zonation between these populations based on similarities in gene expression as shown in **Figure 2.3C**.

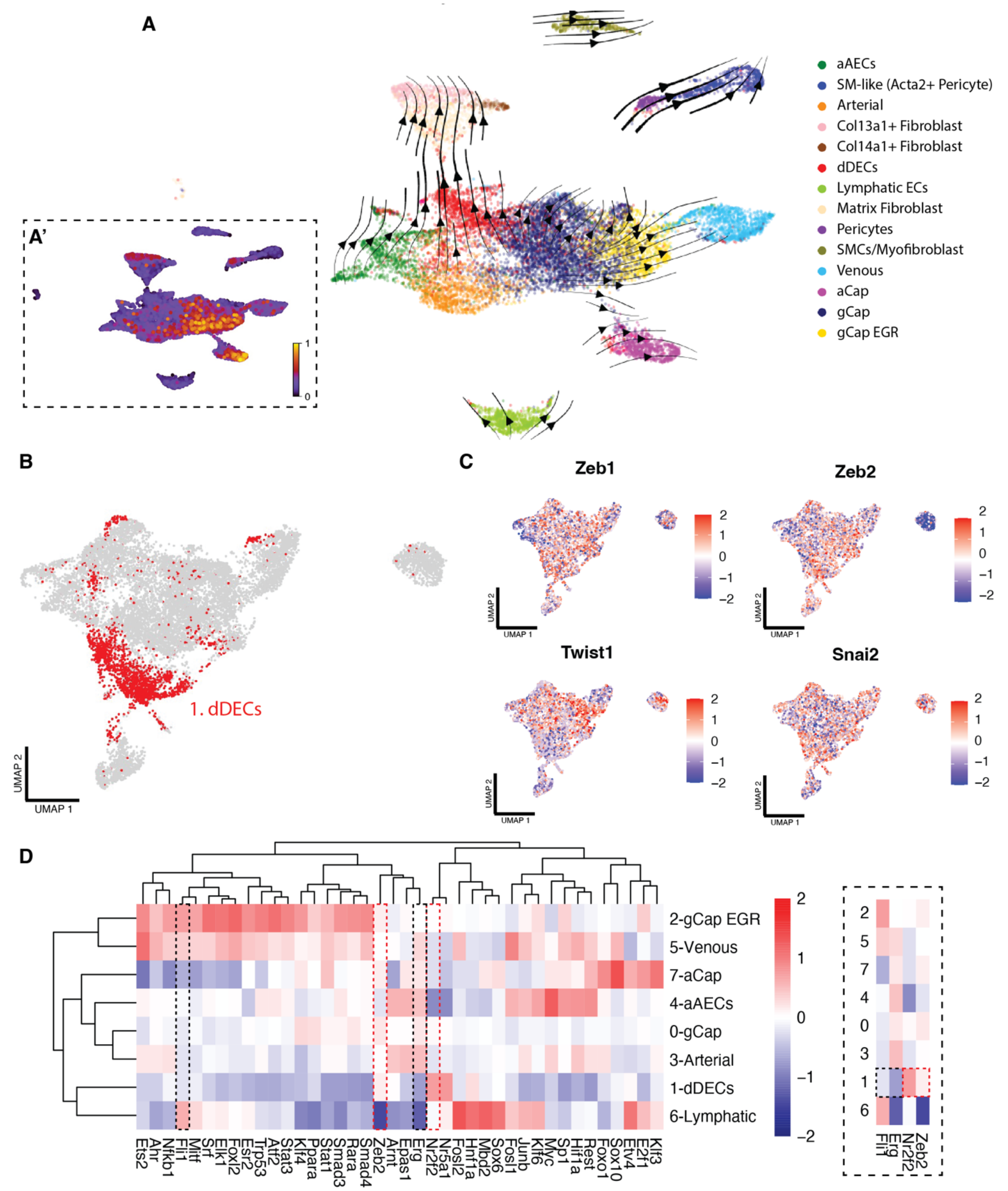

Figure 2.8: RNA velocity analysis indicates endothelial to mesenchymal transition.
A) RNA velocity analysis of endothelial and stromal cell populations using scVelo's dynamical model and CellRank demonstrate velocity vectors from aAEC and arterial EC populations, going through the dDEC cluster to fibroblast populations. RNA velocity vectors are also seen between classical pericytes SM-like (*Acta2*+) pericytes. Inset (A') highlights the latent time analysis which estimates cellular differentiation and shows that gCap, aCap, fibroblasts, and classical pericytes

approximate a more terminal differentiated state, while aAECs, dDECs and SM-like pericytes exhibit a more progenitor-like state. B) EC subset UMAP showing the distribution of dDECs in red. C) UMAP showing the distribution of typical epithelial to mesenchymal transition (EMT) related transcription factor (TF) activities in the EC populations. E) Heatmap of the top 40 most variable TFs in the different EC populations. The insert highlights reduced activity of *Erg* and *Fli1*, ETS family TFs that control endothelial identity, within cluster 1 (dDECs) and increased activity of *Nr2f2* and *Zeb2*, which have been implicated in EndMT.

2.5 Discussion

PAH is characterized by marked pruning of the pulmonary arteriolar bed which, together with complex arterial remodeling, leads to progressive increases in pulmonary vascular resistance; yet the mechanisms underlying these dramatic vascular changes remains unclear. The rat SU/CH model of PAH provides an ideal opportunity to study functional, structural, and molecular changes during the onset and development of PAH, rather than only at late stages of disease when typically, clinical lung tissue is available.

Using multiplexed scRNA-seq we analyzed four timepoints, spanning early to late disease, comparing SU/CH to healthy control animals. Major transcriptomic changes were observed in nearly all lung cell populations at 1-week post SU/CH, including immune, stromal, and vascular cells. Notably, ‘transitional’ monocytes, exhibiting characteristics between those of classical and interstitial monocytes, were among the top five most transcriptionally affected in the PAH model based on the Augur machine learning algorithm and exhibited the greatest number of DEGs at week 1. This is consistent with an important early inflammatory response to injury induced by VEGFR2 inhibition coupled with hypoxia. However, at later timepoints, there was substantial normalization in gene expression profiles in nearly all lung cell populations, with the notable exception of the ‘activated’ arterial EC (aAECs) cluster. This finding was surprising considering that the major pathological and hemodynamic changes in this model manifest at later time points. In particular, the lack of persistence of a transcriptional signature for inflammation is remarkable given the abundant evidence that implicates immune mechanisms in the pathogenesis of PAH.[76] However, this may in part reflect overrepresentation of cells from the distal parenchyma and microcirculation in the lung isolate, which account for by far the greatest number of cells after dispersion, whereas larger vessels, which exhibit more marked pathologically inflammatory changes, make up only a small proportion of total cells. Nonetheless, we did observe some intriguing immune signals including a persistent, albeit modest, increase in DEGs in interstitial macrophages and a robust expansion of the NKT population in later stages of disease. This is consistent with a previous single cell transcriptomic analysis of large pulmonary arteries from patients with severe PAH, which showed a significant increase in NKT cells, along with T cells and neutrophils, compared to control.[122]

In contrast, persistent and robust changes in transcriptional activity were seen selectively in one endothelial cluster, aAECs, suggesting that this population may be playing a central role in the progression of vascular disease in this model. Since the effects of SU and hypoxia would no longer be operative at later timepoints beyond 3 weeks, this raises the question of what drives the persistent transcriptomic response in the aAEC cluster. It has been reported that complex arterial remodeling in this model is dependent on perturbed pulmonary hemodynamics,[44] likely due to pathological levels of shear stress, which would have the greatest impact on the distal arteriolar bed.[197] Using micro-CT, we demonstrated a progressive loss of arteriolar volume in the SU/CH model, which was significant as early as 1 week, preceding any evidence of occlusive arterial remodeling. This suggests that early arteriolar loss, probably as a direct consequence of widespread EC apoptosis, may be the primary mechanism for the initial hemodynamic abnormalities in this model. As well, since in a dispersed lung cell preparation, distal arteriolar ECs will greatly outnumber those from larger arteries, the 'arterial' EC populations that we identified by scRNA-seq would be predominately arteriolar in origin. Thus, by virtue of being largely derived from the distal arteriolar bed, aAECs would have been among the cells the most affected by the abnormal shear forces associated with developing PH,[197] which provides a likely stimulus for the persistent transcriptomic activity seen in this population. Indeed, this EC population may be the link between perturbed pulmonary hemodynamics and complex arterial remodeling that was previously described.[44,198]

At the 1 week timepoint, aAECs and dDECs exhibited a similar transcriptional signature characterized by the transient expression of genes related to cell proliferation and repair. However, at later time points (5 and 8 weeks), only aAECs exhibited a persistent dysfunctional gene expression profile that was consistent with dysregulated cell growth and reduced capacity for vascular repair and angiogenesis. Thus, using single cell transcriptomic analysis we have been able to map the origin of hyperproliferative and apoptosis-resistant ECs which have long been implicated in occlusive arterial remodeling in PAH.[199] We have also demonstrated that aAECs can be distinguished from other EC populations by high expression of *Tm4sf1*, a trans-membrane protein which is also found in many cancer cells.[183] Using immunofluorescence staining, we were able to show that TM4SF1$^+$ ECs were abundant in complex arterial lesions in the SU/CH model and as well as in lung sections from patients with PAH, particularly in regions of occlusive arteriopathy, consistent with a dominant role for this EC population arterial remodeling. Interestingly, this marker was also expressed by the SM-like pericytes and, in the healthy lung, TM4SF1 staining was associated with pericytes surrounding alveolar capillaries. However, in the diseased lung, 3G5$^+$ muscularized regions of remodeled arteries exhibited lower TM4SF1 staining, consistent with their differentiation to a more mature SMC phenotype. This finding also suggests that the SM-like pericyte cluster, which by RNA velocity analysis was derived from the classical Pdzd2$^+$ 'classical' pericytes, may contribute importantly to distal arterial muscularization in PAH, as has been previously suggested.[200–202]

Hong et al. identified a similar arterial EC cluster expressing *Tm4sf1* in both the rat monocrotaline (MCT) model and SU/CH model in late-stage PH.[104] However, the published transcriptomic profile of this *Tm4sf1*$^+$ EC population included expression of genes characteristic of capillary (*Ednrb*), and venous (*Slc6a2, Icam1*), in addition to arterial ECs (*Gja5*). Indeed, we also found that *Tm4sf1* was expressed by venous, but not capillary ECs, but at much lower levels than in aAECs, which also uniquely demonstrated a persistent transcriptomic signature of dysregulated cell growth. As well, we also showed that ECs within occlusive arterial lesions in both the SU/CH model and human PAH patients strongly expressed TM4SF1, consistent with a key role for this population in complex arterial remodeling. While TM4SF1 may be a useful marker to identify aAECs, it is also possible that it may contribute to growth dysregulation. TM4SF1 is a trans-membrane protein belonging to the tetraspanin superfamily that regulates numerous signaling pathways modulating cell development, activation, growth, and motility.[183] Increased *Tm4sf1* expression has been observed in cancer cells, particularly in breast, lung and ovarian cancers,[183] and is a promising target for novel cancer therapies.[203–205] Therefore, similar strategies to antagonize or silence *Tm4sf1* may have benefits in reducing EC growth and arterial remodeling in PAH.

We also identified a novel, relatively de-dedifferentiated EC population in the PAH model, dDECs, that emerged early in disease and exhibited reduced expression of tight junction related genes such as *Cdhn5* and *Cldn5*, indicative of a loss of endothelial integrity, along with upregulation of antigen presentation related genes such as *Cd74* and *RT1-Da*. Interestingly, upregulation of CD74 expression was previously reported in the endothelium of pulmonary arteries and cultured ECs from PAH lungs.[206] As a receptor for macrophage migratory inhibitory factor (MIF), CD74 may contribute to inflammatory cell recruitment which is well known to be associated with arterial remodeling in PAH.[36] Enriched expression of *Cd74* was also described in a single cell transcriptomic analysis of lung ECs isolated from a SU/CH mouse model of PH;[121] however, this was seen across multiple EC populations including capillary, arterial, and venous. As well, the mouse model, unlike the rat, does not exhibit occlusive arterial remodeling and the authors found no evidence of EC proliferation in their single cell transcriptomic analysis.[121] In our study, we were able to determine that *Cd74* enriched ECs represented a discrete subset of ECs that were characterized by a relatively dedifferentiated state. As well, we demonstrated a clear transcriptomic signature for cell proliferation, which was represented in the UMAP as a ‘proliferative node’ consisting of cells from several clusters, including the aAECs and dDECs, both of which expanded markedly during PAH progression.

In addition to any role in promoting vascular inflammation, our study provides novel evidence that dDECs that are primed to undergo endothelial to mesenchymal transition (EndMT) to give rise to vascular stromal cells, a process that has been long thought to contribute to adventitial remodeling and arterial stiffness in PAH.[192,207] EndMT shares many similarities with epithelial to mesenchymal transition (EMT),[193] and is a phenomenon characterized loss of expression of canonical genes necessary for functional integrity, typically cell-cell junction proteins, with the adoption of motile and invasive cell behaviors. Interestingly, our RNA velocity analysis showed numerous strong vectors within the dDEC cluster directed towards various fibroblast populations. Moreover, latent time analysis showed that dDECs approximated a progenitor cell fate whereas the gCap EC populations were closer to a 'terminal' state of cell differentiation. While we were able to infer increased activity of TFs implicated in EndMT in this population, such as *Zeb2* and *Nr2f2*, it has increasingly been recognized that EndMT is a complex process and cannot be defined based on a small number of molecular markers.[193] Indeed, dDECs showed a number of other features consistent with EndMT, including a marked reduction in the activity of *Erg*, a 'master' endothelial TF that promotes endothelial homeostasis via regulation of lineage-specific enhancers and super-enhancers.[194] Indeed, a previous study showed that knockdown of *Erg* together with another ETS family transcription factor, *Fli1*, was sufficient to induce EndMT.[195] Notably, the dDEC cluster was the only endothelial population that exhibited a very low activity of both *Erg* and *Fli1* (**Figure 2.8D**). Therefore, it is not surprising that canonical endothelial tight junction genes were downregulated in dDECs, along with increased activity of pathways associated with inflammation and apoptosis, which have been implicated in EndMT,[208,209] as well as selective upregulation of several other EndMT related genes, including *Tpt1*,[13] *Crip1*,[210] and *S100a4*.[207]

Therefore, we used serial single cell transcriptomics to identify disease-specific EC and stromal cell populations that play a central role in arterial remodeling during the progression of PAH. Notably, we show that *Cd74*-enriched dDECs represent a distinct EC population exhibiting features of dedifferentiation and loss of functional integrity, that are primed to undergo EndMT, thereby contributing to the generation of profibrotic arterial fibroblasts that play an important in adventitial remodeling in PAH. As well, we have demonstrated that the aAEC cluster exhibits a marked growth dysregulated transcriptional state, possibly in response to ongoing hemodynamic perturbation, that disproportionally impacts the distal lung arteriolar bed. As well, for the first time, we provide evidence that the aAEC and SM-like pericyte populations are spatially localized to regions of complex arterial remodeling and contribute to intimal obliteration and distal muscularization, respectively, in both the SU/CH model and PAH patients. Moreover, since they are characterized by high *Tm4sf1* expression, this may be a promising target for therapeutic strategies to prevent or reverse arterial remodeling in PAH.

2.6 Acknowledgements

We would like to thank Anli Yang for her technical assistance with all animal experiments and Elmira Safaie Qamsari for her assistant sectioning fresh frozen tissues for immunofluorescent staining. Additionally, we thank the following Ottawa Hospital Research Institute core services Stemcore laboratories for single cell library preparation and sequencing, OHRI Bioinformatics core for preprocessing of single cell data, and the University of Ottawa's Animal Care and Veterinary Services core.

2.7 Sources of Funding

This work was supported by a Foundation award from the Canadian Institutes of Health Research (FDN – 143291) to DJS. NDC acknowledges scholarship support from the Canadian Institutes of Health Research, and the Canadian Vascular Network.

2.8 Competing Interests

None

2.9 Author Contributions

NDC has contributed to all aspects of this work including conception, experimental design, performing the experiments, data analysis and preparation of this manuscript. EM contributed to data analysis and figure preparation. RSG assisted with collection of the first experiment of single cell samples and preliminary analysis. YD was instrumental in preparation and collection of the lung samples for microCT analysis and in all animal studies. KS performed the IPA analysis. AS performed the RNA velocity analysis and contributed to figure preparation. DPC assisted with single cell transcriptomic analysis and provided valuable support in initial experimental design. SEL performed immunofluorescent staining on all human samples and contributed to figure preparation. TK performed immunofluorescent staining on fresh frozen rat sections. KY collected images on rat lung sections, assisted with figure preparation and data interpretation, and manuscript review. SB provided access to human PAH samples, contributed expertise to interpretation of results, and manuscript review. DJS was involved in the conception, experimental design, data analysis and interpretation, figure design, and drafting the manuscript. DJS is accountable for all aspects of this work.

Chapter 3: Single-cell microencapsulation improves lung retention of endothelial colony forming cells after intravascular delivery and unmasks therapeutic benefit in severe pulmonary arterial hypertension

Nicholas D. Cober[1,2*]; Ketul R. Chaudhary [1,3*]; Yupu Deng [1]; Chyan-Jang Lee [1]; Katelynn Rowe [1]; David W. Courtman [1]; Duncan J. Stewart [1,2]

[1]Sinclair Centre for Regenerative Medicine, Ottawa Hospital Research Institute, Ottawa, ON, Canada
[2]University of Ottawa, Faculty of Medicine, Department of Cellular and Molecular Medicine, Ottawa, ON, Canada
[3]Department of Physiology and Biophysics, Faculty of Medicine, Dalhousie University, Halifax, NS. Canada
* Both authors contributed equally to the work

ORCID IDs:
NDC: 0000-0001-8061-806X
DJS: 0000-0002-9113-8691
KRC: 0000-0003-1725-7438

Corresponding author: Duncan J Stewart, djstewart@ohri.ca.
Executive Vice-President Research, The Ottawa Hospital; CEO & Scientific Director, Ottawa Hospital Research Institute; The Evelyne & Rowell Laishley Chair and Professor, Department of Medicine, University of Ottawa
501 Smyth Road, Box/C.P. 511, Ottawa, ON, K1H 8L6
613-739-6686

Authorship Contributions:

NDC has contributed to all aspects of this work including conception, cell encapsulation optimization, performing experiments, data analysis and preparation of this manuscript. KR contributed equally to this work including conception, initial cell isolation and characterization, experimental work, data analysis and manuscription preparation. YD and KR were involved with all animal studies. CJL designed and prepared all viral vectors used for bioluminescence cell tracking. DWC contributed to conception of the encapsulation platform, and interpretation of results. DJS was involved the conception and design of experiments, data analysis and interpreting results, and drafting this manuscript.

3.1 Abstract

Background: Pulmonary arterial hypertension (PAH) is triggered by pulmonary vascular endothelial cell apoptosis and microvascular loss; therefore, therapies that can regenerate lost vasculature may offer therapeutic benefit. Endothelial colony forming cells (ECFCs) can directly repair damaged blood vessels and may have therapeutic potential for the treatment of PAH. However, poor retention of ECFCs in the lungs following intravenous delivery greatly limits their therapeutic application. Therefore, we studied whether cellular microencapsulation could enhance ECFCs viability and retention in the lung after systemic delivery and improve therapeutic efficacy of ECFCs in a rat monocrotaline (MCT) PAH model.

Methods: ECFCs were encapsulated by vortex-emulsion using various concentrations of agarose, and capsule size and initial cell viability were assessed. Encapsulated and free ECFCs were transduced with luciferase and administered to Sprague-Dawley rats three days after injection of MCT. ECFCs were tracked *in vivo* by bioluminescence imaging (BLI) to assess cell persistence and bio-distribution. At end-study, right ventricular systolic pressure (RVSP) and right ventricular hypertrophy were assessed for therapeutic efficacy.

Results: Microgel encapsulation using 3.5% agarose improved cells survival and supported cell migration from capsules. At 15 minutes after delivery, BLI radiance were similar for free and microencapsulated ECFCs; however, only encapsulated cells could be detected by BLI at 4 and 24 hours. Transplantation of microencapsulated ECFCs led to significant improvement in RVSP three weeks after delivery compared to non-encapsulated ECFCs.

Conclusion: Together, microencapsulation increased retention of ECFCs within the lungs. Furthermore, even a modest increase in ECFCs persistence over 24 hours can provide an important therapeutic benefit in the rat MCT model of PAH.

3.2 Introduction

Cell-therapy has emerged as a promising option for treatment of various diseases and its potential is clearly evident by the ever-incising number of clinical trials using a wide variety cell types. Despite the tremendous promise that cell therapies offer for repairing and regenerating damaged tissues or organs, there has been only limited success in their translation into clinical therapies.[211] A major factor in these mixed results is poor cell retention and survival of the transplanted cells.[98,129,212,213] Endothelial progenitor cells (EPCs) have been used to promote the regrowth and repair of damaged vasculature in many pre-clinical models of vascular diseases.[127,135,214] These cells are classified as early-EPCs (E-EPCs or circulating angiogenic cells) or late-outgrowth EPCs (or endothelial colony forming cells; ECFCs) based on the time of appearance in culture.[215] ECFCs are highly proliferative cells with an endothelial cell-like cobblestone morphology and are capable of forming functional blood vessels.[216] While E-EPCs act mainly by paracrine mechanisms, ECFCs are thought to participate directly in the repair and regeneration of blood vessels.[124]

Pulmonary arterial hypertension (PAH) is a devastating lung vascular disease with 79% 3-year mortality.[217] PAH is caused by damage and loss of the effective lung microvasculature, either by a degenerative mechanism or by occlusive arterial remodeling, leading to increased vascular resistance, as evidenced by increased pulmonary vascular resistance and pulmonary arterial pressures with eventual right ventricular failure.[164,218] Current treatment options are limited, and available pharmacotherapies focus on targeting an imbalance between vaso-constrictor and -dilator factors within the pulmonary microcirculation.[219,220] While current vasodilator therapies can improve symptoms and functional status, with the exception of parenteral prostacyclin their effects on survival are less certain and they are not curative. Since progressive lung arterial pruning is the fundamental pathological feature in PAH, a curative therapy would necessarily regenerate lost lung vasculature. In preclinical models of PAH, E-EPCs have been used to repair the lung microcirculation, with some improvements in pulmonary hemodynamics.[98,127,221] While E-EPCs were effective in preventing PAH in a monocrotaline (MCT) induced rat model,[127] ECFCs failed to improve pulmonary hemodynamics.[98,129] We hypothesize that since ECFCs act directly by engraftment and incorporation into newly formed blood vessels, this lack of efficacy is most likely due to poor survival and retention after intravenous delivery.

Encapsulation of cells creates a protective microenvironment, which can improve transplanted cell survival and increase retention at the site of injury. Single cell microencapsulation provides a temporary micro-niche for the cells during transplantation and allows the delivery of cells into the circulation as a suspension. Microencapsulation of mesenchymal stromal cells within an agarose hydrogel increased survival of suspended cells, and improved cellular retention within a rat hind limb model.[152] Microencapsulation of explant derived cardiac cells (EDCs) within nanoporous hydrogels promoted cell retention within the heart, reducing scar size and improving left ventricular ejection fraction post myocardial infarction.[160,161]

Therefore, we studied whether microencapsulation of ECFCs would result in enhanced retention of ECFCs within the lungs, leading to increased therapeutic efficacy in an experimental model of PAH. We now demonstrate increased lung retention of microencapsulated ECFCs after intravascular delivery leading to the significant reduction on pulmonary arterial pressures and remodeling in the rat MCT model, which has not been previously demonstrated with ECFCs.

3.3 Methods

3.3.1 Endothelial cell isolation and culture

Rat bone marrow ECFCs and human L-EPCs were cultured and characterized.[98] In brief, the mononuclear cell fraction of rat bone marrow or human peripheral blood was obtained by layering the cell suspension over Histopaque®-1083 (density: 1.083 g/mL, Sigma, ON, Canada) or Ficoll (density: 1.2 g/mL, Fisher Scientific, ON, Canada), respectively, followed by centrifugation at 400 g for 40 min. Mononuclear cells were collected from white layer at the interface of media (top) and Histopaque/Ficoll (bottom). Bone marrow mononuclear cells were plated in endothelial growth medium 2 + 10% fetal bovine serum (FBS) (EGM-2MV, Lonza, Switzerland) on fibronectin coated plates and cultured at 37ºC in 5% CO_2 incubators. Colonies with cells showing cobble stone-like endothelial cell morphology appeared in culture between 9 and 14 days after plating mononuclear cells. Endothelial-like colonies were isolated and further sub-cultured at 37ºC in 5% CO_2 incubators, passaging as necessary. In a separate procedure, all the cells cultured were passaged further without colony selection using the same cell culture procedure, and these cells were termed: culture modified bone-marrow cells (CM-BMCs). Otherwise, both ECFCs and CM-BMCs were processed similarly. Human umbilical vein endothelial cells (HUVEC, Lonza, Switzerland) were used in preliminary encapsulation experiments. HUVEC were cultured in endothelial growth medium 2 (EGM-2, Lonza, Switzerland) at 37ºC in 5% CO_2 incubator, passaging as necessary. Cells were used in experiments between P6 and P9.

3.3.2 Flow cytometry

Rat ECFC or human L-EPCs were harvested and passed through 40 μm cell strainer to obtain single cell suspension (500,000/100 μL). Cells were incubated with primary antibodies (**Table 3.1**) for 30 min at 4 ºC in dark. Following primary antibody, cells were washed 3 times in flow buffer followed by secondary antibody incubation for 30 min at 4 ºC in dark. Cells were washed again for 3 times with flow buffer and then analyzed using Attune® Acoustic Focusing Flow Cytometer (ThermoFisher Scientific, ON, Canada), with analysis performed using FlowJo v 8.3 (FlowJo LLC, Ashland, OR, USA).

Table 3.1: Antibody source and concentration used for flow cytometry.

Target	Species	Source	Cat#	Dilution
vWF	Rat, human	Dako	A008202-5	1:400
CD31	Human	BD Pharmingen	555446	1:100
	Rat	Novus Biologics	NB100-2284	1:50
VEGFR2	Human, Rat	Cell Signaling Technology	2479S	1:100
CD45	Human	BD bioscience	555482	1:5
	Rat	Biolegend	202207	1:50
CD34	Human	BD-Pharmingen	555822	1:5
	Rat	Santa Cruz	sc-7324	1:20
VE-Cadherin	Rat	Santa Cruz	sc-6458	1:20
CD146	Rat	R & D	MAB3250	1:50
CD14	Human	BD-Pharmingen	555398	1:5
CD73	Rat	BD-Pharmingen	551123	1:50

3.3.3 Acetylated low density lipoprotein (Ac-LDL) uptake and lectin binding

Rat ECFC or human L-EPCs (500,000/well) were plated on a 6 well plate and 24 hr later media was removed, cells were washed with PBS and incubated with DiI-Ac-LDL (10 µg/mL) for 3 hr at 37ºC in 5% CO_2 incubator. Following Ac-LDL incubation, cells were washed with PBS, harvested, and incubated with Fluorescein labeled Griffonia (Bandeiraea) Simplicifolia Lectin 1 (1:100) for 1 hr at room temperature. Following lectin binding cells were washed with PBS and fixed in 4% paraformaldehyde and analyzed by flow cytometry.

3.3.4 Matrigel network formation assay

To confirm network forming ability of rat ECFC, cells were harvested and plated on growth factor-reduced Matrigel (Corning™ Matrigel™, Fisher Scientific, ON, Canada) in 96-well flat-bottom plate in EGM-2MV media and incubated for 16 hr at 37ºC in 5% CO_2 incubator. Images were captured using TS100 microscope (Nikon, ON, Canada).

3.3.5 Lentiviral transduction

Rat ECFCs were transfected with a lentivirus construct under the murine stem cell virus (MSCV) promoter to overexpress red fluorescent protein (RFP) and luciferase. Fluorescently activated cell sorting was performed to isolate the RFP+ stably transfected cells, at the flow cytometry facility at the Ottawa Hospital Research Institute.

3.3.6 Cellular encapsulation

ECFCs or HUVEC were re-suspended in PBS (Gibco, ON, Canada) with fibrinogen (0.05 mg/ml, Sigma Aldrich, ON, Canada), fibronectin (0.005 mg/ml, Roche, Switzerland) and Pluronic F-68

(0.33%, Sigma Aldrich, ON, Canada), prior to mixing with heated ultra-low gelling agarose type XI (Sigma Aldrich, ON, Canada). The well mixed cell-hydrogel suspension was added dropwise to warm dimethylpolysiloxane (PDMS, Sigma Aldrich, ON, Canada), vortexed for 1 minute, and placed in an ice bath for 10 minutes. As previously described [152], encapsulated cells were washed with Hank's balanced salt solution (HBSS, Gibco, ON, Canada) to remove PDMS phase, and filtered to establish the encapsulated cell population.

3.3.7 Assessment of cell viability of encapsulated cells

Encapsulated cells were assessed *in vitro* for viability by WST-1 assay and Calcein AM staining. Encapsulated or adherent cells were plated in a 96 well plate for 24 or 48h when WST-1 reagent (Roche, Switzerland) was added, or Calcein AM (Invitrogen, ON, Canada) and Nuclear Blue live ready reagent (Invitrogen, ON, Canada) were added. WST-1 assay was assessed by absorbance after 2 hours with an Omega PolarStar (BMG Labtech, Germany). Live imaging was performed using a Zeiss Observer Z1 inverted microscope (Zeiss, Germany) and images were quantified using FIJI for ratio of calcein positive cells to total counted nuclei.

3.3.8 Assessment of cell migration from agarose microcapsules

Migration of encapsulated cells was performed with a Boyden chamber assay in a 24 well plate as per manufacturer's recommendations. Briefly, encapsulated cells were plated in basal media on the top and complete media containing 20% FBS was added to the bottom well. Cells were incubated for 24h. Cells were stained with Nuclear Blue live ready reagent (Invitrogen, ON, Canada) and images were acquired with the Zeiss Observer Z1 inverted microscope (Zeiss, Germany). Images were quantified as before using FIJI.

3.3.9 Monocrotaline model of PAH and cell injections and hemodynamic measurements

All animal experiments were approved by the University of Ottawa Animal Care Committee and conducted according to the guidelines from the Canadian Council for Animal Care. Female Sprague Dawley (SD) rats (150 – 175g; Charles River) were injected with monocrotaline (MCT) (50mg/kg, Sigma Aldrich, ON, Canada) by intra peritoneal (i.p.) injection three days before cell injections. For cell injections, rats were anaesthetized using isoflurane inhalation (induction: 5% isoflurane 1 L/min; maintenance: 2% isoflurane 1 L/min), right jugular vein was isolated, and the angiocath was inserted into the jugular vein. Each animal received 1,000,000 cells or vehicle (0.5 mL PBS). Following injection, topical bupivacaine was applied immediately after wound closure and twice daily for one day post-surgery. Buprenorphine (s.c., 0.03mg/kg) was administered 1 hour prior to surgery and once daily for two days post-surgery for pain management. At 24 days post MCT animals were anaesthetized by an i.p. injection of ketamine (35 mg/kg) and xyalzine (7 mg/kg) and the right ventricular systolic pressure (RVSP) was measured, as previously described. [64,127] The lungs and heart were harvested for histology and protein, and the ratio of right ventricle (RV) to left ventricle plus septum (LV+S) was measured, as previously described.[64,127]

3.3.10 Cell retention analysis by qPCR

To study cell retention, we injected male cells into female rats and assessed cell retention using qPCR for sex-determining region of Y chromosome (Sry) gene. Briefly, female rats were subjected to MCT model and on day-3 male ECFCs were injected. Samples were collected at 15 min and 21 days after ECFCs injection. DNA was extracted from lung samples and 5,000,000 male ECFCs using DNeasy Blood & Tissue Kit (Qiagen, ON, Canada) and quantified using Quant-iT™ PicoGreen™ dsDNA Assay Kits (ThermoFisher Scientific, ON, Canada). Standard curve of different ratios of male ECFC DNA to female rat lung DNA was prepared (1, 0.1, 0.001, 0.0001 ng/1000 ng total DNA) and final sample DNA concentration was adjusted to 125ng DNA/μL. qPCR analysis of standards and samples was performed using QuantiTect SYBR Green PCR Kit (Qiagen, ON, Canada) as per manufacturer's recommendation using primers for amplifying Sry gene (Sry Forward- AAGTCAAGCGCCCCATGA, Sry reverse-TGAGCCAACTTGTGCCTCTCT). Amount of male DNA in total DNA of lung samples was calculated from standard curve and used to quantify cell retention.

3.3.11 Assessment of the effect of encapsulated ECFCs in MCT model

SD rats were treated with MCT and, ECFCs (300,000 cells in 0.5 mL PBS), encapsulated-ECFCs (300,000 cells in 0.5 mL PBS) or empty capsules (equivalent to 300,000 encapsulated cells in 0.5 mL PBS) were injected through jugular vein as described above. The dose of capsulated cells was lowered as higher dose of capsules were not tolerated by MCT treated rats.

3.3.12 In vivo bioluminescent imaging

At 0, 4 and 24 hr post cell injection (**Supplemental Figure 3.1**), animals were injected with D-luciferin (150 mg/kg, ip; Biovision, CA, USA). These animals were subsequently anaesthetized by isoflurane and imaged using the IVIS spectrum (PerkinElmer, MA, USA) at the University of Ottawa Preclinical Imaging Core (RRID:SCR_021832). Animals were euthanized before subsequent open chest and *ex vivo* lung images were taken to account for the thickness of the rat's tissue. Bioluminescent imaging (BLI) was quantified using Living Image 2.0 software (PerkinElmer, MA, USA).

3.3.13 Immunohistochemistry

As previously described,[64] lungs were inflated with 1:1 ratio of OCT:Saline and fixed in 4% paraformaldehyde solution (Electron Microscopy Science, PA, USA) before dehydration and paraffin embedding. Sections of fixed lung tissue (5µm thickness) were cut and stained with hematoxylin (Vector Laboratories, CA, USA) and eosin (ThermoFisher Scientific, ON, Canada) using standard protocol. Alternatively, sections were blocked with 2% goat serum (Rockland Immunochemicals, PA, USA) and stained with primary rabbit anti-firefly luciferase antibody (Abcam, Cambridge, UK) 1:100 overnight at 4ºC followed by Alexa Fluor 594 goat-anti rabbit secondary antibodies (Invitrogen, ON, Canada) at 1:400 for 1 hr at room temperature. Immunofluorescent images were analyzed with a Zeiss M2 (Zeiss, Germany) and prepared with FIJI. Analysis of vascularization was done by grading blood vessels that were non-muscularized (0), partially muscularized (1), or fully muscularized (2), representative images shown in **Supplemental Figure 3.2**, as previously performed.[98] All vessels were counted and assessed in one lung section per animal by a blinded reviewer.

3.3.14 Statistical Analysis

All data are presented as means ± SEM. Differences between groups were analyzed by one-way analysis of variance (ANOVA), with appropriate post-hoc comparisons. A p-value of $p<0.05$ was considered significant. All statistical analysis was performed with Graph Pad Prism 7.0 (Graph Pad, CA, USA).

3.4 Results

3.4.1 Microgel encapsulation supports endothelial cell survival

The vortex emulsion method was optimized using HUVECs and we compared cells encapsulated in 2 to 5% agarose capsules supplemented with or without fibronectin and fibrinogen (**Figure 3.1A**). The resulting microcapsules were heterogeneous in size, ranging from 10 – 70 µm in diameter. Higher concentrations of agarose (5%) produced larger capsules compared to lower concentrations of agarose (2%) (**Figure 3.1B**). Next, we evaluated the effect of agarose concentration on cell survival and egress from the capsule as these are important characteristics for the effectiveness of cell therapy. We observed decreased cell egress over 24 hours from capsules with increasing agarose concentration (**Figure 3.1C**). These data suggest that the stiffer hydrogels delayed the egress of cells. The concentration of agarose had no significant impact on cell survival under normal condition, as assessed by WST-1 assay and CalceinAM staining (**Figure 3.1D,E**; respectively). However, in response to serum starvation, conditions that better reflect those that cells are exposed to during cell transport and delivery, cells encapsulated in 3.5 and 5% agarose exhibited superior survival compared to adherent cells (28% vs 71% reduction, respectively) (**Figure 3.1F**). Based on these results and previous work,[161] 3.5% agarose capsules were used for the *in vivo* studies.

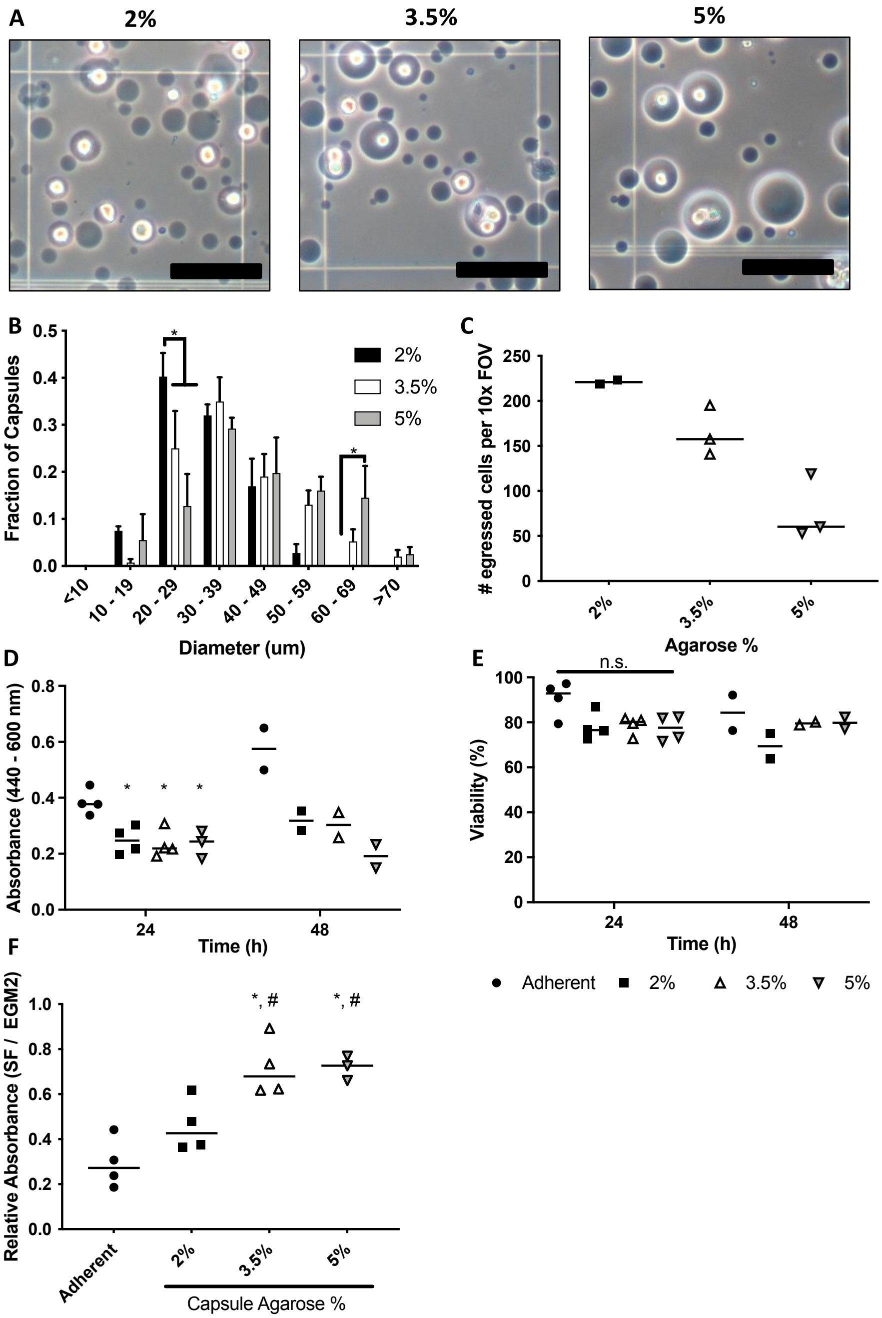

Figure 3.1: Varied agarose concentration has minimal effect on cell viability.
(A) Representative phase contrast images of encapsulated cells in 2-5% agarose microgels, scale bars represent 100 µm. (B) Capsules containing cells appear to increase in diameter with increasing concentration of agarose in the hydrogel mixture. (C) Higher concentrations of agarose capsules appears to slow migration of cells from the capsules. Viability was unaffected by agarose capsule concentration as assessed by (D) WST-1 assay and (E) CalceinAM staining. Capsules provided a protective niche during 24h culture in serum free condition, shown by (F) raw WST-1 absorbance and (G) reduction in absorbance. Scale bar represents 100µm, * represents $p < 0.05$ vs adherent, # represents $p < 0.05$ vs 2% agarose. Data represents means ± SEM, n = 2-4.

3.4.2 ECFCs were ineffective in severe pulmonary arterial hypertension

Rat ECFCs were isolated from the SD rat bone marrow and displayed typical endothelial growth characteristics. Cell morphology and surface markers of ECFCs were compared to human L-EPCs and CM-BMCs (**Figure 3.2**). ECFCs displayed a cobblestone morphology when cultured on plastic similar to that of L-EPCs and HUVECs (**Figure 3.2A**) whereas CM-BMC exhibited more mesenchymal cell morphology. ECFCs demonstrated significant proliferative potential *in vitro* (**Supplemental Figure 3.3**). Furthermore, human L-EPCs and rat ECFCs shared common endothelial characteristics including uptake of ac-LDL, lectin binding, and expression of vWF and CD31. Rat ECFCs additionally expressed vascular endothelial cadherin, and low levels of vascular endothelial growth receptor 2 (VEGFR2), CD146, and CD34 (**Figure 3.2B**). Moreover, human L-EPCs and rat ECFCs completely lacked markers of leukocyte or monocyte cell lineage such as CD45 and CD14 (**Figure 3.2B**). Importantly, while CM-BMCs did exhibit some endothelial features (acLDL uptake, lectin binding and low vWF expression), they expressed the mesenchymal marker, CD73. These data confirm the endothelial identity of ECFCs and suggest that selection of cells is required to avoid contamination of mesenchymal-like cells from bone marrow.

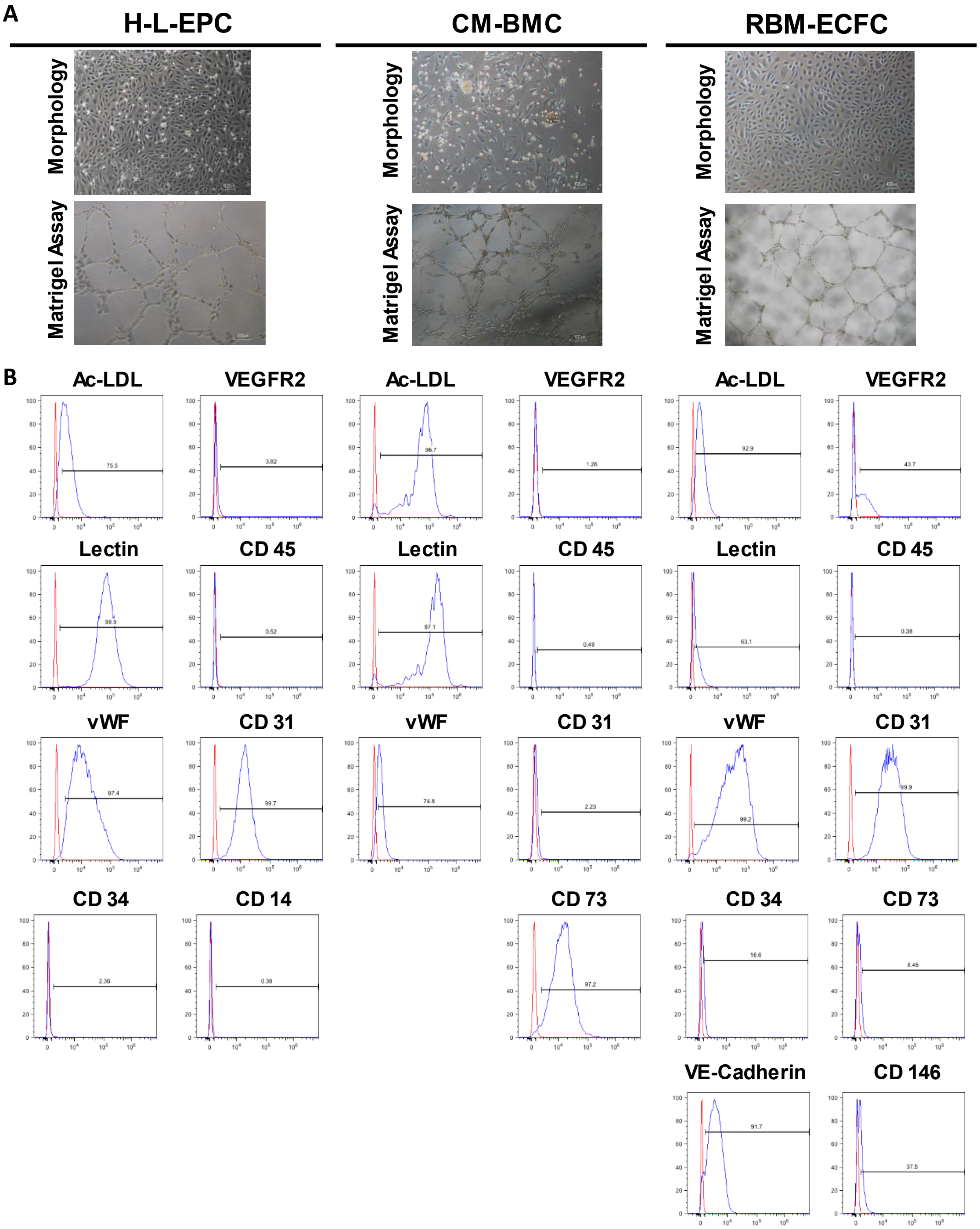

Figure 3.2: Rat ECFCs share morphology and surface markers with human L-EPCs. (A) Representative images of human L-EPC, rat CM-BMC, and rat ECFCs demonstrating the cobblestone morphology commonly observed in cultured endothelial cells. (B) Surface marker characterization by flow cytometry demonstrating the similarities between human and rat derived L-EPCs positive for ac-LDL, lectin, von Willebrand Factor, and CD31, while negative for CD45. The red line depicts isotype control and blue line represents staining with specific marker.

Next, we assessed the therapeutic efficacy of ECFCs in the MCT model of PAH. ECFC were delivered by intrajugular vein injection (1,000,000 cells) 3 days after MCT. Compared with vehicle control (PBS), treatment with ECFCs resulted in no detectable improvements in RVSP or RV remodeling at day 24, 3 weeks after cell delivery (**Supplemental Figure 3.4**). We assessed retention of the cells in the lungs by qPCR. At 15 minutes, we observed 80% retention of cells in the lungs; however, at the end study, cells were not detectable suggesting poor retention of syngeneic ECFCs following injection (**Supplemental Figure 3.4**).

3.4.3 Encapsulation of ECFCs increased their retention within the lungs of MCT treated rats

To enhance the survival and retention of ECFCs, we performed microencapsulation in 3.5% agarose. A dose of 300,000 ECFC loaded microgels were injected by intrajugular vein injection. Bioluminescent imaging allowed tracking of live cells containing luciferase luminescent reporter. The baseline signal within 30 minutes of cell injection was comparable between encapsulated and non-encapsulated ECFC treated animals; however, the signal for non-encapsulated cells was rapidly lost within 4 hours of cell injection and there was no detectable signal with either live or *ex vivo* imaging (**Figure 3.3A,B**). In contrast, encapsulated ECFCs could be detected up to 24 h post cell injection (**Figure 3.3A,B**), but not after 72 h even with *ex vivo* imaging. The retention of encapsulated cells was further verified by H&E and immunohistochemical staining with anti-luciferase antibody at 4h and up to 72h (**Figure 3.3C,D**). Additionally, empty capsules were found to persist *in vivo* for up to 21 days (**Supplemental Figure 3.5**). Therefore, encapsulation of ECFCs lead to a significant prolongation of lung retention in monocrotaline-treated rats.

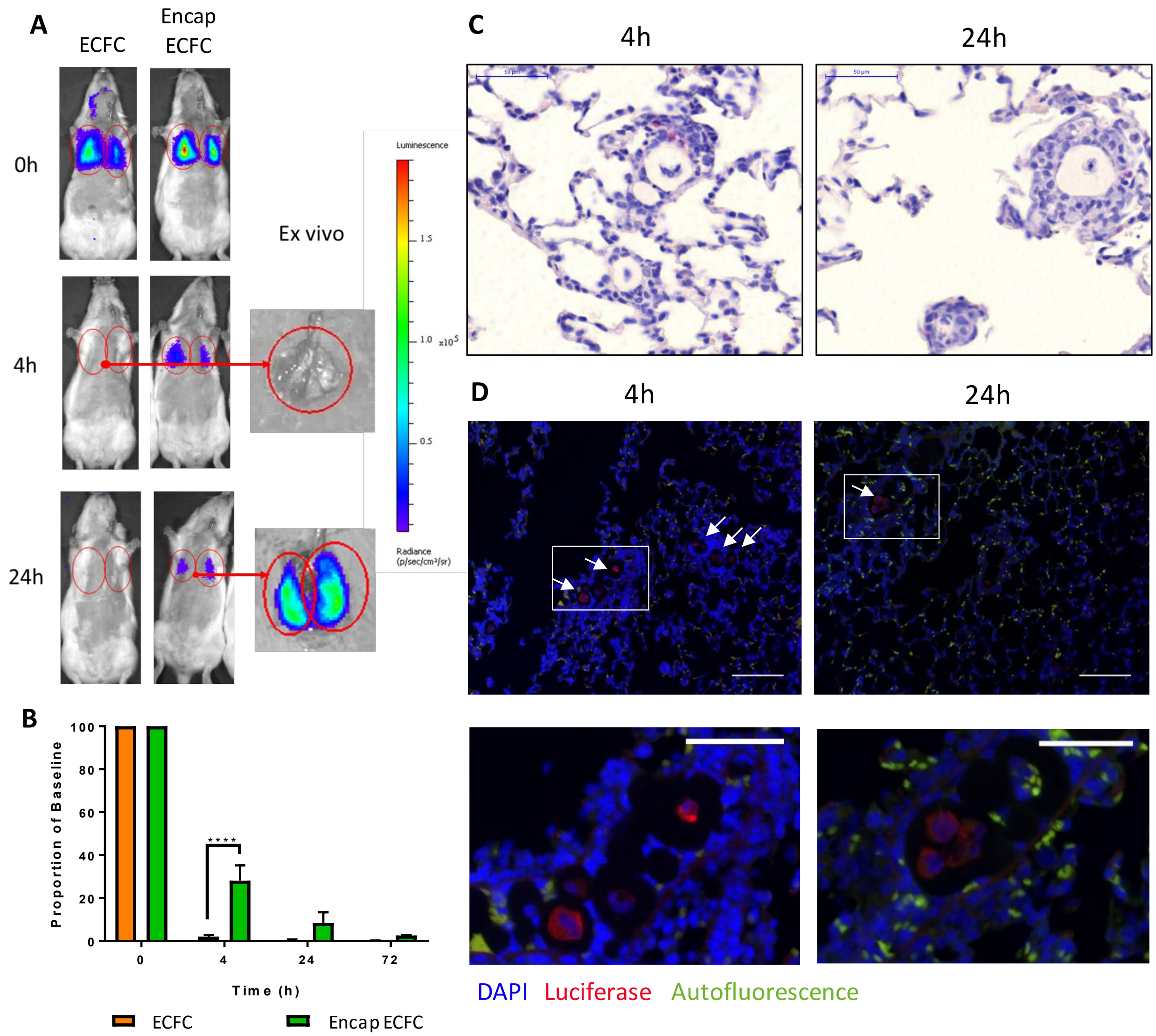

Figure 3.3: Encapsulated ECFCs are retained significantly longer than non-encapsulated cells. (A) Representative images of the bioluminescent signal emitted by luciferase transfected ECFCs 15 minutes after luciferin injection, including *ex vivo* images of lungs containing encapsulated cells. The encapsulated cells were detectable in the lungs up to 24h whereas non-encapsulated cells were cleared after 4h and not detectable even with *ex vivo* imaging. (B) The proportion of the baseline signal demonstrates at 24h ~10% of the encapsulated cells were detectable by bioluminescent imaging. Representative images of encapsulated cells with H&E (C) (scale bar – 50um) or stained with anti-luciferase antibody (red), DAPI (blue), and auto fluorescence overlap (green) (D) at 4 and 24h post injection (scale bar – 100µm, or 50µm for zoomed image, demonstrating persistence of encapsulated cells *in vivo*. Data represented as mean ± SD, n =3-4.

3.4.4 Encapsulated ECFCs prevented the onset of severe PAH and improved lung vascular morphology

Animals were followed for 24 days post MCT injection to assess the effect of cell delivery of pulmonary hemodynamics and vascular remodelling. No significant survival difference between ECFC treated rats and PBS treated rats was observed. Survival was also similar for rats treated with empty capsules or encapsulated ECFCs. Importantly, a trend towards lower survival in the groups treated with capsule was evident compared to the groups receiving capsules (empty capsules compared to PBS and encapsulated ECFCs compared to ECFCs). The only significant difference in survival was observed between ECFCs treated rats and empty capsules (**Figure 3.4A**). Again, animals treated with non-encapsulated ECFCs showed no improvement in RVSP or RVH compared to control-vehicle treated animals (**Figure 3.4B,C**). However, animals receiving encapsulated ECFCs demonstrated a significant improvement in RVSP ($p < 0.05$) compared to rats treated with vehicle control or empty capsules (**Figure 3.4B**). MCT-induced pulmonary hypertension was associated with arterial muscularization with an increase in the ratio of partially (33.8%) and fully (60.3%) muscularized vessels (**Figure 3.4D,E**). Non-encapsulated ECFCs or empty capsules had no effect on the severity of arterial muscularization. In contrast, treatment with encapsulated ECFCs significantly reduced muscularization (**Figure 3.4D**), yet no changes in overall lung vasculature were observed by MicroCT (**Supplemental Figure 3.6**). Taken together, these data suggest that the modest increase in retention of ECFCs resulting from microencapsulation was sufficient to uncover a therapeutic benefit in a model of PAH.

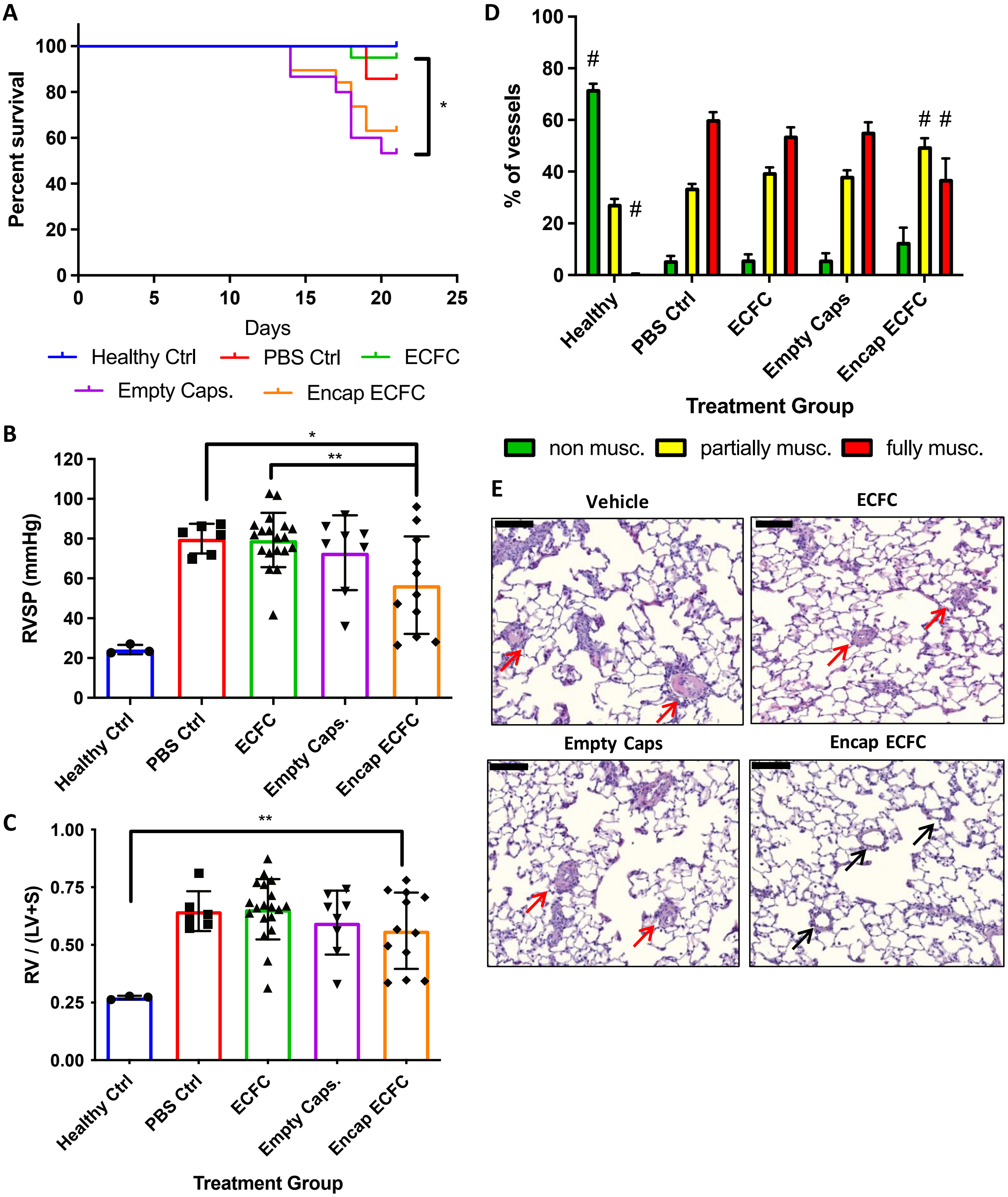

Figure 3.4: Capsules may be detrimental in animal survival, yet encapsulated ECFCs provided a therapeutic benefit to preventing development of severe PAH.
(A) Survival curve demonstrating a slight detrimental effect of capsules on animal survival. (B) RVSP and (C) RVH for all surviving animals demonstrate the beneficial effect offered by encapsulated ECFCas in preventing the onset of severe PAH. (D) Severity of muscularization was graded and assessed to be (0) non-muscularized, (1) partially muscularized, or (2) fully

muscularized, where animals treated with encapsulated ECFCs had fewer fully muscularized blood vessels, # represents $p < 0.01$ vs PBS ctrl. (E) Representative images of H&E stained histological sections demonstrating severe muscularization of blood vessels (red arrows) 24 days post MCT in animals treated with PBS vehicle, ECFCs, and empty capsules, whereas animals treated with encapsulated ECFCs had improved vascular remodelling (black arrows). Scale bar represents 100µm. Data represented as means ± SEM, n = 3 – 20 for panels A, B, and C, n = 3 (Control) – 5 (Treatments) for Panels D and E.

3.5 Discussion

ECFCs have tremendous promise for the treatment of vascular diseases due to their exceptional proliferative and angiogenic potential. ECFCs have been successfully used to repair and regenerate vasculature in many cardiovascular diseases[222] Therefore, it is surprising that ECFCs have failed to be effective in preclinical models of PAH,[98,129] despite the critical role of arterial pruning in its pathogenesis.[164] However, unlike E-EPCs which act nearly exclusively by paracrine mechanisms, ECFCs (or L-EPCs) are thought to act directly to regenerate blood vessels by engraftment and differentiation.[214] Thus, the lack of cell persistence in the lung after intra venous delivery may be a major limitation to their potential repair of the lung arterial bed through direct integration. Therefore, we investigated whether a strategy to enhance the retention of ECFCs within the lungs would enhance their therapeutic potential using single cell microencapsulation.

Microencapsulation of cells within agarose hydrogels supplemented with fibrinogen and fibronectin offers a protective niche for the cells during transplantation. Similar strategies have been employed with MSCs,[152] and EDCs for myocardial infarction.[160,161] By incorporating integrin binding proteins it creates a protective niche within the hydrogel preventing anoikis and enhancing cell survival.[152] In this report, we investigated the impact of hydrogel concentration for ECs encapsulation, to maintain cell viability under serum starved conditions, while allowing cell migration from capsules. Unlike macro-encapsulation that aims to permanently isolate cells from the host immune cells,[223] single-cell microencapsulation provides a temporary shield to protect the cells during the traumatic effects of transplantation, yet allows cell egress within the first few days. The size of the cell-loaded microgels allows for ease of delivery by intravenous injection. There is also evidence that microencapsulation can promote increased paracrine secretions compared in 2D cell culture or bulk encapsulation systems[224] providing additional benefits to this delivery system.

Moreover, microencapsulation of ECFCs improved local retention of cells within the lungs, since even the smallest capsules were too large to traverse through the lung capillary bed and most would be retained within pre-capillary arterioles. In contrast, free ECFCs were rapidly cleared from the lungs within 4h of injection. We observed that the increase in retention of microencapsulated ECFCs within the damaged lung unmasked a therapeutic effect in the MCT model of PAH that was not evident with cells alone. Considering that the dose of microencapsulated ECFCs was only 300,000, compared to previous studies delivering up to 1.5 million free cells,[98] this strongly supports the critical importance of ECFC retention for enhancing therapeutic effects. Although, the capsules provided short term improvement in ECFC retention, there was no evidence of cell persistence beyond 72 hours, whereas empty capsules could be found in the lung for at least three weeks post injection. This suggests that cells did not remain in capsules indefinitely, and either egressed from the capsules or underwent apoptosis after several days. However, even if a substantial proportion of cells exited the capsules, they did not persistent in the lung in sufficient numbers to be detectable by bioluminescent imaging, implying that the observed benefit may have involved paracrine mechanisms. Indeed, microencapsulation has previously been shown to enhance the paracrine effects of both MSCs and EDCs.[161,224]

There are some limitations of our study. Despite the ease of encapsulation using the vortex-emulsion method, the capsules produced are heterogenous in size and many do not contain cells. Additionally, the current capsule formulation persists within the lungs for prolonged periods. The persistence of these capsules *in vivo*, and the variability in size, likely contributes to a weak trend toward worsening survival. It is possible that this could be due to a detrimental effect of the agarose hydrogel. For example, capsules with diameters above 50µm could block larger arterioles, thereby aggravating the underlying pruning of the arteriolar bed seen in this model, possibly explaining why there was no improvement in lung arterial architecture by micro-CT. This might be avoided by using a microfluidic technique to generate more homogeneous capsules and reduce the number of empty capsules.[224,225] Reduction in capsule size heterogeneity, ratio of encapsulated cells to empty capsules, and degradability may allow larger doses of capsules to further enhance the therapeutic efficacy of this technology. Furthermore, optimization of the biomaterial composition could reduce the inflammatory response and allow enhanced degradability of the matrix for use in pulmonary vascular regeneration.[226]

This study represents a proof-of-principle for the potential of microencapsulation technology to enhance the efficacy of ECFCs for treatment of PAH. Our microencapsulation strategy increased lung retention of ECFCs compared to the non-encapsulated controls. Furthermore, short term increases in retention resulted in hemodynamic improvement in the MCT model of PAH, although there is room to improve this approach by further optimizing the consistency and biocompatibility of the hydrogel capsules.

3.6 Authorship Contributions

NDC has contributed to all aspects of this work including conception, cell encapsulation optimization, performing experiments, data analysis and preparation of this manuscript. KR contributed equally to this work including conception, initial cell isolation and characterization, experimental work, data analysis and manuscription preparation. YD and KR were involved with all animal studies. CJL designed and prepared all viral vectors used for bioluminescence cell tracking. DWC contributed to conception of the encapsulation platform, and interpretation of results. DJS was involved the conception and design of experiments, data analysis and interpreting results, and drafting this manuscript. DJS is accountable for all aspects of this work.

3.7 Acknowledgements

The authors would like to thank Anli Yang for her assistance with all animal work.

3.8 Sources of Funding

This work was supported by a Foundation award from the Canadian Institute of Health Research (FDN – 143291) held by DJS. NDC acknowledges scholarship funding from the Canadian Institute of Health Research, and the Canadian Vascular Network. KRC received postdoctoral fellowship from the Heart and Stroke Foundation of Canada and Canadian Vascular Network.

3.9 Disclosures

None

Chapter 4: Targeting extracellular vesicle delivery to the lungs by microgel encapsulation

Nicholas D. Cober[1,2], Katelynn Rowe[1], Yupu Deng[1], Ainara Benavente-Babace[3], David W. Courtman[1], Michel Godin[3], Duncan J. Stewart[1,2]

[1] Sinclair Centre for Regenerative Medicine, Ottawa Hospital Research Institute, Ottawa, ON, Canada
[2] University of Ottawa, Faculty of Medicine, Department of Cellular and Molecular Medicine, Ottawa, ON, Canada
[3] University of Ottawa, Faculty of Science, Department of Physics, Ottawa, ON, Canada

ORCID IDs:
NDC: 0000-0001-8061-806X
DWC: 0000-0002-6403-271X
MG: 0000-0002-9360-0675
DJS: 0000-0002-9113-8691

Corresponding author: Duncan J Stewart, djstewart@ohri.ca.
Executive Vice-President Research, The Ottawa Hospital; CEO & Scientific Director,
Ottawa Hospital Research Institute; The Evelyne & Rowell Laishley Chair and
Professor, Department of Medicine, University of Ottawa
501 Smyth Road, Box/C.P. 511, Ottawa, ON, K1H 8L6
613-739-6686

Author Contributions

NDC has contributed to all aspects of this work including conception, performing the experiments, data analysis and preparation of this manuscript. KR and YD were involved with all animal studies. KR contributed technical knowledge and helped perform the biodistribution and *in vivo* digestion flow cytometry experiments. ABB and MG contributed expertise for the operation and maintenance of the microfluidic encapsulation device. DWC contributed to conception of the encapsulation platform, and in interpretation of results. DJS was involved in the conception and design of experiments, data analysis and interpreting results, and drafting this manuscript.

4.1 Abstract

Extracellular vesicles (EVs) secreted by stem and progenitor cells have significant potential as cell-free ‘cellular’ therapeutics. Yet, small EVs (<200 nm) are rapidly cleared after systemic administration, mainly by the liver, presenting challenges targeting EVs to a specific organ or tissue. Microencapsulation using natural nano-porous hydrogels (microgels) has been shown to enhance engraftment and increase the survival of transplanted cells. We sought to encapsulate EVs within microgels to target their delivery to the lung by virtue of their size-based retention within the pulmonary microcirculation. Mesenchymal stromal cell (MSC) derived EVs were labelled with the lipophilic dye (DiR) and encapsulated within agarose-gelatin microgels. Endothelial cells and bone marrow derived macrophages were able to take up EVs encapsulated in microgels *in vitro*, but less efficiently than the uptake of free EVs. Following intrajugular administration, microgel encapsulated EVs were selectively retained within the lungs for 72 hours, while free EVs were rapidly cleared by the liver. Furthermore, microgel loaded EVs demonstrated greater uptake by lung cells, in particular CD45+ immune cells, as assessed by flow cytometry compared to free EVs. Microencapsulation of EVs may be a novel tool for enhancing targeted delivery of EVs for future therapeutic applications.

Subject Keywords: Extracellular vesicles; biodistribution; biomaterials; microencapsulation; pulmonary circulation

4.2 Introduction

There is increasing evidence that extracellular vesicles (EVs) play an essential role in cell-to-cell communication.[227] EVs are nano-sized membrane bound particles loaded with proteins, mRNAs, and miRNAs from their host cell which provide important signaling cues to their recipient cell.[227] EVs can be categorized based on their size; small EVs are <150nm in size likely contain the exosome fraction of endosomal origin, whereas EVs between 150-1000nm contain primarily microvesicles.[142] Mesenchymal stromal cells (MSCs) represent a multi-faceted therapeutic cell with important angiogenic and immunomodulatory potential and have been reported to have therapeutic effects in a number of models of cardiovascular disease.[228] The actions of MSCs are thought to be mediated largely by paracrine mechanisms, in particular related to the release of therapeutic EVs.[229] Therefore, there is considerable interest in developing MSC derived EVs, particularly small EVs, as a cell-free 'cellular' therapeutic product.[229] In fact, MSC-EVs have been studied as a therapy for a variety of cardiovascular diseases including pulmonary arterial hypertension (PAH)[135,136,140], acute myocardial infarction[136,230], acute lung injury[231], and broncho-pulmonary dysplasia[232].

EVs have a number of potential advantages over intact cells. EVs have the potential to mirror the benefits of cell-based therapies without some of the risks associated with delivery of intact cells, including tumorigenicity, immunoreactivity, product shelf life, and viability.[233] As MSC-EVs are cell by-products they are unable to replicate and cannot directly form tumors. Furthermore, the transplantation of allogenic cells presents a risk of immunoreactivity from foreign antigens, whereas EVs derived from MSCs generally lack components of the major histocompatibility complex.[234] Finally, unlike intact cells where efficacy is dependent on cell viability that can be lost during storage,[235] EVs possess good long term stability at -80°C[236] and do not have post thaw viability requirements that may hinder their use.

However, unlike intact cells which can be used to target the lung through size-based filtration in the distal lung arteriolar bed, small EVs, in the nanometer range, would not be expected to lodge in the precapillary arteriolar bed and are rapidly cleared from the circulation by the liver and spleen[146,148], limiting their therapeutic potential. Indeed, Gupta et al. have shown in a pharmacokinetic study that EVs have a very short half-life *in vivo* and are cleared from the blood within minutes of delivery.[147] Furthermore biodistribution may be impacted by cell origin; while EVs from many cell types largely accumulate in the liver and spleen,[148] EVs derived from breast cancer cells may preferentially target the lung,[149] as well as by modifications, such as glycosylation,[150] or genetic modification.[237]

Biomaterials are commonly used to create cell compatible microenvironments, promoting cell viability and facilitating transplantation,[153] and can be engineered to target distribution to a particular organ. Microencapsulation can enhance local organ retention of intact cells[152] and has been shown to promote therapeutic outcomes in experimental models of acute myocardial infarction.[161] More recently, bulk EV encapsulation has been used to create large regenerative tissue patches for cardiac repair[162]. Despite relatively poor lung uptake after intravascular delivery[148], EVs have been shown to be effective in the treatment of preclinical models of pulmonary arterial hypertension (PAH).[238] Therefore, the objective of this study was to determine whether microencapsulation of EVs within nanoporous hydrogels (microgels) would increase lung targeting in the monocrotaline (MCT) preclinical model of (PAH). We hypothesized that microencapsulation of EVs would enhance local EV retention within the diseased lung, facilitating increased cellular uptake. We now report markedly enhanced retention of EV-loaded microgels within the lungs as compared to free EVs, with enhanced local cellular uptake, supporting the use of microencapsulation as a novel strategy to efficiently target EVs to the lung.

4.3 Methods

4.3.1 Mesenchymal stromal cell culture and extracellular vesicle isolation

Sprague Dawley rat bone marrow mesenchymal stromal cells (MSCs) were isolated from rat bone marrow as previously described[239] or acquired from Cyagen (Cyagen Bioscience, Santa Clara, CA, USA). Isolated rat bone marrow MSCs were cultured in alpha MEM (ThermoFisher Scientific, Burlington ON, Canada) with 10% fetal bovine serum (ThermoFisher Scientific, Burlington ON, Canada) and 1% pencilin/streptomycin (Life Technologies, Carlsbad, CA, USA), Cyagen sourced MSCs were cultured in StemXVivo mesenchymal stem cell expansion media (R&D systems, Toronto, ON, Canada) inside tissue culture incubators at 37°C with 5% CO_2, passaging as necessary.

4.3.2 Extracellular vesicle isolation and labelling

MSCs between passage 3 and 5 were used for EV isolations. For EV isolation, MSCs were cultured to 80-90% confluency, washed 2x with PBS and changed to serum free alpha-MEM

(Invitrogen, Waltham, MA, USA) with 1% pencilin-streptomycin for 24h collection period. After 24h, MSC-conditioned media was collected and purified using sequential ultracentrifugation and tangential flow filtration (TFF) (KrosFlow KR2i, Repligen, Waltham, MA, USA). Since TFF coupled with ultra-centrifugation may lead to co-precipitation of protein aggregates, we were careful to apply consistent production processes in these experiments to minimize any confounding effects from uptake of protein aggregates. In brief, conditioned media (CM) was spun at 2500g for 10min at 4°C, the supernatant was then spun at 20,000g for 20min at 4°C. The resulting conditioned media was processed by TFF to remove small protein and particles with a 500,000 MWCO MidGee hoop ultrafiltration cartridge (GE Lifesciences, Vancouver, BC, Canada). Diafiltration was performed with sterile filtered PBS and concentrated sample was collected. To further purify small EVs, conditioned media was spun at 100,000g for 30min at 4°C and pellets were resuspended in sterile PBS. For DiR (ThermoFisher Scientific, Burlington, ON, Canada) and DiD (ThermoFisher Scientific, Burlington, ON, Canada) labelling, concentrated EVs from the TFF were stained with DiR or DiD at 0.5 µg/ml for 15min then spun at 100,000g for 30min at 4°C to wash unbound dye and pellets were resuspended in PBS. For pkh26 (Sigma Aldrich, Oakville, ON, Canada) labelling, concentrated EV fraction following TFF was spun at 100,000g for 30min at 4°C, and pellets were resuspended in dilutant C. pkh26 (0.002mM; Sigma Aldrich, Oakville, ON, Canada) was added for 15 min following which sample was spun at 100,000g for 30min at 4°C to concentrate and wash the EV fraction. Labelled EVs were resuspended in PBS, aliquoted and stored at -80°C until use.

4.3.3 Extracellular vesicle characterization

MSC derived small EVs were characterized for protein concentration using the bicinchoninic acid (BCA) assay (Sigma Aldrich, Oakville, ON, Canada). Nanoparticle tracking analysis was performed using ZetaView (Particle Metrix, Mebane, NC, USA) to determine particle number and size distribution. Western blot was performed to confirm presence of canonical EV protein markers CD63, CD9, TSG101, or negative selection marker GM-130. Samples were lysed in 1x RIPA buffer (Millipore, CA, USA) + Halt protease inhibitors (ThermoFisher Scientific, Burlington, ON, Canada) with sonication and vortexing for protein quantification, as above. Loading buffer was added and samples were heated at 70°C for 10min. Samples (10-15µg protein/lane) were run by electrophoresis on pre-cast SDS-Page Stain Free Gels (Bio-Rad, Hercules, CA, USA). Separated proteins were transferred to low fluorescence PVDF membranes using the TransBlot Turbo (Bio-Rad, Hercules, CA, USA), and blocked in TBS-T (TBS with 0.1% Tween 20) with 5 % non-fat dry milk for 1h at room temperature. Membranes were washed 5x times with TBS-T and stained overnight at 4°C with gentle agitation with primary antibodies: mouse anti-rat CD63 (1:200 dilution, BD Biosciences, Mississauga, ON, Canada), rabbit anti-rat CD9 (1:500 dilution, ThermoFisher Scientific, Burlington, ON, Canada), rabbit anti-rat TSG101 (1:500 dilution, ThermoFisher Scientific, Burlington, ON, Canada), or rabbit anti-mouse GM-130 (1:500 dilution, ThermoFisher Scientific, Burlington, ON, Canada). After washing membranes 5x in TBS-T membranes were incubated with appropriate horseradish peroxidase (HRP)-conjugated secondary antibodies (1:5000, Jackson ImmunoResearch West Grove, PA, USA) for 1h at room temperature. Clarity Western ECL (Bio-Rad, Hercules, CA, USA) was used to detect HRP signal imaging with ChemiDoc MP imaging system (Bio-Rad Hercules, CA, USA). Images were analyzed with Image Lab v6 (Bio-Rad, Hercules, CA, USA). Data shown in **Supplemental Figure 4.1**.

4.3.4 HUVEC uptake experiments

Human umbilical vein endothelial cells (HUVEC) were cultured in endothelial cell (EC) growth media with 5% FBS, 1% pen/strep and supplements (ScienCell, Carlsbad, CA, USA), in a tissue culture incubator at 37°C with 5% CO_2, passaging as needed. HUVEC between passages 4 and 6 were used for experiments. HUVEC were seeded at 100,000 cells/ well in a 6 well plate (Corning, Corning, NY, USA), after 24h DiR or DiD labelled free EVs were added at 1μg or 3μg of EV protein. After 24h of uptake, cells were washed with PBS, lifted with trypLE (Life Technologies, Carlsbad, CA, USA), and resuspended in PEB: PBS + 2mM EDTA (ThermoFisher Scientific, Burlington, ON, Canada) + 0.5% bovine serum albumin (BSA, Wisent Bioproducts, Saint-Jean-Baptiste, QC, Canada). Cells were counted, washed, and resuspended in staining buffer containing: 1:100 dilution V450 mouse anti-human CD31 (BD Biosciences, Mississauga, ON, Canada), 1:10 dilution PE mouse anti-human CD34 (BD Biosciences, Mississauga, ON, Canada), for 30min at 4°C in the dark. Appropriate unstained, fluorescent minus one (FMOs), and compensation controls were prepared. Following staining cells were washed with PEB and loaded into 5ml flow tube (Corning, Corning, NY, USA) for flow analysis on the Attune NXT (ThermoFisher Scientific, Burlington, ON, Canada), or the AMNIS ImageStream X (Luminex, Austin, TX, USA) for intracellular visualization. Subsequent analysis was performed in FlowJo version 10 (FlowJo LLC, Ashland, OR, USA).

4.3.5 Bone marrow derived macrophage isolation, characterization, and uptake

Rat bone marrow derived macrophages were derived, as adapted from Souza-Moreira et al.[240] Rat bone marrow was isolated, mononuclear cells were counted, and frozen in 90% heat inactivated (HI) FBS (ThermoFisher Scientific, Burlington, ON, Canada) + 10% DMSO (Sigma Aldrich, Oakville, ON, Canada). Rat bone marrow mononuclear cells were thawed and cultured at 4-6 million in a 10 cm dish (Falcon) using differentiation media containing: DMEM (ThermoFisher Scientific, Burlington, ON, Canada), 20% HI FBS, 1% Pen/strep, 1% Glutamax (ThermoFisher Scientific, Burlington, ON, Canada), and 20 ng/ml macrophage colony stimulating factor (MCSF, Sigma Aldrich, Oakville, ON, Canada) in a tissue culture incubator at 37°C, 5% CO_2. Additional media was added after 3-4 days. After 6-7 days macrophages were lifted using cold PBS and scraping then counted. Bone marrow derived macrophages were plated at 1 million per well, in a 6 well plate in DMEM + 10% HI FBS, 1% Pen-strep, 1% glutamax with or without LPS (50 ng/ml, Sigma Aldrich, Oakville, ON, Canada) + interferon gamma (IFNγ, 5 ng/ml PeproTech Inc., Cranberry, NJ, USA) or interleukin 4 (IL4, 10 ng/ml, PeproTech Inc., Cranberry, NJ, USA) stimulation. Macrophages were characterized for presence and absence of canonical markers using flow cytometry PE-Cy5 mouse anti-rat CD45 (BD Biosciences, Mississauga, ON, Canada), BV786 mouse anti-rat CD11b/c (BD Biosciences, Mississauga, ON, Canada), and PE mouse anti-rat CD34 (Novus Biologicals, Littleton, CO, USA) (**Supplemental Figure 4.2**). For uptake experiments macrophages were cultured, lifted, and plated for 24h of stimulation with or without LPS+IFNγ. Subsequently, macrophages were washed with PBS, and fresh media was added with or without IL4, and DiR labelled EVs at 1µg of EV protein. After 24h macrophages were lifted, washed, counted, and stained. Staining was performed with 1:200

dilution eFluor 450 mouse anti-rat CD45 (eBioscience, San Diego, CA, USA), and FITC mouse anti-rat CD86 (eBioscience, San Diego, CA, USA), for 30min at 4°C in the dark. Following which cells were washed and analyzed by flow cytometry as previously described.

4.3.6 Microfluidic EV encapsulation

Extracellular vesicles were encapsulated using a novel microfluidic device designed for cell and small particle encapsulation, in a similar manner as described for cell encapsulation[225,241]. A known quantity of EV protein (10-20µg) was mixed with 1% ultra-low gelling temperature agarose (Sigma Aldrich, Oakville, ON, Canada), 1% gelatin (Sigma Aldrich, Oakville, ON, Canada) and kept at 37°C during encapsulation. Following microfluidic encapsulation, microgels were kept at 4°C to ensure complete gelation, and 3x PBS washes with 1000g for 5min centrifugation spins to remove the residual oil. Microgels were counted using the hemocytometer and used for experiments based on initial EV protein incorporated into total batch of microgels. Microgels were stored at 4°C for up to 24h prior to *in vivo* injection. For fluorescent visualization gelatin labelled with Oregon green 488 (ThermoFisher Scientific, Burlington, ON, Canada) was added to capsules at a diluted concentration (0.5%). Fluorescently labeled EV loaded and empty microgels were visualized with both a Zeiss M2 imager epi-fluorescent and a Zeiss LSM900 confocal microscope.

4.3.7 MCT Model of PAH and biodistribution

All animal experiments were approved by the University of Ottawa Animal Care Committee. As previously described,[127] male Sprague Dawley (SD) rats (200-250g) were injected with monocrotaline (MCT) (60 mg/kg, Sigma Aldrich, Oakville, ON, Canada) by intra peritoneal (i.p.) injection seven days before EV injections. For EV injections, animals were anaesthetized by isoflurane inhalation for jugular vein cut down and cannulation. After wound closure, topical bupivacaine was applied, and administered twice daily for one day following surgery. Buprenorphine (s.c. 0.03 mg/kg, Ceva Santé Animale, Libourne, France) was also administered 1 hour prior to surgery for pain management. Treatments were delivered by intra jugular vein (i.j.) injection using PBS (ThermoFisher Scientific, Burlington, ON, Canada) vehicle. For biodistribution experiments of DiR labeled free or encapsulated EVs (20µg protein content) were tracked at 4h, 24h, and 72h post injection by ex vivo imaging with the IVIS spectrum (Perkin Elmer, Waltham, MA, USA) at the University of Ottawa Preclinical Imaging Core (RRID:SCR_021832). Animals were euthanized, organs (lungs, liver, spleen, kidney, and heart) were isolated and fluorescent images were acquired. Region of interest selection for average radiant efficiency were selected using Living Image Software v 3.2 (Perkin Elmer, Waltham, MA, USA) intensity and fluorescent background was subtracted using vehicle controls.

4.3.8 Lung digestion and flow analysis

As described, EVs or microgel-EVs were injected 7 days following MCT injection. Lung digestion was performed as previously described.[166,242] 24h post injection animals were euthanized, and lungs were flushed with PBS perfusion through the right heart. Lungs were extracted, manually diced and placed in OCTO-Macs dissociation tubes (Miltenyi Biotec, Bergisch Gladbach, Germany) with digestion buffer [collagenase type 1 (Worthington Biochem., Lakewood, NJ, USA) neutral protease (Worthington Biochem., Lakewood, NJ, USA), and DNAase I (Sigma

Aldrich, Oakville, ON, Canada) in Hank's Balanced Salt Solution (HBSS, ThermoFisher Scientific, Burlington, ON, Canada)]. Dissociation was performed using OCTOmacs dissociator (Miltenyi Biotec, Bergisch Gladbach, Germany). Following which, digested lungs were filtered through 70µm filters (Corning, Corning, NY, USA) and washed with PEB. Red blood cell lysis was performed with 1x RBC lysis buffer (eBioscience, San Diego, CA, USA) for 3min at room temperature, followed by washing with PEB. Cells were counted in PEB and ~1 million cells were taken for staining and appropriate controls. Cells were stained with first Live/Dead Fixable yellow (ThermoFisher Scientific, Burlington, ON, Canada), and then 1:200 dilution of Alexa Fluor 488 mouse anti-rat CD45 (BioLegend, San Diego, CA, USA), PE mouse anti-rat CD31 (BD biosciences, Mississauga, ON, Canada) for 30 min at 4°C in the dark. Cells were washed with PEB, mixed with CountBright Plus absolute counting beads (ThermoFisher Scientific, Burlington, ON, Canada), and analyzed by flow cytometry on the Attune Nxt (ThermoFisher Scientific, Burlington, ON, Canada), with subsequent analysis performed in FlowJo v10 (FlowJo LLC, Ashland, OR, USA). Gating strategy shown in **Supplemental Figure 4.3**.

4.3.9 Statistical Analysis

All data are presented as means ± SEM. Differences between groups were analyzed by one-way with Tukey's post-hoc test for multiple comparisons or two-way analysis of variance (ANOVA) with Sidak's post-hoc test for multiple comparisons. An adjusted p-value of $p<0.05$ was considered significant. All statistical analysis was performed with Graph Pad Prism 8.0 (Graph Pad, San Diego, CA, USA).

4.4 Results

4.4.1 Differential uptake of extracellular vesicles by cell type

Small EVs are known to play a role in cellular communication in part mediated by uptake by other cells. Small MSC-derived EVs labelled with the near infrared lipophilic dye DiR were incubated with HUVEC or bone marrow-derived macrophages *in vitro*. Less than a third of HUVECs (29 ± 2%) were observed to take up DiR labelled EVs over 24h at 1µg of protein (**Figure 4.1A-C**), although this increased with higher protein concentration (62 ± 3% at 3ug). Visualization with the AMNIS image stream (**Figure 4.1B**) and subsequently confocal imaging (**Supplemental Figure 4.4**) demonstrated the labelled EVs were internalized, not only bound to the cell surface. Compared to HUVECs, a greater proportion of untreated macrophages (MØ) were readily able to take up EVs (75 ± 4% at 1ug) (**Figure 4.1D-E**) which had no discernable effect on MØ morphology (**Supplemental Figure 4.5**). Pretreatment with IL4 to induce a M2 alternative activation state, but not LPS+IFNγ which promotes an M1 phenotype, significantly reduced the uptake of MSC EVs (p=0.03) (**Figure 4.1D-E**). Since lipophilic dyes, including DiR, may form micelles during labelling, a control experiment was performed in which DiR was added the vehicle (PBS) and prepared and processed in the same manner as DiR labelled EVs. Post ultracentrifugation DiR-Pellets (which would contain any micelles) or DiR-supernatant (Sup) were incubated with HUVECs. While there was very minimal labelling of HUVECs with DiR-Pellet, DiR-Sup containing soluble dye produced a strong DiR signal (**Supplemental Figure 4.6**).

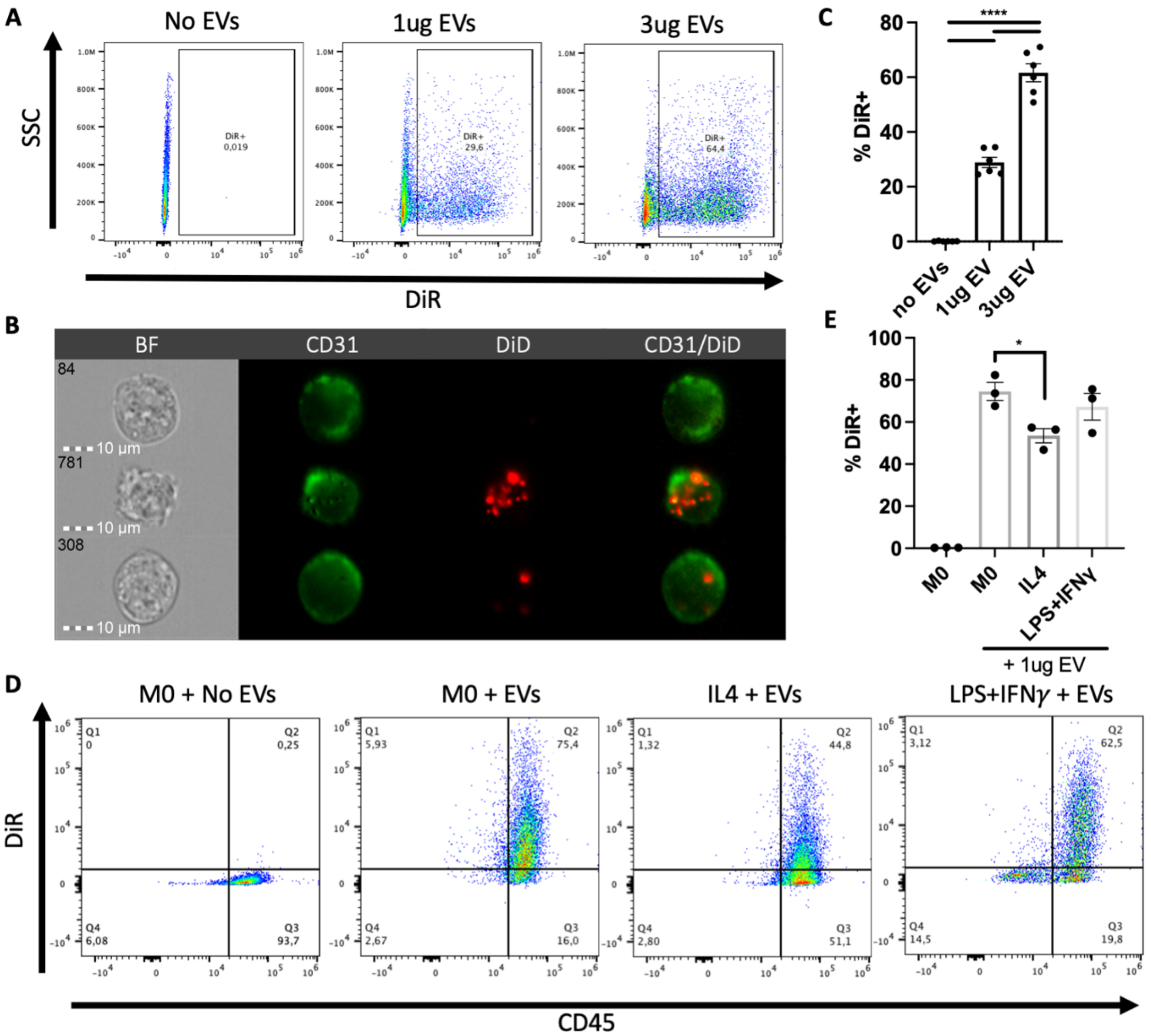

Figure 4.1: Endothelial cells and macrophages have differential MSC-EV uptake. HUVEC and macrophages were exposed to DiR labelled MSC-EVs *in vitro*. EV uptake by HUVEC was characterized after 24h by (A) flow cytometry and (B) AMNIS analysis revealing the internalization of EVs by a limited population of HUVEC, as quantified (C). Unstimulated macrophages (MØ), IL4 stimulated and LPS/IFNg stimulated macrophages readily took up macrophages as shown in representative flow plots (D) and quantified (E). Data represents mean ± SEM.

4.4.2 Encapsulation of EVs in microgels

Nanoporous hydrogels have been previously used to encapsulate single cells forming a "microgel" niche to protect cells for *in vivo* delivery.[161] A microfluidic approach[225,241] was employed to encapsulate EVs labelled with pkh26 in 1% agarose-1% gelatin producing microgels of uniform size (47 ± 0.4 µm) (**Figure 4.2A-C**). Using confocal imaging z-stacks, labelled EVs were observed to be distributed throughout the spherical microgel, and appeared to be spatially co-localized with the labelled gelatin (**Figure 4.2D**). Furthermore, *in vitro* encapsulated EVs were taken up by both endothelial cells (9.7 ± 1%) and MØ (64 ± 4%) over 24 hours (**Figure 4.2E-F**), and again, uptake of EVs was greater for MØ. Integrated fluorescence density per cell was calculated as a measure of relative EV uptake. Interestingly, there was no difference in the proportion of MØ taking up free versus encapsulated EVs (p=0.27), however individual MØ took up significantly more free EVs than encapsulated EVs evidenced by higher fluorescent intensity (p=0.003). This demonstrates that microencapsulation delays the uptake of EVs thereby potentially providing a system for controlled delivery of EVs to a target tissue. Interestingly, while the proportion of HUVECs taking up encapsulated EVs was lower than for free EVs, the amount of uptake per cell was if anything higher (**Figure 4.2F**), again illustrating important differences in the uptake of EVs between cell types.

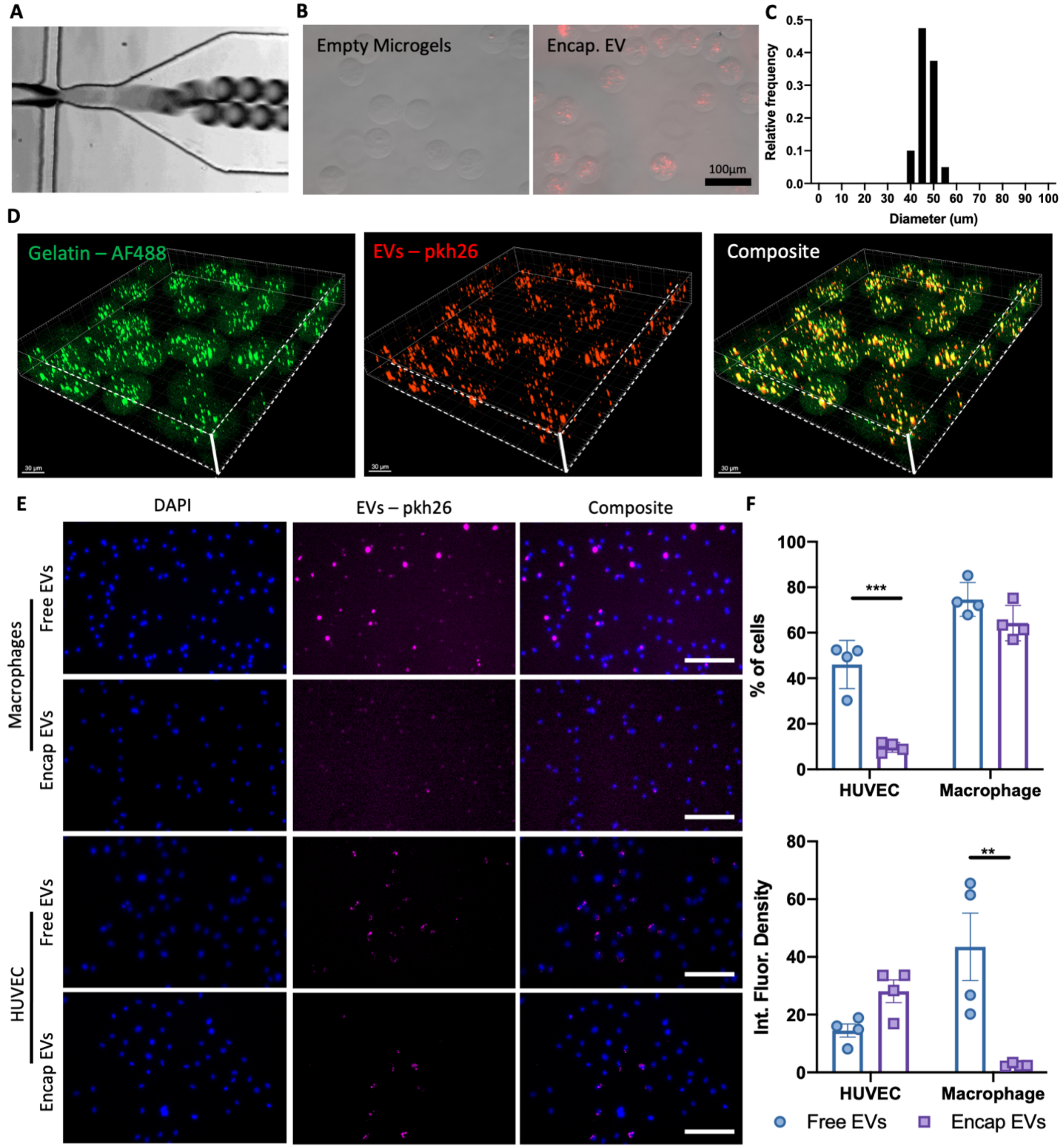

Figure 4.2: Microencapsulation of MSC-EVs within nanoporous hydrogels.
(A) Microfluidic encapsulation was performed with 1%agarose-1%gelatin hydrogels using an oil immersion process to form a homogenous population of EV-loaded microgels. Pkh26 labelled encapsulated EVs were visualized by fluorescent microscopy (B) and microgel diameter quantified (C). Confocal z-stacks demonstrate the loading of EVs throughout the hydrogels (D). Uptake of encapsulated EVs was compared to free EVs after 24h by immunofluorescent imaging (E) and quantification (F) demonstrated the reduced rate of EV uptake compared to free EVs. Data represents mean ± SEM.

4.4.3 Microencapsulated EVs enhance local lung specific delivery

To evaluate the impact of encapsulation on EV retention, biodistribution experiments were performed using DiR labeled EVs which has a near-infrared fluorescent signal (ex. 750nm; em. 780nm) where tissues have improved optical transparency for *in vivo* imaging and limited auto-fluorescent. Free or encapsulated EVs and vehicle controls were injected through the jugular vein of SD rats 7 days after administration of MCT (**Figure 4.3A**). At 24h there was a clear difference in biodistribution between free EVs which were predominately taken up by the liver with lung representing only 7.5 ± 0.4% of the measured fluorescent signal, whereas EV-loaded microgels were efficiently retained within the lung (**Figure 4.3B-C**) representing 81 ± 12 % of the signal ($p=0.0001$). In contrast, EV-loaded microgels show minimal accumulation within the liver at 24h (10 ± 3%) compared to 74 ± 2% for free EVs ($p=0.0001$). Accumulation of free and encapsulated EVs was not statistically significant in any other organ examined, including spleen, kidney, and heart (**Supplemental Figure 4.7**). The fluorescent signal measured in the lungs of encapsulated EVs appeared to increase overtime (**Figure 4.3D-E**), which is surprising since the microgels are too large to pass through the pulmonary circulation, and one would anticipate retention at the pre-capillary arteriolar level on first passage. Therefore, the maximal number of encapsulated EVs would be expected immediately after injection. However, the phenomenon of aggregation caused quenching (ACQ) has been well described[243] resulting in loss of fluorescence signal when fluorescent molecules are densely packed into a restricted space, as with encapsulation. Therefore, it is likely that at early time points the low fluorescent signal was caused by quenching of the fluorescent signal of EVs tightly packed inside microgels[244] and that the quenching is reduced as EVs are released over time and become distributed over a greater area. An alternative explanation would be that EVs are taken up over time from the circulation; however, this is unlikely since there was no similar increase in lung signal after the injection of free EVs, which based on their small size would have a much greater opportunity for recirculation. Moreover, vortex-emulsion produced empty 1% agarose-1% gelatin microgels are largely cleared over the first 72h (**Supplemental Figure 4.8**). While vortex-emulsion microgels were more heterogenous in size, the average diameter was similar (35±15 µm). Finally, it should be noted that the lipophilic dye will persist in the membrane of cells after uptake of EVs and this likely accounts for the relatively stable signal intensity from 4 to 72h after delivery of free EVs in the liver, spleen, kidney, and heart (**Supplemental Figure 4.7**). Therefore, in aggregate, these findings demonstrate that microencapsulation of small EVs can lead to significant improvement in local lung delivery compared to systemic injection of free EVs.

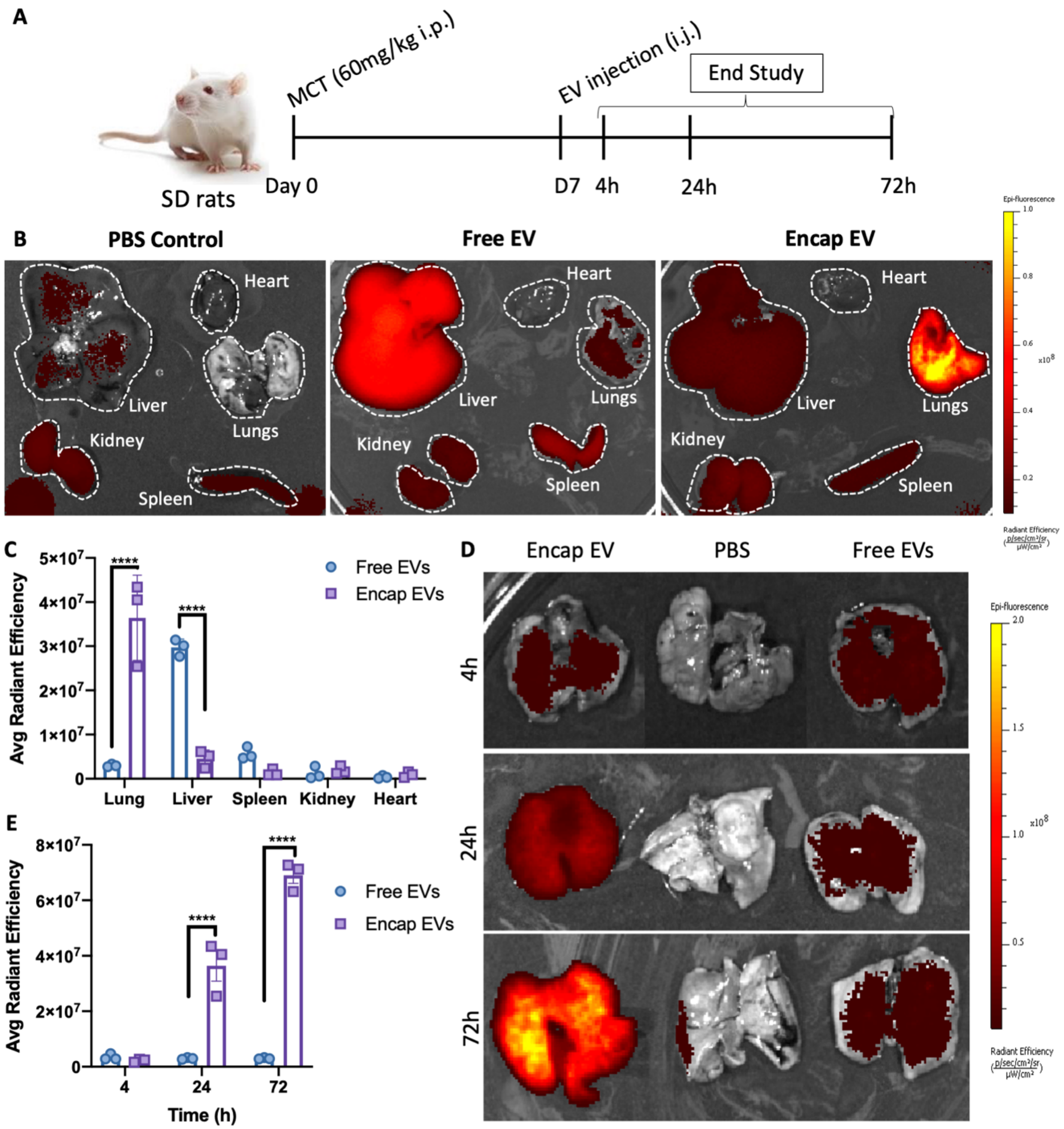

Figure 4.3: EV loaded microgels were retained within the lungs.
(A) Free and encapsulated DiR labelled EVs were administered 7 days after monocrotaline (MCT) which induces a model of pulmonary arterial hypertension. (B) Representative images from IVIS analysis demonstrate the level of background fluorescence observed at 24h in PBS controls compared to free and encapsulated EVs. (C) Quantification of average radiant efficiency at 24h from the lungs, liver, spleen, kidney, and heart demonstrate the significant increase in lung specific retention by encapsulated EVs while free EVs were rapidly cleared to the liver. (D) Representative lung samples from 4h, 24h and 72h time points demonstrate the low level of free EV retention within the lungs, which is further quantified (E). Data represents mean ± SEM.

4.4.4 Encapsulated EVs were taken up by lung resident immune cells in vivo

While the distribution kinetics of free EVs have been studied following systemic administration, little is known about the cellular uptake of these membrane-bound particles in the target organs. We performed lung digestion combined with flow cytometric analysis following the *in vivo* administration of DiR labelled encapsulated or free EVs to identify which cells were interacting with the administered EVs in the lung. The digestion and isolation procedure was biased towards immune cells, with a large proportion of cells being CD45+ across all treatment groups (**Figure 4.4A-B**). Intravenous injection of microgels, with or without, EVs resulted in an increase in CD45+ cell recruitment to the lungs compared to healthy controls (**Figure 4.4B**), consistent with a proinflammatory effect of agarose-based hydrogel. Histological data corroborated this finding demonstrating cellular influx surrounding microgels (**Supplemental Figure 4.8**). No statistical difference was observed between the number of endothelial cells (CD45-CD31+) in control lungs and those from animals receiving microgels; while there was a modest increase in other CD45- cells (e.g., fibroblasts) between empty microgels and other groups, consistent with a reactive response (**Figure 4.4B**). Interestingly, at 24h, only animals treated with EV-loaded microgels showed statistically significant accumulation of DiR+ EVs within both the CD45+CD31- and CD45+CD31lo immune cell populations compared to all other treatment groups (**Figure 4.4C-D**). Despite the relative low yield of endothelial cells (CD45-CD31+) from the digestion, EV uptake was seen only in animals receiving EV-loaded microgels. No differences were observed in the CD45-CD31- cells uptake of DiR+ EVs between all the treatment groups (**Supplemental Figure 4.9**). Therefore, these findings demonstrate that EVs are predominately taken up by immune cells *in vivo*, and encapsulation enhances EV uptake.

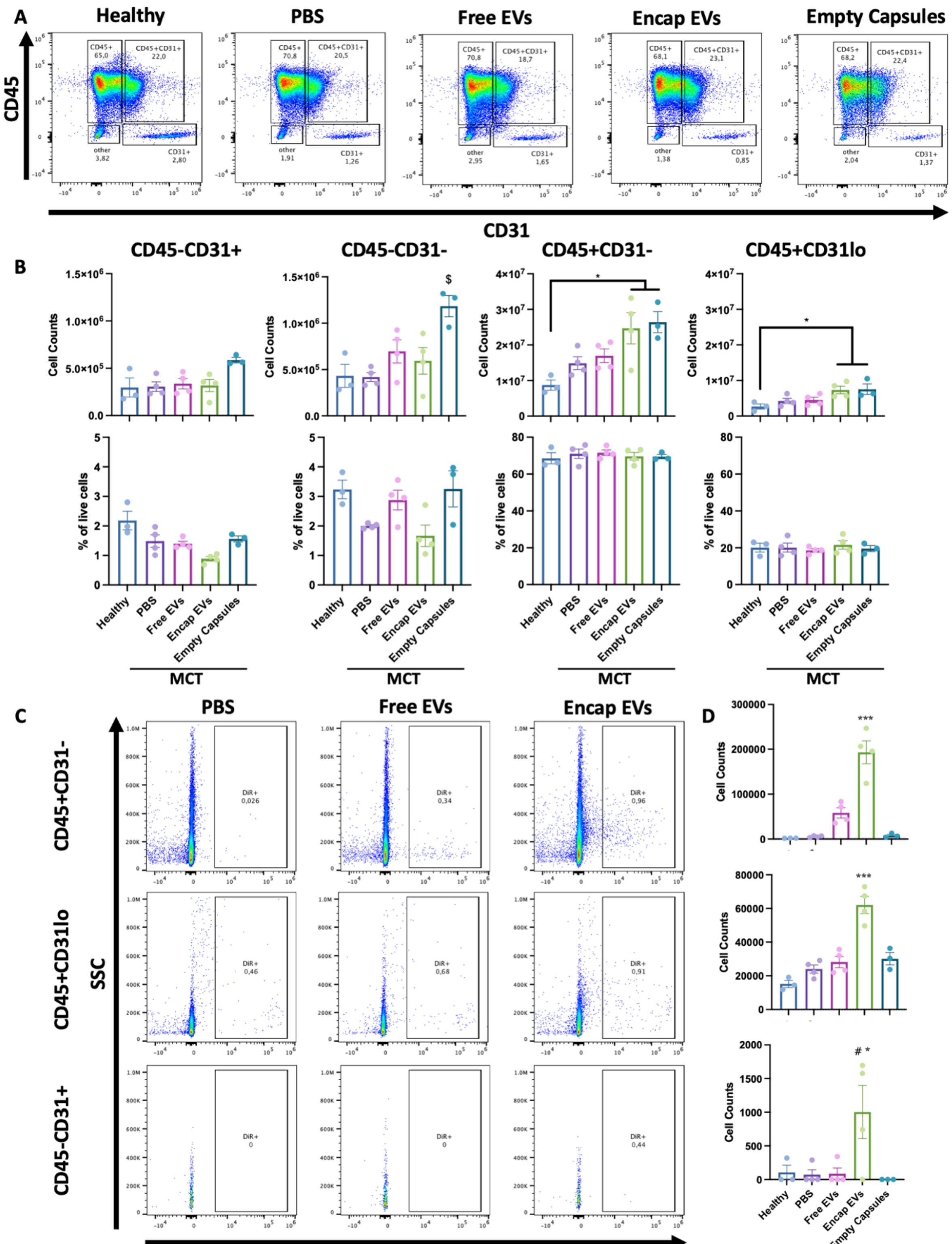

Figure 4

Figure 4.4: Local immune cell EV uptake increased by microencapsulation.
Lungs were isolated, digested, and prepared for flow cytometry analysis 24h after DiR labelled EV administration. (A) Representative flow plots demonstrate consistent proportions of lung

endothelial (CD45-CD31+), immune (CD45+CD31- or CD31lo), and other (CD45-CD31-) populations, which was quantified as cell counts, and proportions (B) demonstrating increased numbers of immune cells with the presence of microgels. EV uptake was assessed by evaluation of DiR labelling, representative flow plots are shown (C) and quantification (D) demonstrates significant EV uptake by CD45+CD31- and CD45+CD31lo cells when exposed to encapsulated EVs. Data represented as mean ± SEM, * $p<0.05$ PBS, Free EVs, and Empty Capsules compared to Encap. EVs, *** $p<0.0005$ all Tx compared to Encap EVs, # $p = 0.07$ healthy compared to Encap EVs.

4.5 Discussion

Systemic delivery of free EVs is a promising treatment for a variety of lung diseases,[245] including PAH.[140] However, after intravenous administration, EVs are rapidly cleared from the circulation, primarily by the liver and spleen,[147,246–248] representing a significant challenge for therapies requiring targeted delivery of EVs to other tissues and organs, such as the lungs. Therefore, strategies to improve organ specific EV retention and prolong the opportunity for EVs to interact with target host cells could greatly enhance efficacy of EV therapies. In this study, we demonstrated that encapsulation of MSC-EVs in nano-porous microgels significantly improved lung targeted EV retention and enhanced EV uptake by resident lung cells.

Microencapsulation has been previously employed for the delivery of therapeutic stem and progenitor cells.[152,161,225] We sought to apply this technology for the targeted delivery of EVs to the lung. We demonstrated reduced uptake of EVs *in vitro* over 24 hours by macrophages (decreased EV fluorescent signal) and ECs (decreased percentage of EV+ cells) from microgels suggesting that encapsulation restricted access to EVs compared to free EVs which were readily taken up by cells. The marked difference in the way ECs and macrophages interacted with encapsulated EVs suggests cell type has an important impact on EV uptake. Phagocytic cells, such as macrophages, show greater consistency of EV uptake than ECs; however, the magnitude of EV uptake was greatly constrained by encapsulation. In contrast, a smaller proportion of ECs were able to uptake EVs, especially after encapsulation, but the number of EVs taken up remained fairly constant. We cannot rule out that other factors, including differences in cell culture media and additives, might influence EV release from the microgels and cellular uptake. Despite the relatively restricted uptake of encapsulated EVs over 24 hours in cell culture conditions, *in vivo* studies demonstrated much greater retention of EV containing microgels within the lungs up to 72h following injection. This is in contrast to previous pharmacokinetic studies which have shown that free EVs are rapidly cleared from the bloodstream within hours of administration.[147] Therefore, loading EVs into microgels represents an effective strategy to both enhance their delivery to the lung and increase their retention.

While previous studies have evaluated the overall biodistribution of systemically administered EVs, they have generally not examined which cells are responsible for EV uptake. To better understand the mechanisms by which EVs may exert their therapeutic actions, it is necessary to define the specific cell types with which they interact. In this study, we used fluorescently labelled EVs in combination with lung digestion and flow cytometry to gain insights into the cellular uptake of MSC-EVs within the lung. Loading EVs into microgels resulted in a marked increase in uptake by lung resident cells, primarily CD45+ immune cells. Uptake by lung resident immune cells could enhance the therapeutic efficacy of EVs in inflammatory lung diseases, such as acute respiratory distress syndrome. As well, in PAH it is hypothesized that MSC-derived EVs modulate the local inflammatory environment by interacting with immune cells, specifically macrophages.[228] While free EVs were readily taken up by macrophages *in vitro* (**Figure 4.1**), due to the short residence time *in vivo*, their ability to interact with lung host cells was limited resulting in minimal uptake by CD45+ immune cells after systemic delivery (**Figure 4.4**). In contrast, microencapsulation, which reduced *in vitro* uptake by MØ and ECs, greatly enhanced cellular uptake *in vivo* by prolonging the retention of EV-loaded microgels in the lung. However, whether the more efficient lung resident cell uptake of encapsulated EVs translates into greater therapeutic benefits remains to be seen.

The biomaterials used for microgel preparation will impact the tissue residence time and the local microenvironment. An agarose hydrogel formulation was developed for previous studies in our group designed to enhance cell persistence and engraftment following transplantation.[152] This agarose-gelatin formulation was also effective in enhancing local retention of encapsulated EVs in the lung (**Figure 4.3**), yet there are opportunities to optimize the biomaterial formulation going forward. Interestingly, fluorescently labelled gelatin and EVs appeared to co-localize within microgels (**Figure 4.2**), which may be due to protein-protein interactions between the gelatin and EVs during microgel formation and could contribute to the EV protein corona. While modifications to the EV protein corona were not directly studied, changes to the protein corona could influence downstream EV-cell interactions,[249] and the impact of microgel encapsulation on this could be the source of future studies. Immune cells were the primary cells involved in the uptake of EVs from microgels and even empty agarose-gelatin microgels promoted inflammation, as observed by increased number of immune cells within the lung, likely due to biomaterial-immune cell interactions inciting a local foreign body response (FBR). The size and shape of implanted biomaterials has been shown to influence the FBR, although in this study no materials below 100µm were studied.[250]

Novel biomaterials have been developed to reduce the FBR, for example to reduce the inflammatory response to encapsulated pancreatic islets after transplantation.[251] Further studies should seek to optimize the biomaterial formulation to reduce the FBR, particularly in the context of a therapeutic product. Biomaterials can also be modified to optimize the release kinetics of EVs. Recently, it has been reported that translocation of EVs through biomaterials and extracellular matrices is linked to the matrix mechanical properties and the EV deformability,[252] and this represents an opportunity to modify the matrix properties to control the diffusivity of the loaded EVs. Alternatively, introduction of matrix metalloproteinase degradable sites through click-chemistries[226] could further refine the release profile and determine the local retention time by enhancing degradation of the microgels.

This study demonstrates that EV-loaded microgels can be used to enhance EV delivery to the lungs compared to administration of free EVs. Furthermore, EV-loaded microgels act as a sustained release system to increase the time for interaction between host cells and EVs. Lastly, we have demonstrated that increased local retention of EVs results in significantly higher host cell uptake. All of this suggest EV-loaded microgels may offer significant benefits to enhancing delivery of EV therapies.

4.6 Acknowledgements

We want to thank Anli Yang for her technical support during all animal surgeries and end points, and Dr. Dylan Burger for his advice on this manuscript. We would also like to thank the University of Ottawa’s Preclinical imaging core facility and the University of Ottawa’s Cell Biology and Image Acquisition core facility.

4.7 Author Contributions

NDC has contributed to all aspects of this work including conception, performing the experiments, data analysis and preparation of this manuscript. KR and YD were involved with all animal studies. KR contributed technical knowledge and helped perform the biodistribution and *in vivo* digestion flow cytometry experiments. ABB and MG contributed expertise for the operation and maintenance of the microfluidic encapsulation device. DWC contributed to conception of the encapsulation platform, and in interpretation of results. DJS was involved in the conception and design of experiments, data analysis and interpreting results, and drafting this manuscript. DJS is accountable for all aspects of this work.

4.8 Conflicts of Interest

None

4.9 Funding

This work was supported by a Foundation award from the Canadian Institute of Health Research (FDN – 143291) held by DJS. NDC acknowledges scholarship funding from the Canadian Institute of Health Research, and the Canadian Vascular Network.

4.10 Data Availability Statement

The data that support the findings of this study are available from the corresponding author upon reasonable request.

4.11 Chapter 4 Extension

As an extension to this manuscript, we sought to test the efficacy of MSC derived EVs and microgel encapsulation as therapeutics for PAH. We employed the MCT rat model and EV/ microgel injections as described in Chapter 4, with EVs or vehicles injected 7 days post MCT in a late prevention model (**Extended Data Figure 4.5A**). Free EVs and microgel loaded EVs were compared with PBS vehicle and empty microgel vehicles, with healthy animals serving as an additional control. Unfortunately, no statistically significant differences were observed between any of the treatment groups for RVSP or RVH (**Extended Data Figure 4.5B,C**). Variability within vehicle treated control animals was very high, which may have masked therapeutic effects of MSC-derived EVs, and the microgel-loaded EVs, requiring additional power to properly assess statistical significance. Yet, signs point to only a modest benefit with both free and microgel loaded EVs. Therefore, future work should evaluate different cell sources for the most potent EVs, which could include umbilical cord (UC) derived MSCs.

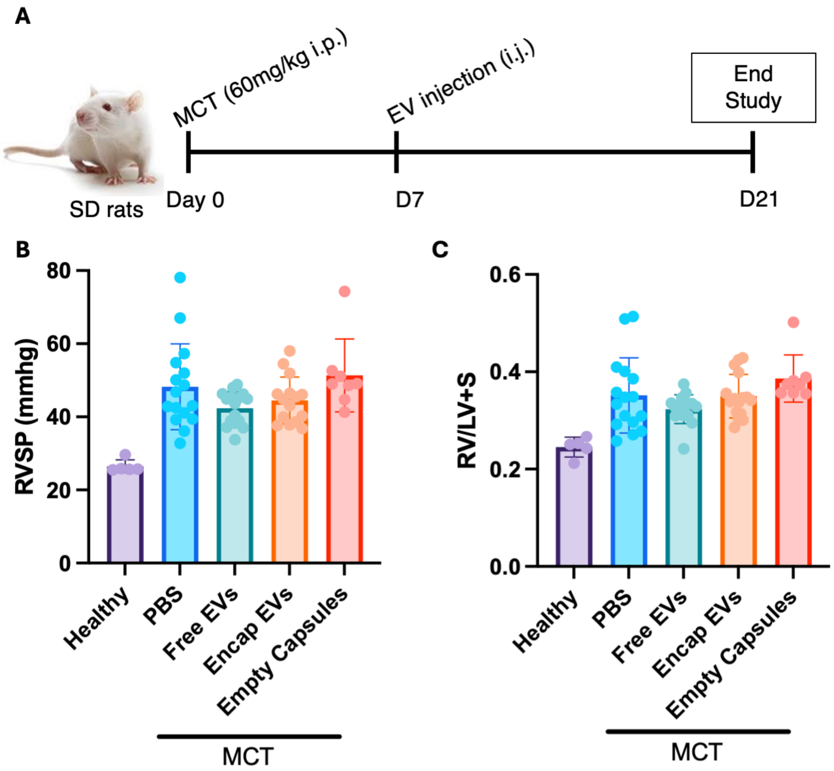

Extended Data Figure 4.5: EVs and microgel loaded EVs to prevent MCT induced PH.
(A) Schematic of monocrotaline (MCT) induced PH and treatment with EVs or microgel loaded EVs. MSC derived EVs were unable to prevent PH progression based on RVSP (B) and RVH (C) parameters. Data presented as mean ± SD, n = 5-16.

Chapter 5: General Discussion and Perspectives

5.1 Summary

PAH is a severe and lethal disease of the pulmonary vasculature, with complex pathogenesis and limited treatment options available. Through these independent studies we have gained new insights into disease progression and potentially regenerative therapeutic options. Sequential scRNA-seq analysis in the SU/CH model identified key cell populations driving PAH progression, notably the aAECs, dCap ECs, and SM-like pericytes. This study is the first to use single cell transcriptomic analysis to unravel some of the complex factors at play at the earliest stages of PH development. Additionally, we evaluated two regenerative treatment strategies to restore the injured pulmonary circulation associated with PAH progression. While ECFCs offered limited therapeutic benefit on their own, microencapsulation of ECFCs both increased cell retention within the lungs and was able to reduce the severity of PAH in the MCT rat model. Stem cell derived EVs have gained popularity as an alternative to regenerative cell therapies, yet biodistribution after administration may limit their therapeutic potential. As an extension from cell encapsulation, microgels were developed for EV delivery. EV loaded microgels were found to significantly enhance lung retention compared to non-encapsulated EVs with a resultant increase in local cell uptake. Thus, supporting the application of microencapsulation technology for enhanced local retention of therapeutic EVs.

5.1.1 Beyond scRNA-seq

Through this work, we demonstrated the utility of sequential scRNA-seq analysis during the onset of PAH to gain deeper insights into disease progression. In our study we took advantage of sample multiplexing to test multiple biological replicates at each timepoint. Yet, costs associated with single cell sample preparation and sequencing meant a limited number of cells per animal could be sampled and sequenced. In future studies the opportunity to increase sequencing depth or the number of cells sampled per animal may improve our ability to resolve more complex cell interactions. While we focussed mainly on the vascular cell compartment, specifically endothelial and stromal cells, our whole lung digestion has provided a rich opportunity to further evaluate changes in immune cell populations during SU/CH development. Changes in transcriptomic profiles within the immune cell populations was mainly limited to the early stages of disease development. In particular, the greatest number of DEGs was seen in transitional monocytes at 1 week in SU/CH model; however, at later stages only interstitial macrophages showed any persistent differential gene expression, and this was at a very low level. This is surprizing given the abundance of evidence that immune mechanisms play an important role in this disease but may reflect the bias towards the small vessels that account for by far the greatest numbers of cells. In contrast, larger arteries, which pathologically exhibit the most marked inflammatory changes, would make up only a trivial proportion of cells in the lung dispersate. Thus, the immune cell populations characterized by scRNA-seq mainly reflect cells with the distal microcirculation and alveolar structures.

However, we were able to resolve key vascular cell populations and elucidate their role in the complex arterial remodeling. Both the aAECs and SM-like pericytes were observed to express *Tm4sf1* and immunofluorescent staining localized these populations within the areas of arteriolar remodeling. Furthermore, TM4SF1 has been implicated in numerous cancers and contributes to cellular migration, and proliferation. Thus, we suggest therapeutic strategies targeting TM4SF1+ cells could have major benefits by removing the dysfunctional aAECs and SM-like pericytes contributing to disease associated vascular remodeling. In fact, TM4SF1 CAR-T cells are in development for cancer treatment[253] and may offer an exciting therapeutic avenue for PAH. Based on our findings, the SU/CH model represents an excellent opportunity to test a TM4SF1 CAR-T therapy in vivo. We observed the presence of *Tm4sf1* expressing ECs throughout the progression of PH, so there are opportunities to target both late and early stages of the disease. A reversal model with CAR-T treatment at later timepoints (5-weeks) is the most translationally relevant. Hopefully, by specifically targeting dysfunctional TM4SF1$^+$ cells we may facilitate regeneration of the damaged vasculature.

Cellular senescence and its role in tissue homeostasis as well as disease has gained significant interest in recent years.[254,255] Increased vascular cell senescence has been suggested to contribute to PAH and cellular dysfunction in a time dependent manner.[48,256] Although this was not included in the manuscript, we found the aAECs exhibited increased levels of several genes associated with senescence (*Serpine1*, *Cdkn1a*, *Tp53*) as early as 1-week into SU/CH (**Figure 5.1**). These findings are in line with broader literature around EC senescence during PAH,[53] and present an interesting direction for further study. Cellular senescence has many different biological roles. In addition to its well-known association with aging and disease, senescence also plays an important role in repair and stem/progenitor differentiation.[255] Thus, the early onset of a senescent gene expression profile within aAECs, the population most impacted in this PAH model, could represent either a failed repair response or a mechanism for disease related inflammation. A study to map the time course of senescence in distinct cell compartments during PAH would be invaluable to increasing our understanding of disease progression. Additionally, targeting senescent cells with senolytics has become an active area of research. Yet, a complete understanding of when proportions of senescent cells increase will help identify the therapeutic window for targeting senescent cells during PAH progression, opening up many possibilities for both drug based senolytic therapies, or immune modulatory strategies to clear senescent cells.

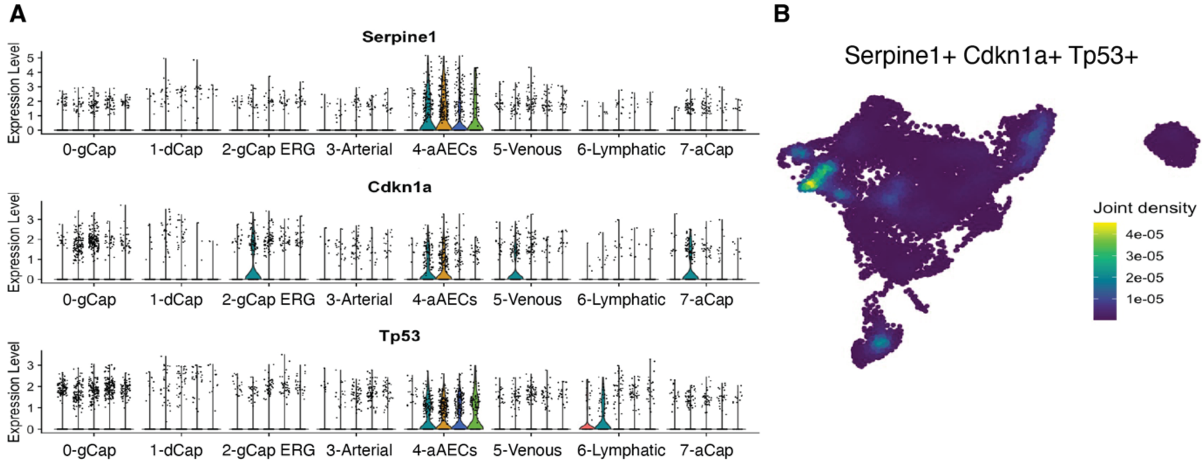

Figure 5.1: Endothelial senescence during PAH.
Gene expression of *Serpine1* (PAI-1), *Cdkn1a* (p21), and *Tp53* (p53) within the endothelial cells shown as (A) volcano plots and combined expression within a (B) nebulosa plot. aAECs demonstrated increased expression of these senescent associated genes as early as 1-week and throughout SU/CH progression.

Increased shear stress has been linked to vascular remodeling through elegantly performed banding studies.[44] Through our lung cell atlas of PAH progression, we have clearly mapped important transcriptomic changes and elucidated key populations driving vascular remodeling, yet we did not evaluate the direct role of shear stress in producing these disease associated populations (aAECs, dCap ECs, or SM-like pericytes). Left pulmonary artery banding (LPAB) prior to onset of the SU/CH model can produce a flow limiting stenosis such that the right lung develops severe occlusive remodeling, while histologically the left lung remains largely unchanged. Future work could implement LPAB coupled with scRNA-seq or more simply flow cytometry or immunofluorescent staining to validate the presence or absence of aAECs, dCap ECs, and SM-like pericytes between the banded and unbanded lungs. Such a study would validate the role of shear stress in the expansion of these cell populations, and thereby its important role in driving PAH.

As more single cell transcriptomic studies are performed in models of PAH or with human patient samples, there is an opportunity to integrate these datasets to validate findings between species (human, mouse, rat), interrogate drug targets based on genes differentially expressed during PAH compared to controls, or evaluate the complexity of cell-cell interactions. This study has provided new insights into key cell populations driving vascular remodeling during PAH progression and has identified significant opportunities to both deepen our understanding of disease pathogenesis and investigate new therapeutic avenues.

5.1.2 Regenerative therapeutics

Characterization of the significant and progressive vascular loss during SU/CH progression suggests that strategies to regenerate the damaged pulmonary vasculature are of utmost importance for restoring lung function to PAH patients. To this end, we evaluated both stem cell and EV therapeutics coupled with biomaterials as potential regenerative strategies. While nonencapsulated ECFCs were found to be ineffective, microencapsulation increased their lung retention and prevented onset of severe PH. This strategy is an exciting advance demonstrating utility of ECFCs for PAH, and the benefit of microencapsulation for cell delivery, yet prevention strategies are not feasible treatment options for patients with PAH. Future studies should seek to identify cell therapy candidates that can reverse PAH. While autologous therapies from patient derived EPCs or MSCs are attractive options from an immune rejection perspective, autologous therapies present serious challenges for a production, logistics and regulatory perspective, and they may not be practical as a commercial therapeutic product. Induced pluripotent stem cells (iPSCs) have the potential to differentiate into almost any lineage, and at the time of writing several companies (Bluerock Therapeutics, Notch Therapeutics) are developing iPSC derived cell therapies for several indications. Perhaps, iPSC derived EPCs coupled with genetic engineering would produce a more therapeutic cell that could be coupled with encapsulation strategies for treatment of PAH. While there are still potential concerns about the safety of iPSC-derived cell therapy products due to the chance for uncontrolled growth and tumour formation, this would not be a concern for iPSC-derived EV products which have no nucleus. Indeed, the use of iPSC-derived or transformed cells can overcome the limitation of using different (and variable) cell sources for EV manufacturing, and thereby can provide a more consistent source for EV products. Strategies to manufacture more consistent EV products and tune their regenerative properties are essential for developing an effective regenerative therapeutic product. iPSCs from a single donor derived master cell bank, rather than the multiple donor isolations used to acquire EPCs or MSCs, could control cell source variability. As these fields develop new technologies, it will be exciting to apply these treatments to PAH in the hope of finding a truly regenerative solution.

In addition, we demonstrated that microencapsulation strategies can be extended to submicron sized EVs, facilitating a targeted delivery strategy and enhancing local retention. These proof-of-concept studies suggest that microencapsulation can facilitate targeted cell or EV delivery, however, refinement of the biomaterials is warranted. We found delivering empty microgels to the lung led to increased immune cell activity in the MCT model of PAH. Ideally the biomaterial chosen would work synergistically with the therapeutic EVs to improve the treatment benefit. Future work can refine the biomaterial composition to tune the desired retention and immunomodulatory properties for the desired application. For example, the size and shape of the transplanted biomaterials has been shown to affect the host cell interactions; large (1.5mm) hydrogel spheres had an abrogated foreign body response compared to sub millimetre sized hydrogel spheres.[250] Additionally, sub-100µm agarose capsules were found to promote less fibrotic response then larger 300-1000µm capsules.[257] The size range of the microgels we used for cell or EV encapsulation was even smaller (<50µm) and thus the microgel size could be further optimized for an improved foreign body response.

The choice of biomaterial has a significant impact on the local microenvironment and the EV release, with numerous options available from natural (agarose, collagen, alginate) to synthetic (PEG) sources. With many advances in the field of biomaterials, there are opportunities to create fully synthetic matrices or enhance naturally derived materials through cross-linking or biochemical modification to control the matrix mechanics (stiffness, elasticity), and presence of biochemical cues.[153,258] One study developed a combinatorial hydrogel library to screen alginate modifications that would reduce a foreign body response in the context of islet transplantation and found a triazole modified surface avoided fibrosis around the implanted material.[251] While another group used biotin-streptavidin interactions to conjugate programmed cell death 1 (PD-L1) on the surface of microgels to act as an immunomodulatory agent for their transplanted cells, prolonging graft survival.[259] Ultimately, optimization of the biomaterial will need to balance local immune responses with EV release kinetics to prevent adverse immune responses and facilitate EV release.

Through this work it is clear that late stage PAH presents with both significant losses in functional pulmonary vascular and dysfunctional cells driving occlusive remodeling. My identification of the key cell populations driving occlusive remodelling presents a number of new therapeutic possibilities, most prominently TM4SF1 targeted clearance of dysfunctional ECs. While the most effective regenerative cell or EV therapeutic for treatment of PAH has yet to be identified, the microencapsulation strategies presented here clearly demonstrate the ability of microgels to improve cell and EV delivery, providing a valuable tool for delivery of future therapeutics. While both targeting dysfunctional cells and lung regeneration strategies hold promise on their own, perhaps, the most effective therapy will combine the two, to both clear diseased cells and simultaneously regenerate the damaged pulmonary circulation to ultimately reverse pulmonary hypertension.

Appendix: Manuscript Supplements

Chapter 2 Supplements

2.1 Supplemental Figures

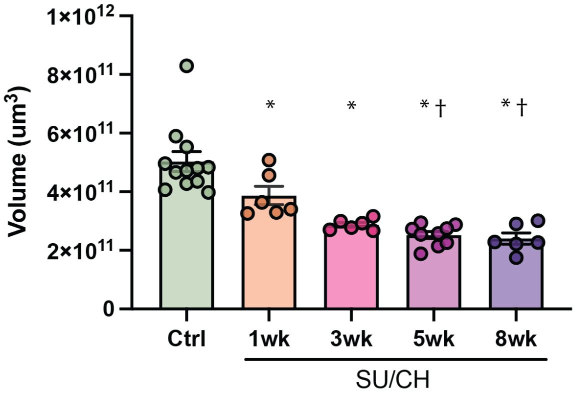

Supplemental Figure 2.1: Loss of pulmonary vascular volume during SU/CH.
Total vascular volume demonstrating progressive loss throughout SU/CH development. Data represented as mean ± SEM, n = 6 – 12 biological replicates, * $p < 0.05$ vs healthy control, † $p < 0.05$ vs 1-week.

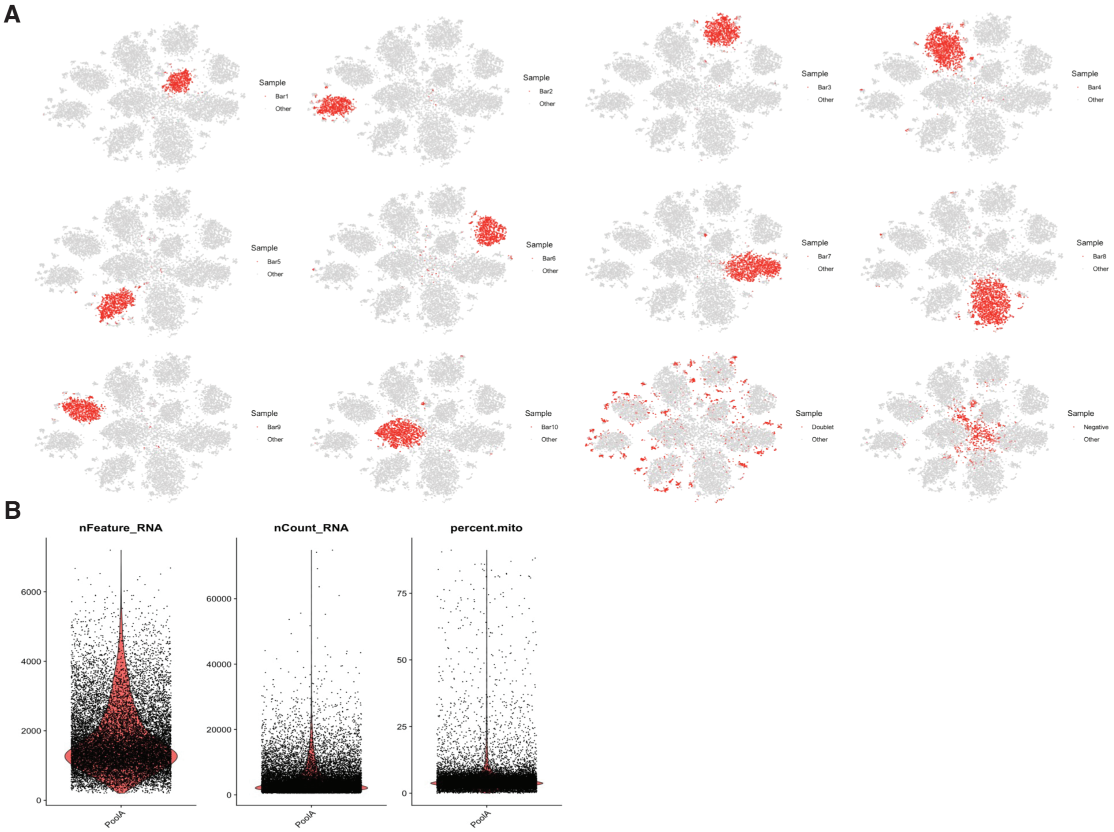

Supplemental Figure 2.2: Quality control metrics during deMultiplex and preprocessing. (A) Representative plots from one lane of 10x Genomics samples while preforming demultiplexing. Cells strongly expressing individual barcodes clustered together (singlets), cells expressing multiple barcodes are seen in small clusters on the periphery (doublets), and cells with insufficient barcode expression clustered in the middle (negative). Only singled identified barcodes were kept. (B) Additional quality control preprocessing in Seurat using features, counts, and mitochondrial content.

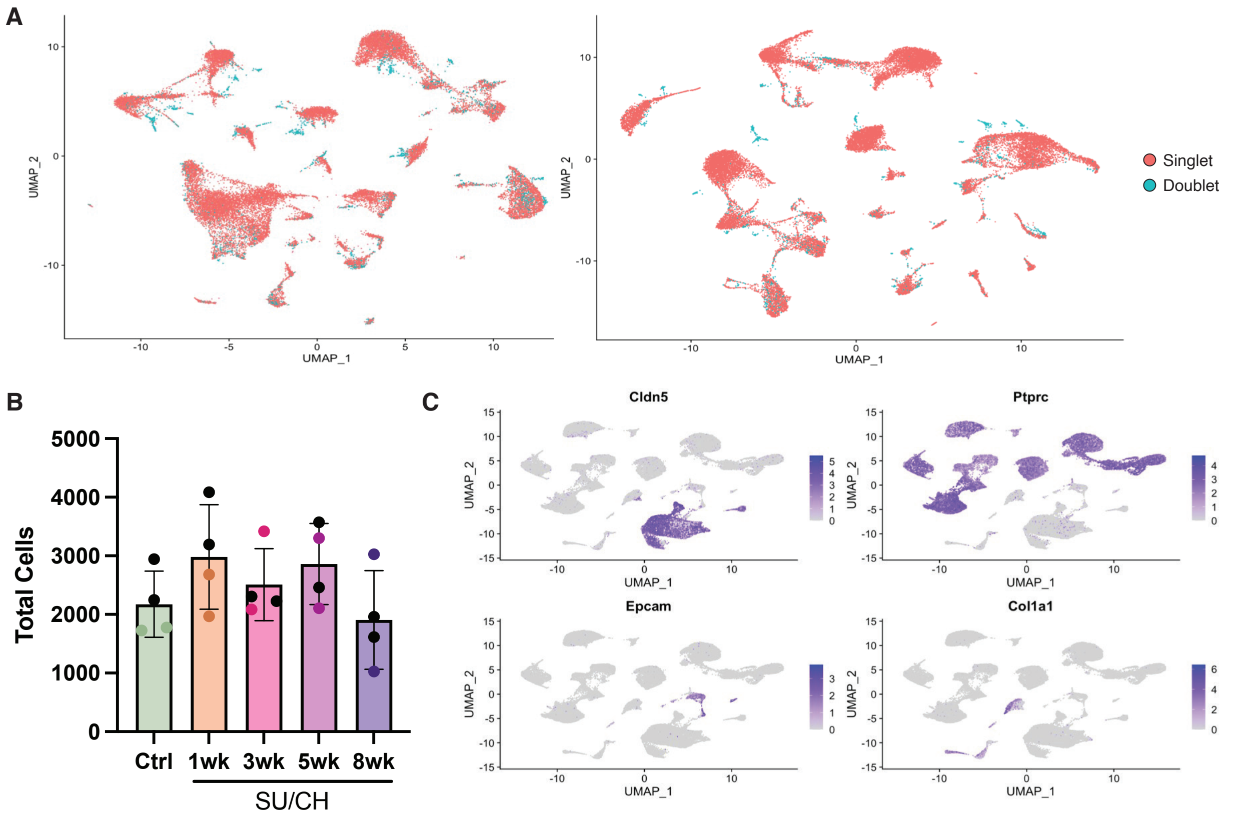

Supplemental Figure 2.3: Doublet removal and bulk population identification.
(A) Prior to merging and integrating the two experiment an additional round of doublet removal was performed with scDblFinder. (B) Total cells for each biological sample in the integrated Seurat object. (C) Identification of major lung cell populations based on common bulk identify genes *Cldn5* (endothelial), *Ptprc* (immune), *Epcam* (epithelial), and *Col1a1* (stromal).

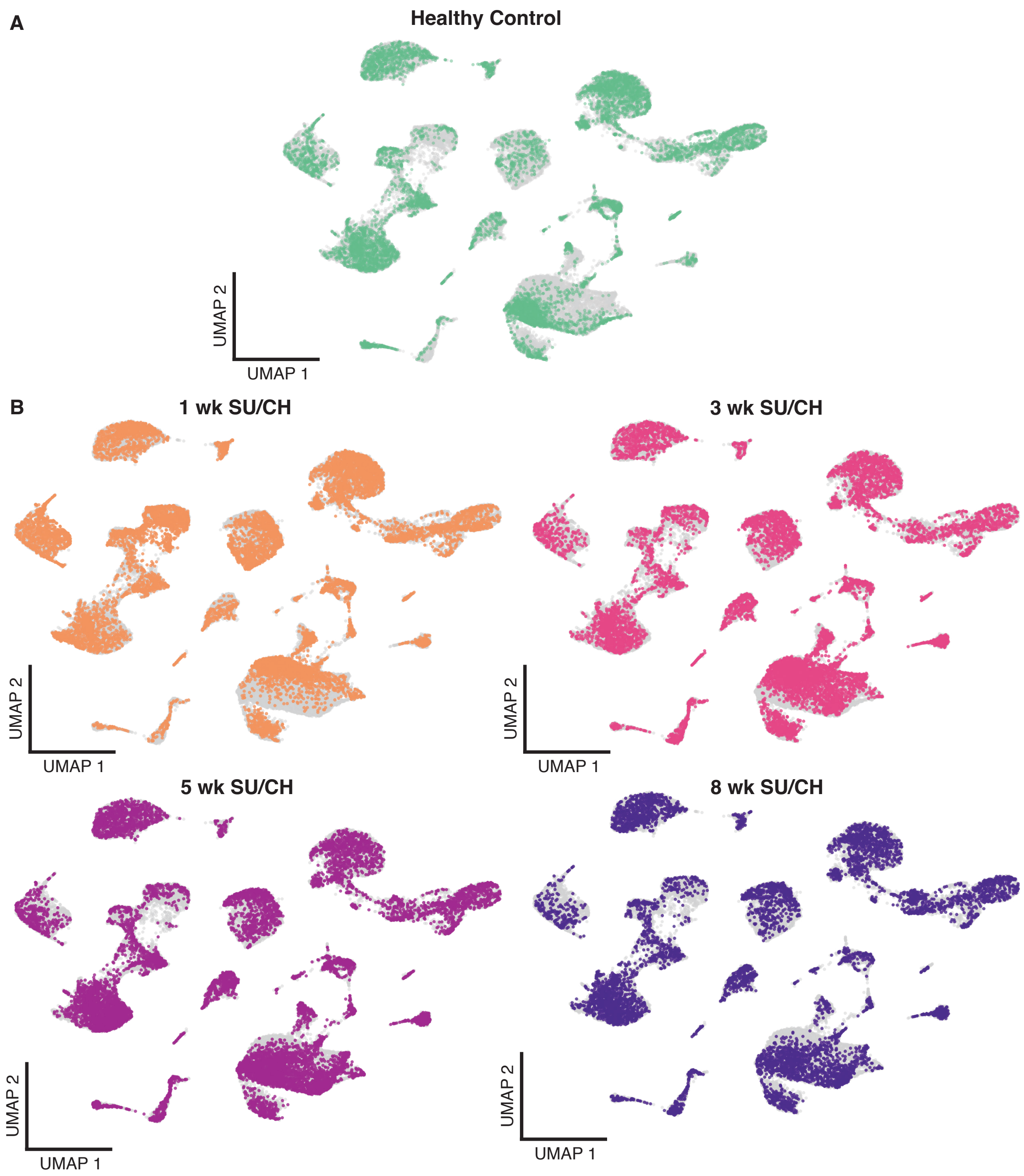

Supplemental Figure 2.4: Global UMAPs by timepoint.
Representative UMAPs showing each timepoint control – green (A), 1wk SU/CH – orange (B), 3 wk SU/CH – pink (C), 5 wk SU/CH – purple, 8 wk SU/CH – dark purple.

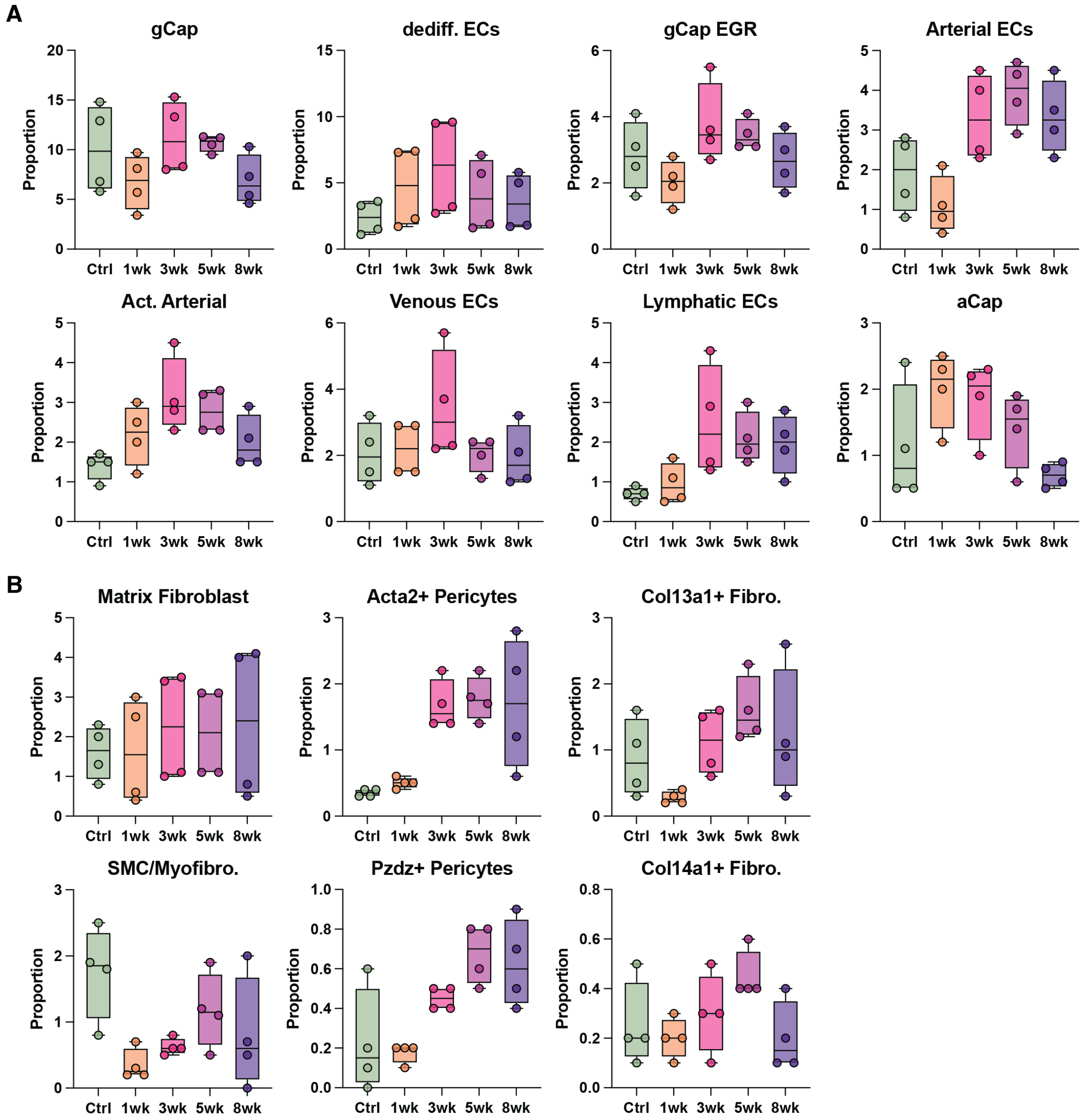

Supplemental Figure 2.5: Global proportions of all endothelial and stromal cells within integrated Seurat object.

Changes in global proportions of cell populations were quantified in the endothelial (A) and stromal (B) subsets by timepoint, demonstrating relative increases in arterial ECs, activated arterial ECs, *Acta2*+ pericytes, and classical pericytes during PAH progression compared to controls. Representing n = 4 biological replicates per timepoint.

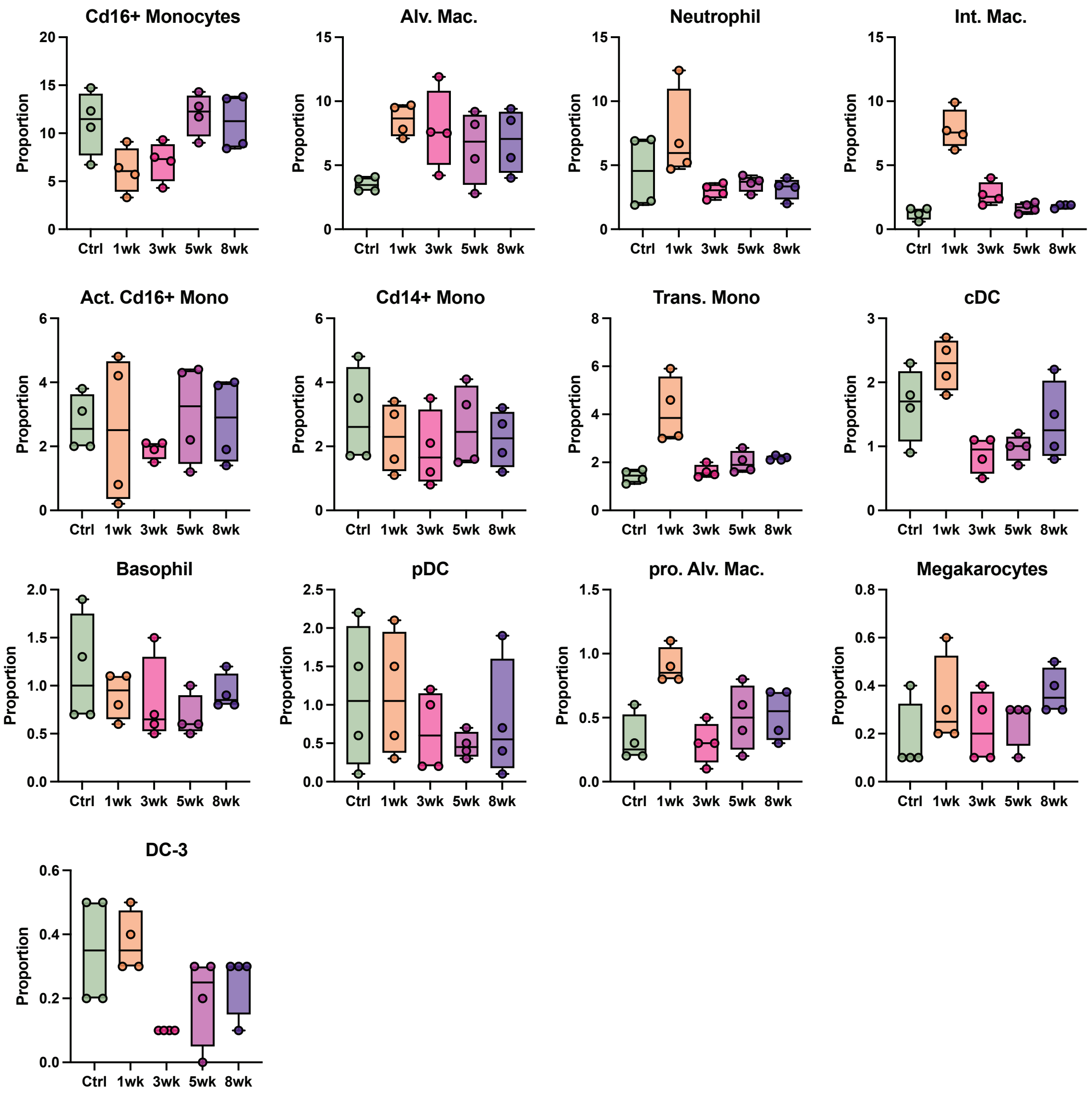

Supplemental Figure 2.6: Global proportions of all myeloid cells within integrated Seurat object.

Representing n = 4 biological replicates per timepoint.

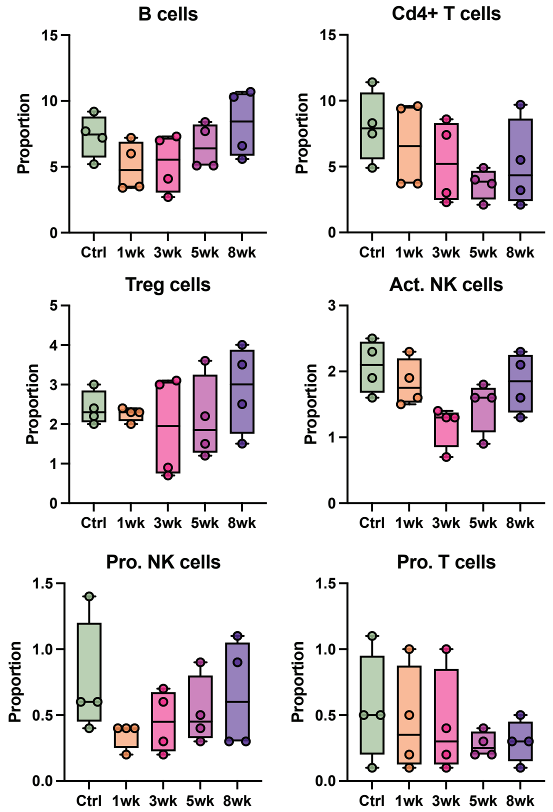

Supplemental Figure 2.7: Global proportions of all lymphoid cells within integrated Seurat object.
Representing n = 4 biological replicates per timepoint.

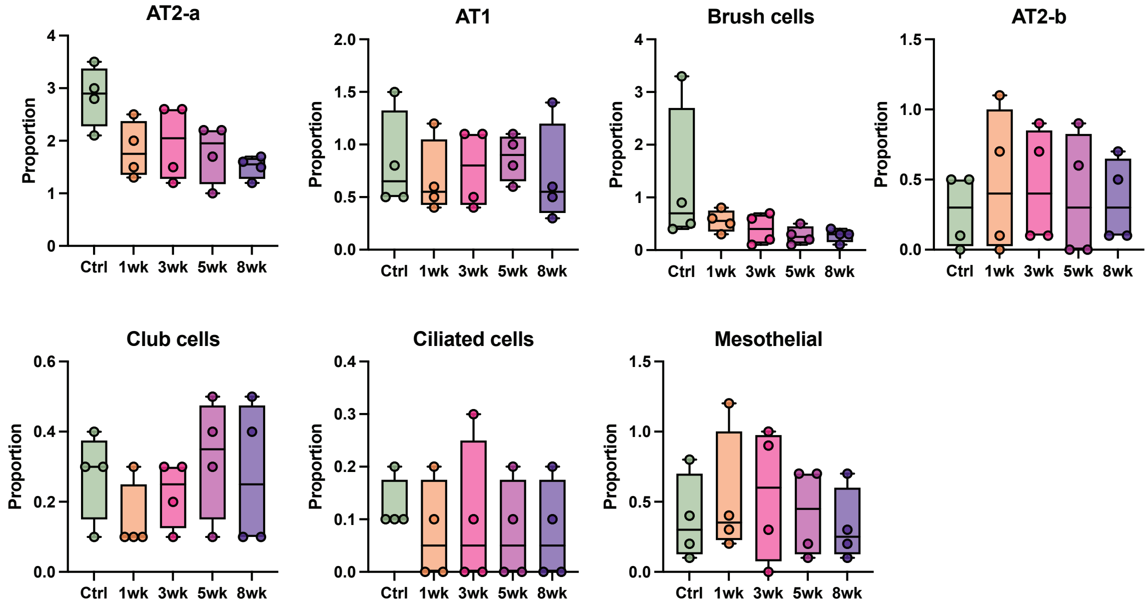

Supplemental Figure 2.8: Global proportions of all epithelial and mesothelial cells within integrated Seurat object.
Representing n = 4 biological replicates per timepoint.

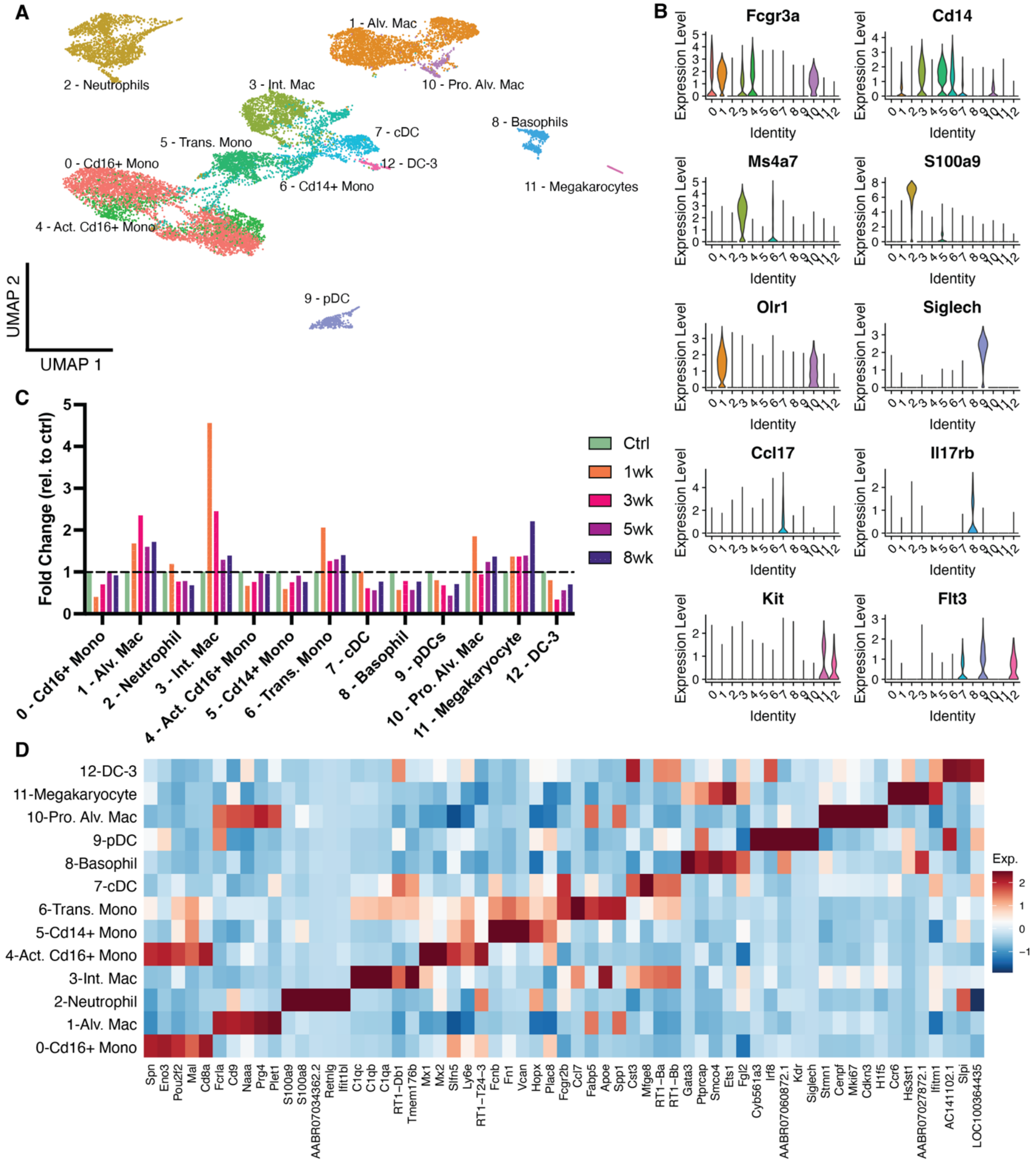

Supplemental Figure 2.9: Myeloid subcluster analysis.
(A) UMAP of myeloid subset representing 13 resolved cell types. (B) Top genes used to identify myeloid populations. (C) Fold change of myeloid populations at each timepoint relative to healthy control samples. (D) Heatmap of the top 5 differentially expressed gene per myeloid cluster.

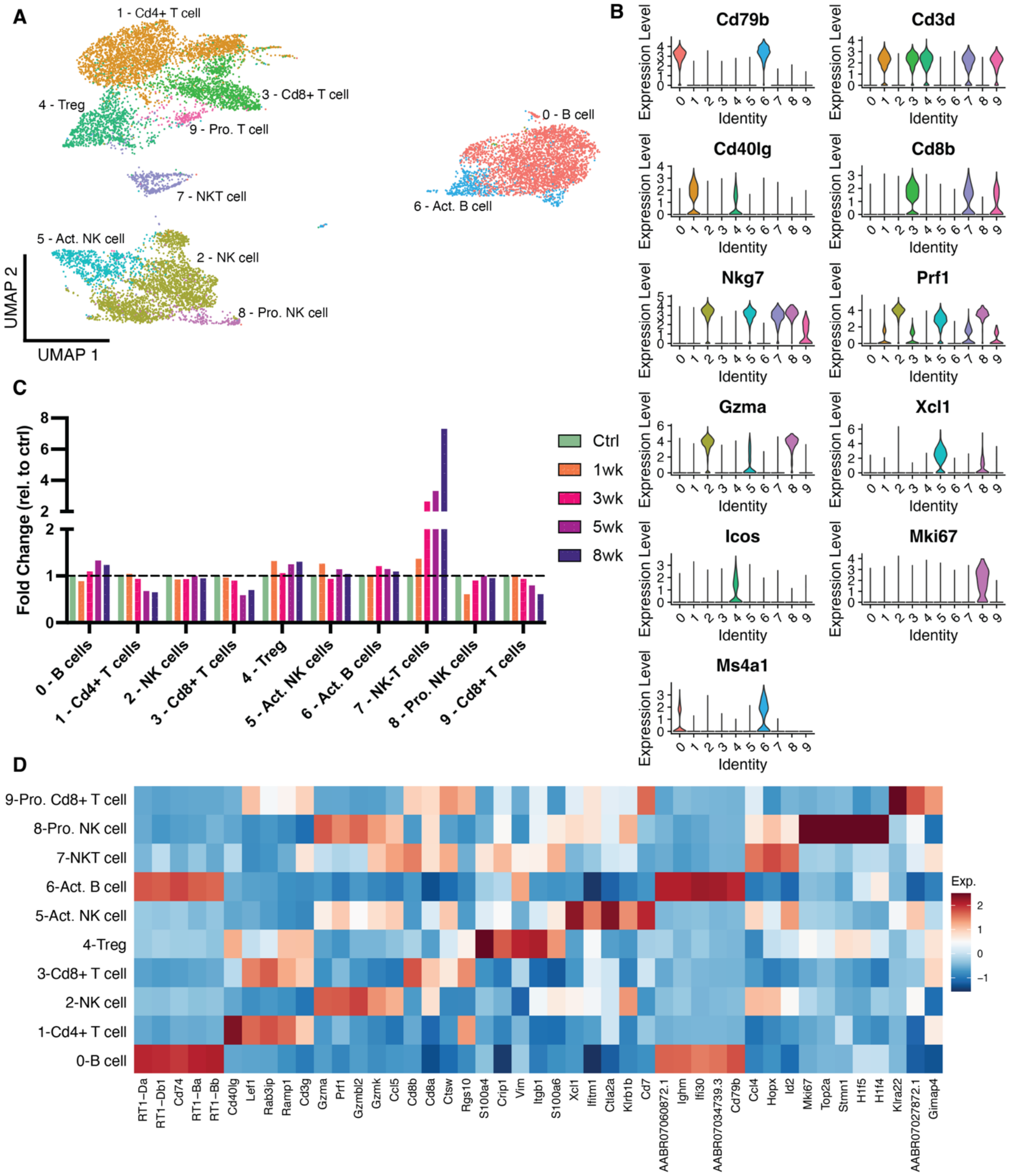

Supplemental Figure 2.10: Lymphoid subcluster analysis.

(A) UMAP of lymphoid subset representing 10 resolved cell types. (B) Top genes used to identify lymphoid populations. (C) Fold change of lymphoid populations at each timepoint relative to healthy control samples. (D) Heatmap of the top 5 differentially expressed gene per lymphoid cluster.

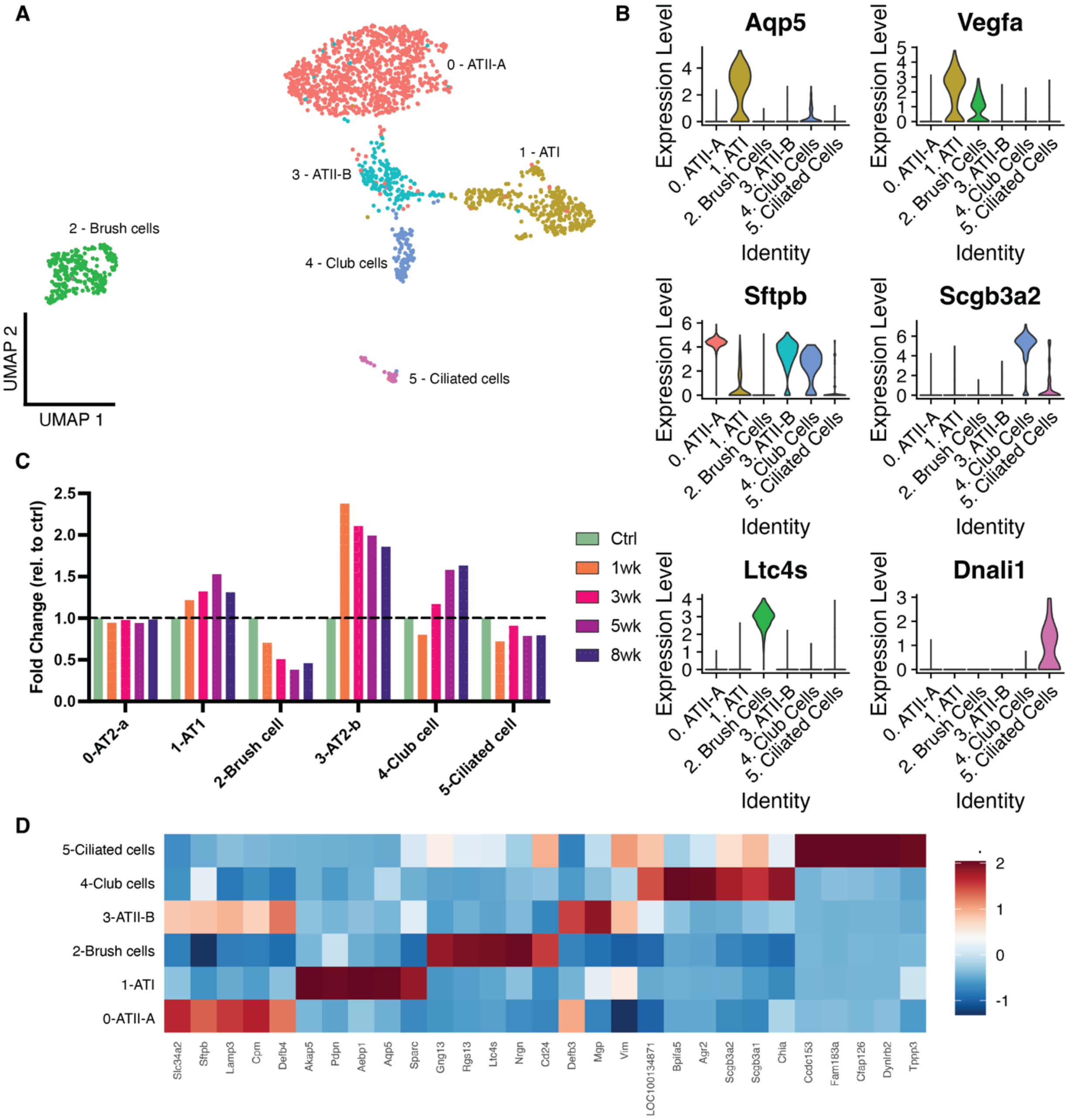

Supplemental Figure 2.11: Epithelial subcluster analysis.
(A) UMAP of epithelial subset representing 6 resolved cell types. (B) Top genes used to identify epithelial populations. (C) Fold change of epithelial populations at each timepoint relative to healthy control samples. (D) Heatmap of the top 5 differentially expressed gene per epithelial cluster.

Chapter 3 Supplements

3.1 Supplemental Figures

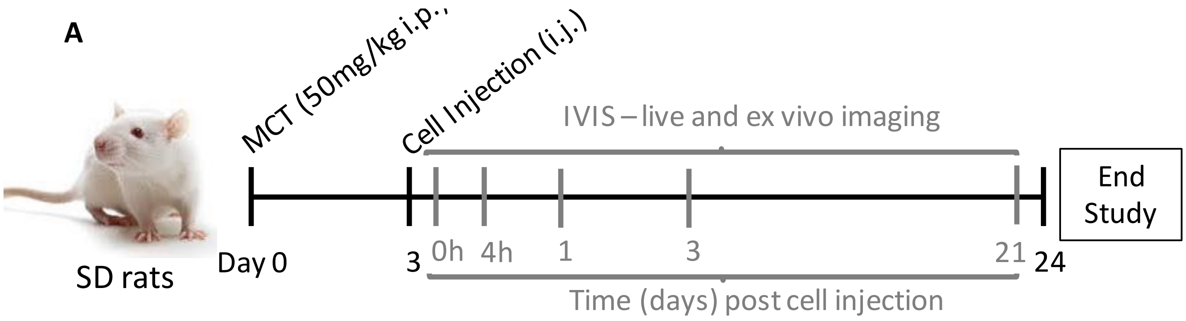

B

Treatment Group	MCT	L-EPC	Capsules
Healthy Control	-	-	-
PBS Vehicle Control	+	-	-
Non-encapsulated ECFC	+	+	-
Encapsulated ECFC	+	+	+
Empty Capsules	+	-	+

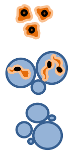

Supplemental Figure 3.1: Study design and treatment groups.
(A) Animals were i.p. injected with MCT, and provided preventive cell therapy 3 days post MCT. Bioluminescent imaging were done at baseline (0h), 4h, 1, 3 and 21 days post cell injection. End study at 24 days post MCT was performed to assess RVSP, RVH, and collect samples for histology. (B) Treatment groups given 3 days post MCT.

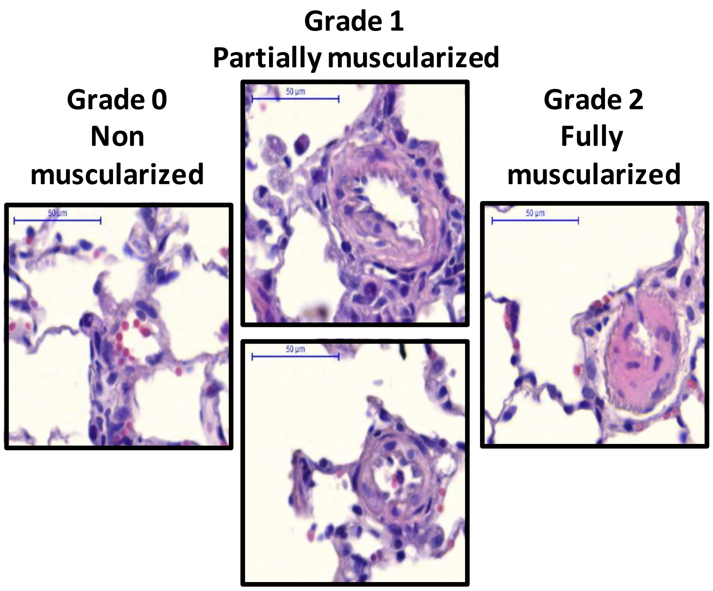

Supplementary Figure 3.2: Examples of blood vessels used for grading vascular muscularization.
Grade 0 indicates no muscularization of blood vessel, Grade 1 indicates minor or partial muscularization of the blood vessel has occurred, grade 2 indicates a severely muscularized blood vessel where only a partial lumen is observed.

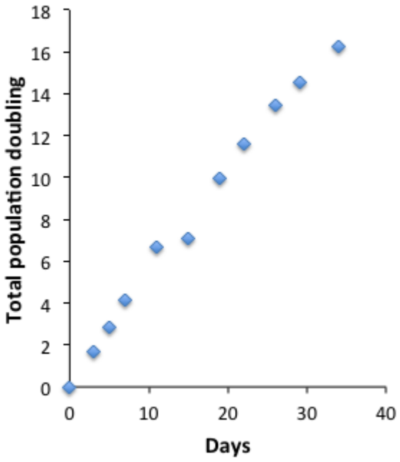

Supplemental Figure 3.3: Characterization of L-EPCs proliferative potential.

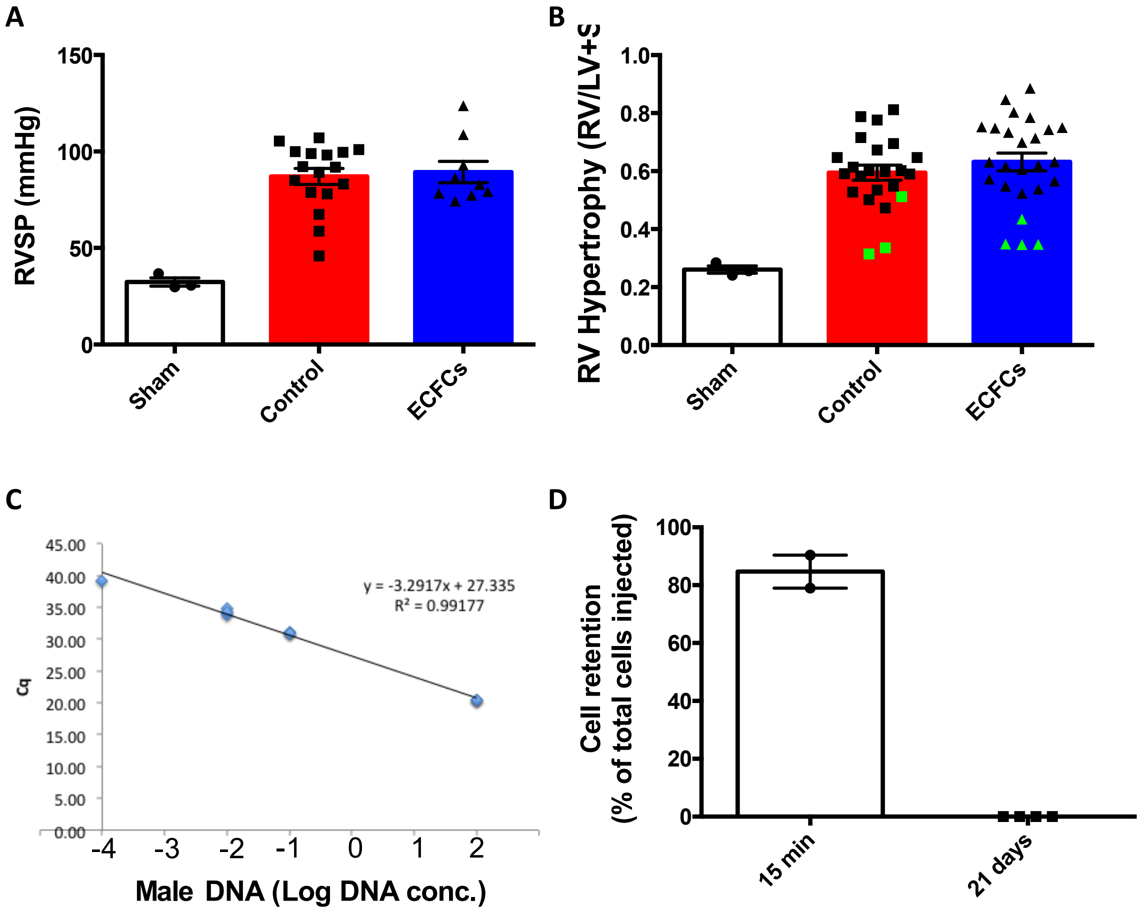

Supplemental Figure 3.4: Lack of retention within MCT treated lungs after 21 days. Green rats were sacrificed before 21 days post cell injection due to reaching humane end-point.

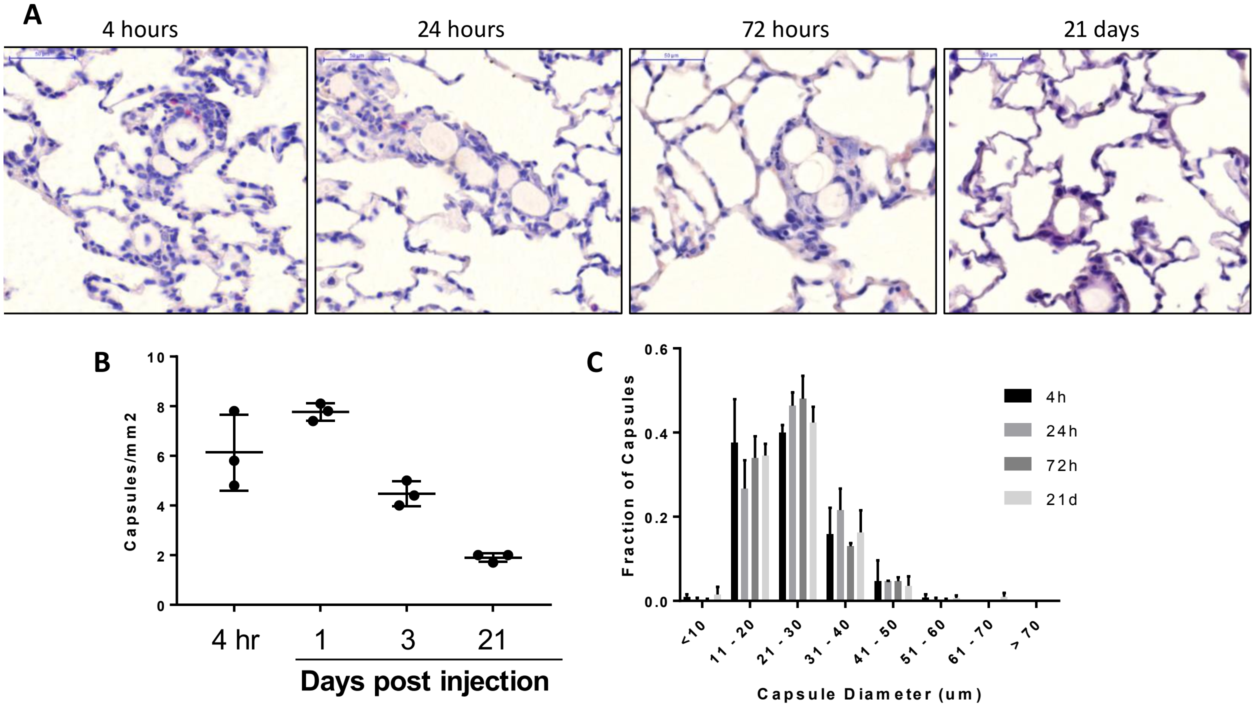

Supplemental Figure 3.5: Capsule degradation.
(A) Representative images of capsules within the lungs after 4, 24, 72 hours or 21 days post cell injection, indicated with black arrows. (B) Average number of capsules counted per mm2 of lung indicating capsules are cleared from the lung over time. (C) Capsule diameter as assessed over time, despite fewer capsules present by 21 days the capsules remaining are not significantly changed in size. n = 3 per time point, data represented as mean ± SD.

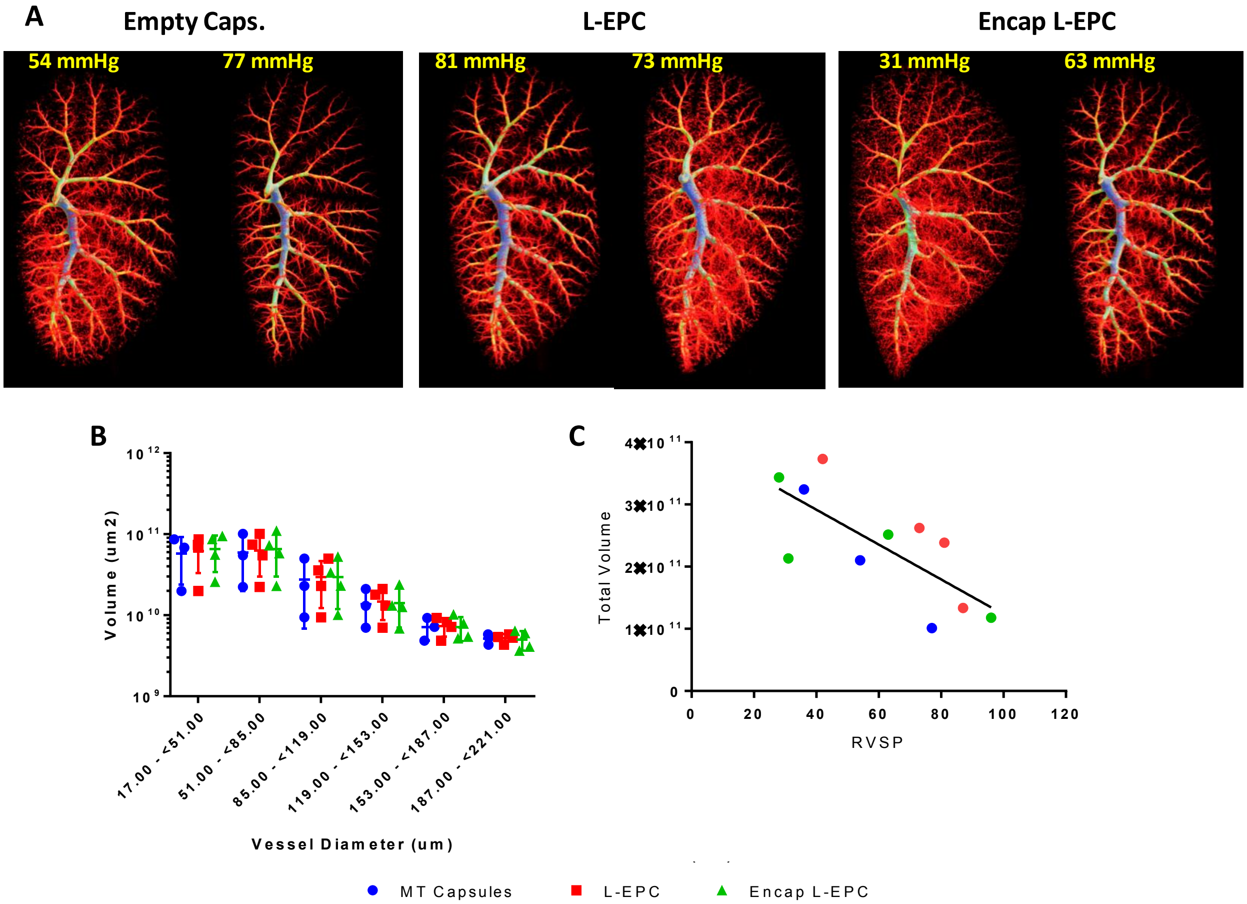

Supplemental Figure 3.6: Right ventricular systolic pressure strongly correlates with vascular volume within the lungs.

(A) Representative images of MicroCT analysis from the left lobes of SD rats given MCT and treated with: empty capsules, L-EPCs, or encapsulated L-EPCs. (B) Vascular volume between treatment groups compared by vessel diameter suggesting this experiment was underpowered to identify differences between these groups. (C) RVSP and total vascular volume had a strong inverse relationship suggesting that high pressures are more likely when total volume is decreased. Data represented as means ± SEM, n = 3 – 4.

Chapter 4 Supplements

4.1 Supplemental Methods

4.1.1 Lipophilic dye micelle controls

To control for formation of micelles during lipophilic dye labelling a series of controls were included, shown in Supplemental Figure 6. In the same manner as EV labelling, PBS was mixed with DiR at 0.5 µg/ml for 15min then spun at 100,000g for 30min at 4°C to wash unbound dye. Supernatant was removed and saved as dye positive control (DiR-Sup), and pellets were resuspended in PBS as control for micelle formation during staining (DiR-Pellet). Controls were incubated with HUVEC in the manner described for HUVEC uptake experiments with 24h of incubation prior to flow cytometry analysis.

4.1.2 HUVEC – EV uptake confocal imaging

Human umbilical vein endothelial cells (HUVEC) were cultured on fibronectin (1mg/ml for 1h at room temperature, Sigma Aldrich, Oakville, ON, Canada) coated chamber slides (ThermoFisher Scientific, Burlington, ON, Canada) at 50,000 cells per slide for 24h in standard culture conditions. After 24h, 0, 1, or 3 µg of pkh26 labelled EVs were added to the chamber and allowed to incubate for 24h. Slides were washed with PBS-T (PBS (Gibco, ON, Canada) with 0.1% Tween-20, Sigma-Aldrich, Oakville, ON, Canada), blocked with PBS + 5% bovine serum albumin (BSA, Wisent), and stained with 1:100 v450 mouse anti-human CD31 (BD Bioscience, Mississauga, ON, Canada) for 1h in the dark. Stained samples were washed again with PBS-T, stained with DRAQ5 at (1:1000 dilution, eBioscience, San Diego, CA, USA) for 10 min in the dark at room temperature. Fully stained samples were washed with PBS-T and fixed with 4% paraformaldehyde (Electron Microscopy Sciences, Hatfield, PA, USA) and mounted with prolong diamond antifade mounting media (ThermoFisher Scientific, Burlington, ON, Canada) prior to imaging with a Zeiss LSM900 confocal microscope. Z-stacks were reconstructed in Imaris Viewer (version 9.6.0, Imaris).

4.1.3 Vortex emulsion encapsulation

Prior to access to the microfluidic encapsulation, vortex-emulsion encapsulation was performed to compare tissue retention and impact on animals' respiratory health following monocrotaline (MCT, Sigma Aldrich, Oakville, ON, Canada) injection. Methodology applies to data presented in supplemental figure 8. As previously described,[260] microgel biomaterials (2% agarose or 1% gelatin – 1% agarose, Sigma Aldrich, Oakville, ON, Canada) were prepared and kept warm at 37°C. Mixtures were added dropwise by a p200 pipette into warm dimethylpolysiloxane (PDMS, Sigma Aldrich, Oakville, ON, Canada) and vortexed for 1 minute. Microgel emulsion was placed on ice for 10 minutes to stabilize microgels. Samples were washed with PBS to remove oil phase and microgels were counted with a hemocytometer. Microgel size was measured from images taken with a Nikon Eclipse TS100 inverted microscope, and diameter quantified in FIJI.[261]

4.1.4 Pulmonary hemodynamics and lung histology

To assess in vivo microgel retention, Sprague Dawley rats were given an intraperitoneal injection of MCT (60 mg/kg), and 3 days later treated with empty microgels (2% agarose or 1% agarose – 1% gelatin) or PBS. Each animal received a dose of 500,000 microgels in PBS delivered through intrajugular vein injection. End points were performed at 1-, 3-, and 7- days post microgel delivery to measure right ventricular systolic pressure (as a measure of lung vascular health) and perform histological analysis for retention of microgels. As previously described,[127] rats were anaesthetized with ketamine (35 mg/kg) and xylazine (7 mg/kg), and right ventricular systolic pressure was measured. Animals were euthanized and lungs were dissected and filled with 1:1 OCT:Saline through the trachea to inflate the lungs. Lungs were stored in 4% paraformaldehyde for 24h, washed in PBS, then in 70% ethanol. Lungs were dehydrated and prepared in paraffin blocks. 5μm sections were cut and H&E staining was performed as previously described.[64] Whole slides were scanned with Pannoramic Desk slide scanner (3D Histech Ltd., Budapest, Hungary), and one whole lung per animal was quantified for presence of microgels using Pannoramic Viewer 1.15.4 (3D Histech Ltd., Budapest, Hungary).

4.2 Supplemental Figures

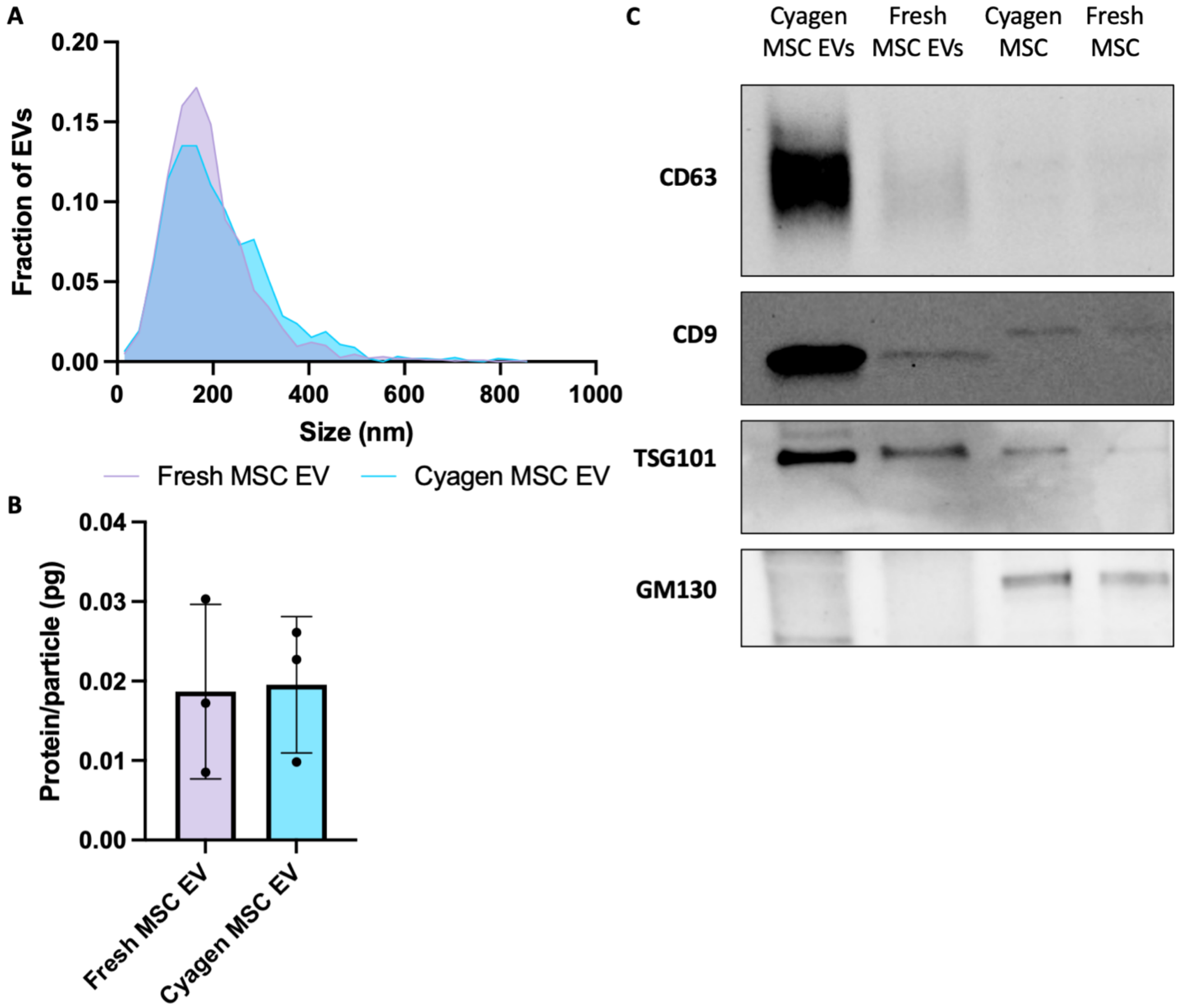

Supplemental Figure 4.1: Mesenchymal stromal cell derived extracellular vesicle characterization.

(A) Size distribution measured by nanoparticle tracking analysis demonstrating EVs with a median size less than 200nm. (B) Protein to particle ratio were consistent between cell sources tested. (C) MSC derived EVs expressed canonical EV markers CD63, CD9, and TSG101 with absence of Golgi membrane protein GM-130 by western blot. Data represents mean ± SD, n = 3 EV isolations.

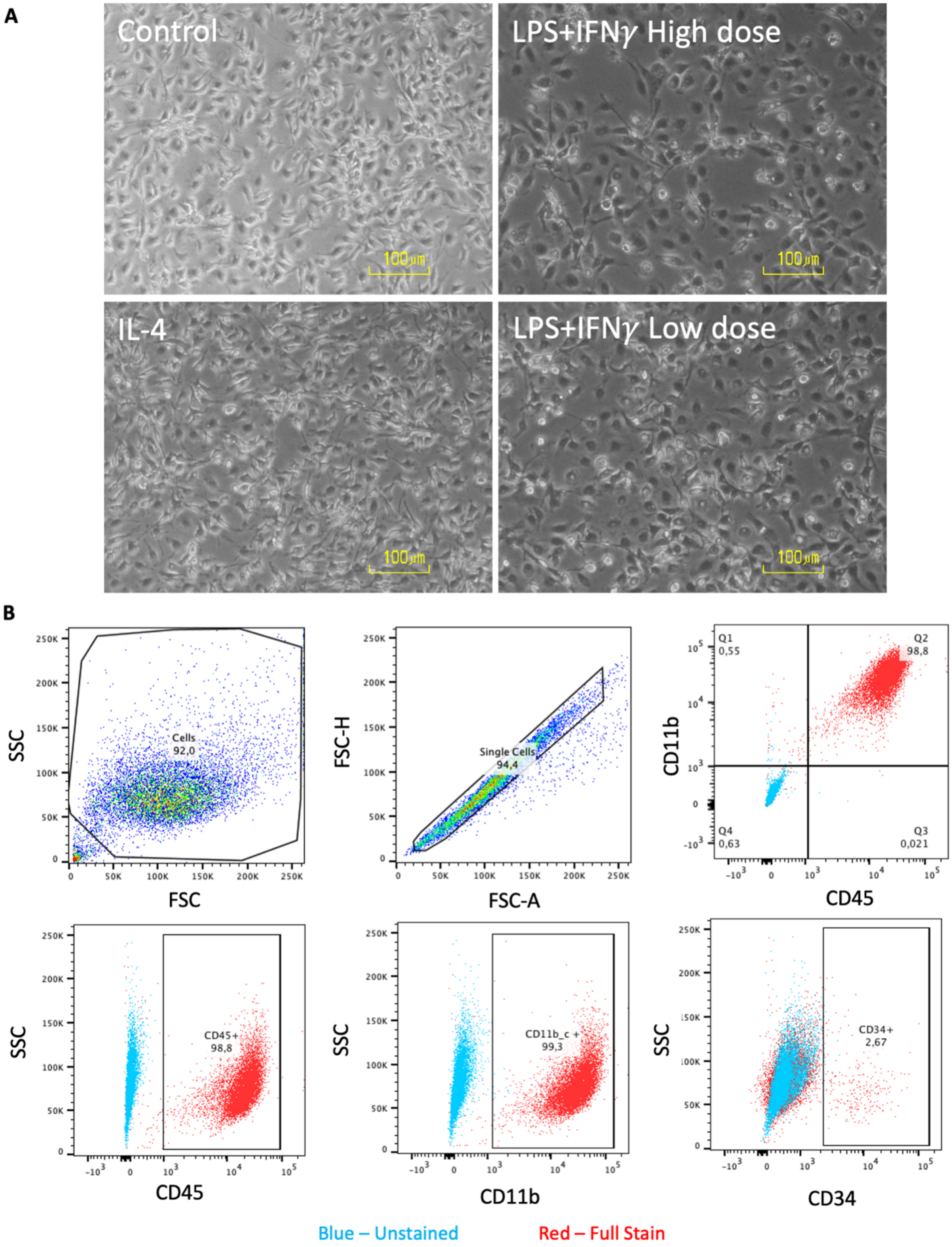

Supplemental Figure 4.2: Bone marrow derived macrophage characterization.
(A) Representative images showing morphology of untreated macrophages (MØ), IL4 stimulated M2-like, and LPS+IFNγ stimulated M1-like macrophages. (B) Representative flow plots showing MØ were positive for immune markers CD45 and CD11b while negative for CD34.

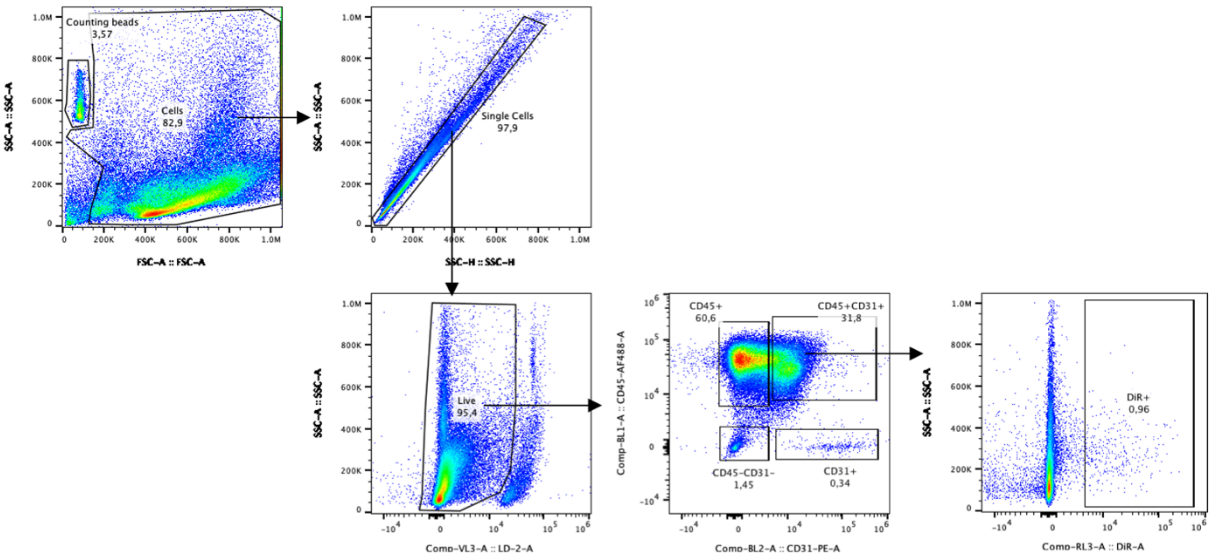

Supplemental Figure 4.3: Gating strategy employed for analysis of lung digestion samples. In brief, debris and counting beads were excluded by FSC-A and SSC-A. Doublets were discriminated with SSC-A vs SSC-H. Dead cells were excluded. CD45 and CD31 were used to separate immune cells (CD45+) from endothelial cells (CD31+) from other (stromal, and epithelial CD45-CD31-). Finally, a DiR gate was applied on each subset to characterize the uptake of DiR labelled EVs. All gates were set using both FMOs and unstained controls.

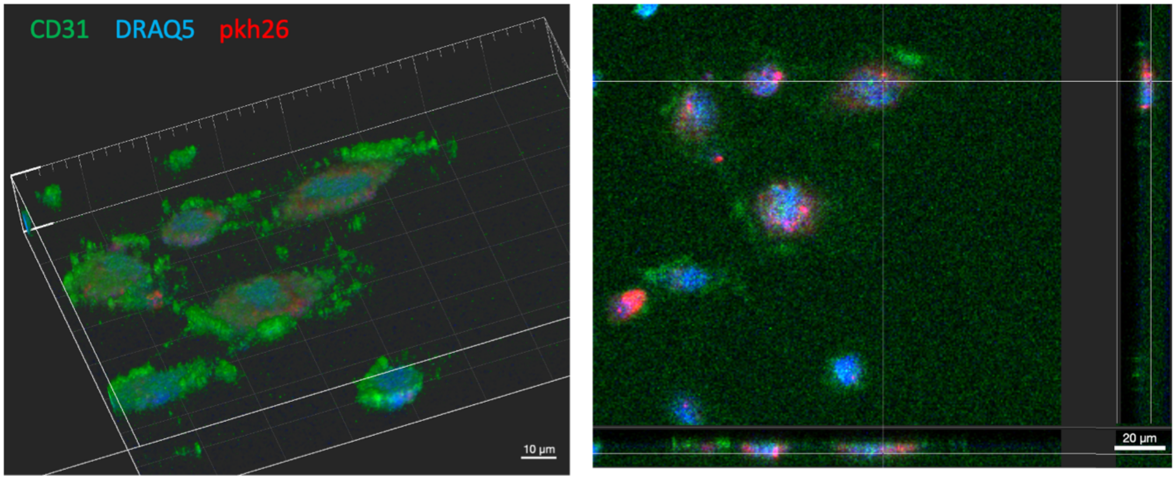

Supplemental Figure 4.4: Human umbilical vein endothelial cells (HUVEC) internalized EVs. Representative confocal images of HUVEC exposed to pkh26 labelled EVs in vitro. Z-stack and layered image demonstrate presence of EVs within cytosolic space of the HUVEC indicating internalization.

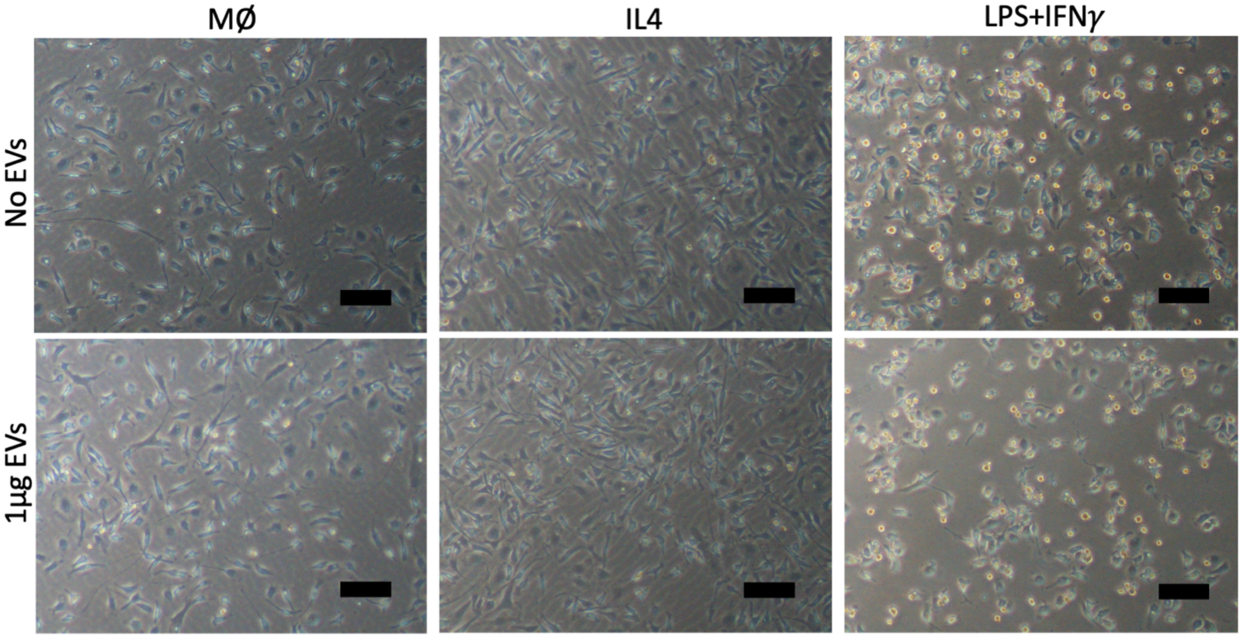

Supplemental Figure 4.5: Macrophage morphology was unchanged by EV exposure. Representative images of all macrophage groups (MØ, IL4, and LPS+IFNγ) with or without exposure to EVs in culture. Scale bar represents 100 µm.

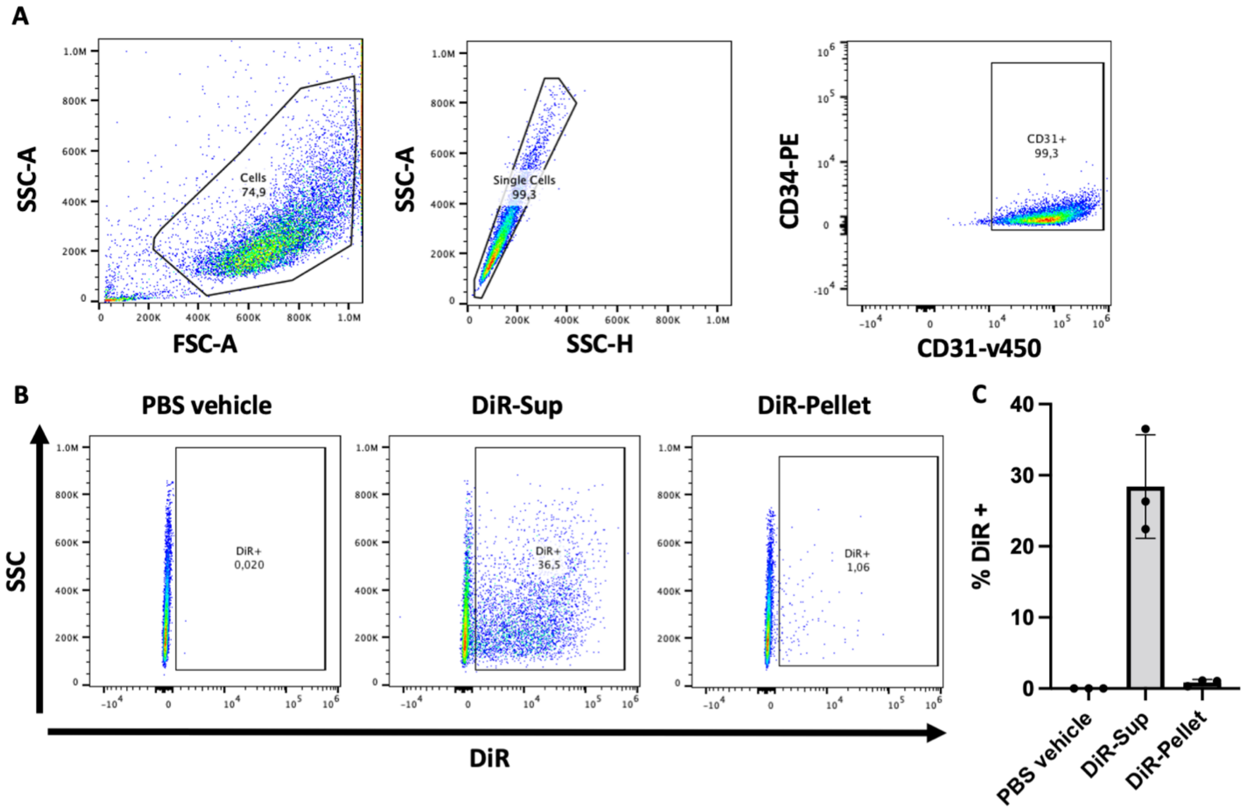

Supplemental Figure 4.6: Minimal DiR-micelles formed in labelling suspension.
(A) Representative flow plots of gating for cells, singlets, and CD31+ cells. (B) Representative flow plots of DiR labelling in HUVEC after PBS vehicle, DiR-Sup, and DiR-Pellet controls. (C) Quantification of DiR+ ECs after 24h treatment with DiR controls, demonstrating minimal accumulation of DiR-Pellet micelles following ultracentrifugation, with DiR-Sup signal representing free dye binding with HUVEC. Data represents mean ± SEM, n = 3.

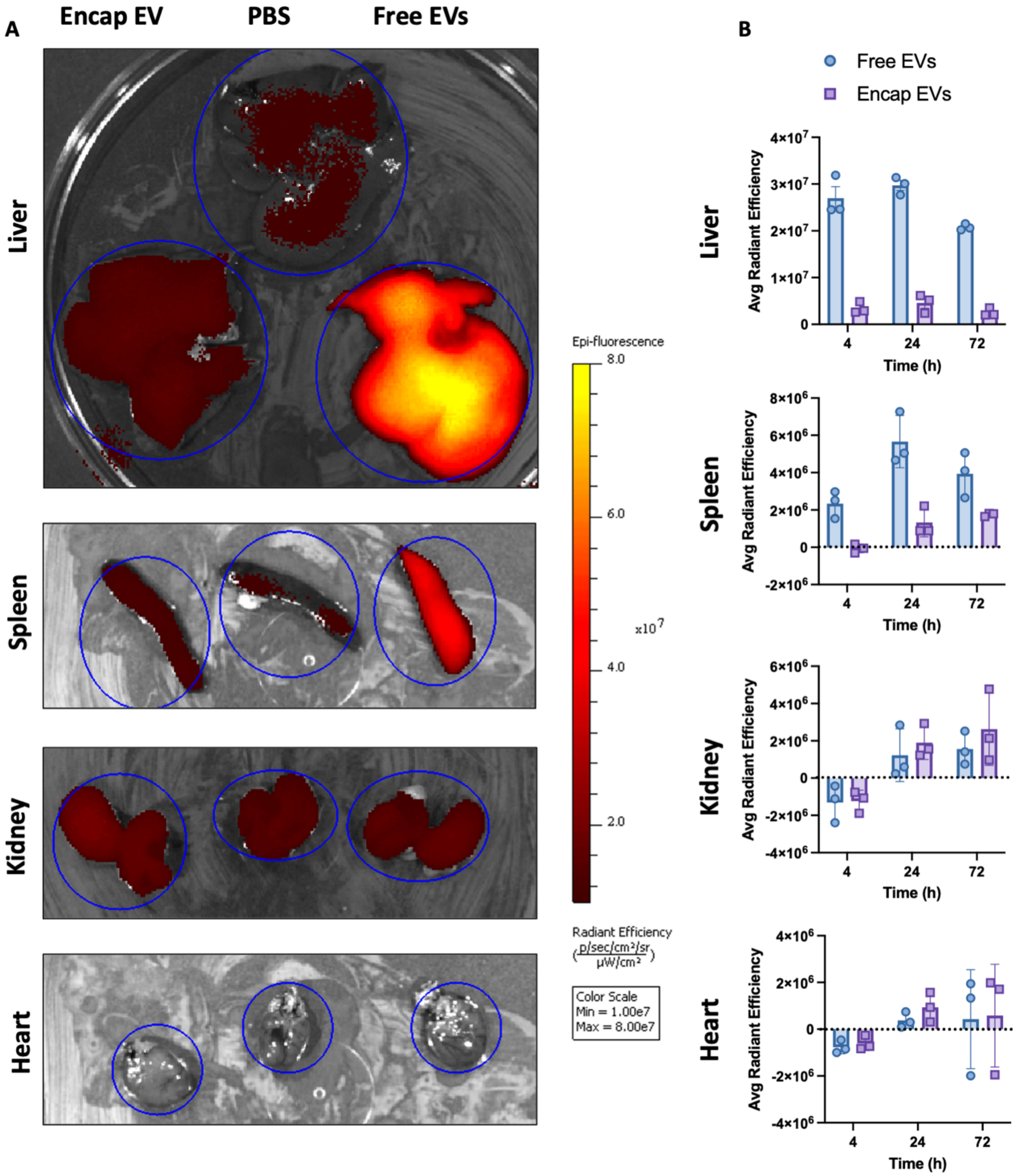

Supplemental Figure 4.7: Free and encapsulated EV uptake in liver, spleen, kidney, and heart. (A) Representative images of IVIS data showing DiR labelled EV distribution within animals treated with encapsulated and free EVs at 24h. PBS vehicle treated animals served as a control for background fluorescence intensity. (B) Quantification of fluorescence EV signal using average radiant efficiency demonstrating high uptake of free EVs in both liver and spleen. Minimal accumulation of encapsulated or free EVs was observed in the kidney or heart. Data represents mean ± SEM, n = 3.

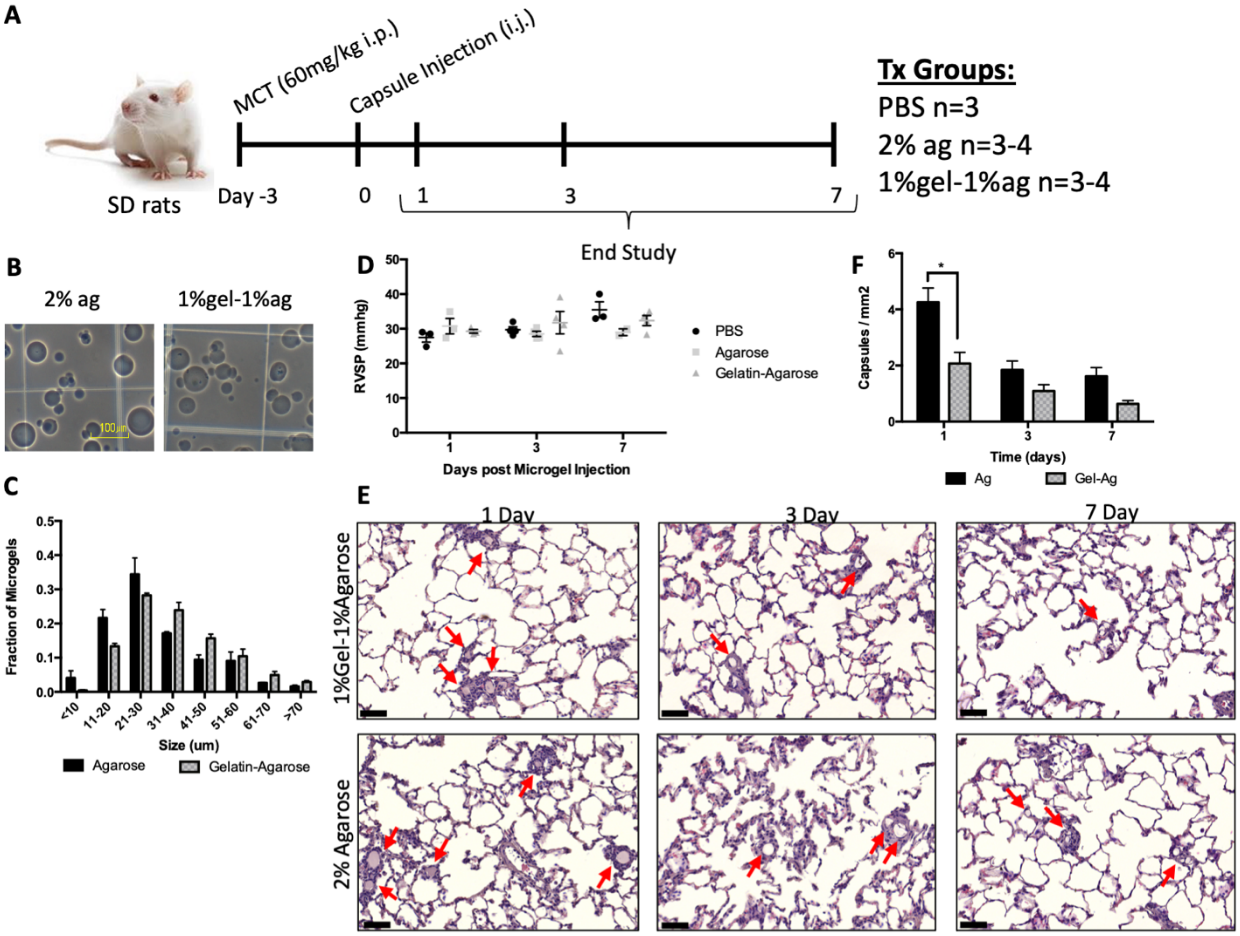

Supplemental Figure 4.8: In vivo microgel degradation.

(A) Schematic of study design. (B) Representative images of empty microgels made of 2% agarose, and 1% agarose - 1% gelatin by vortex emulsion, with size distribution (C) showing no difference in average size between these hydrogel formulations. (D) Empty microgel injection had no impact on right ventricular systolic pressures (RVSP) within these animals. (E) Representative H&E-stained images of lung histology of lungs receiving empty microgels at 1-, 3-, and 7- days post injection. Red arrows indicate presence of microgels with evidence of surrounding immune infiltrate. (F) Quantification of capsules per lung section demonstrating enhanced clearance of 1% agarose - 1% gelatin microgels. Data represents mean ± SEM, n = 3-4. Scale bar represents 50 µm.

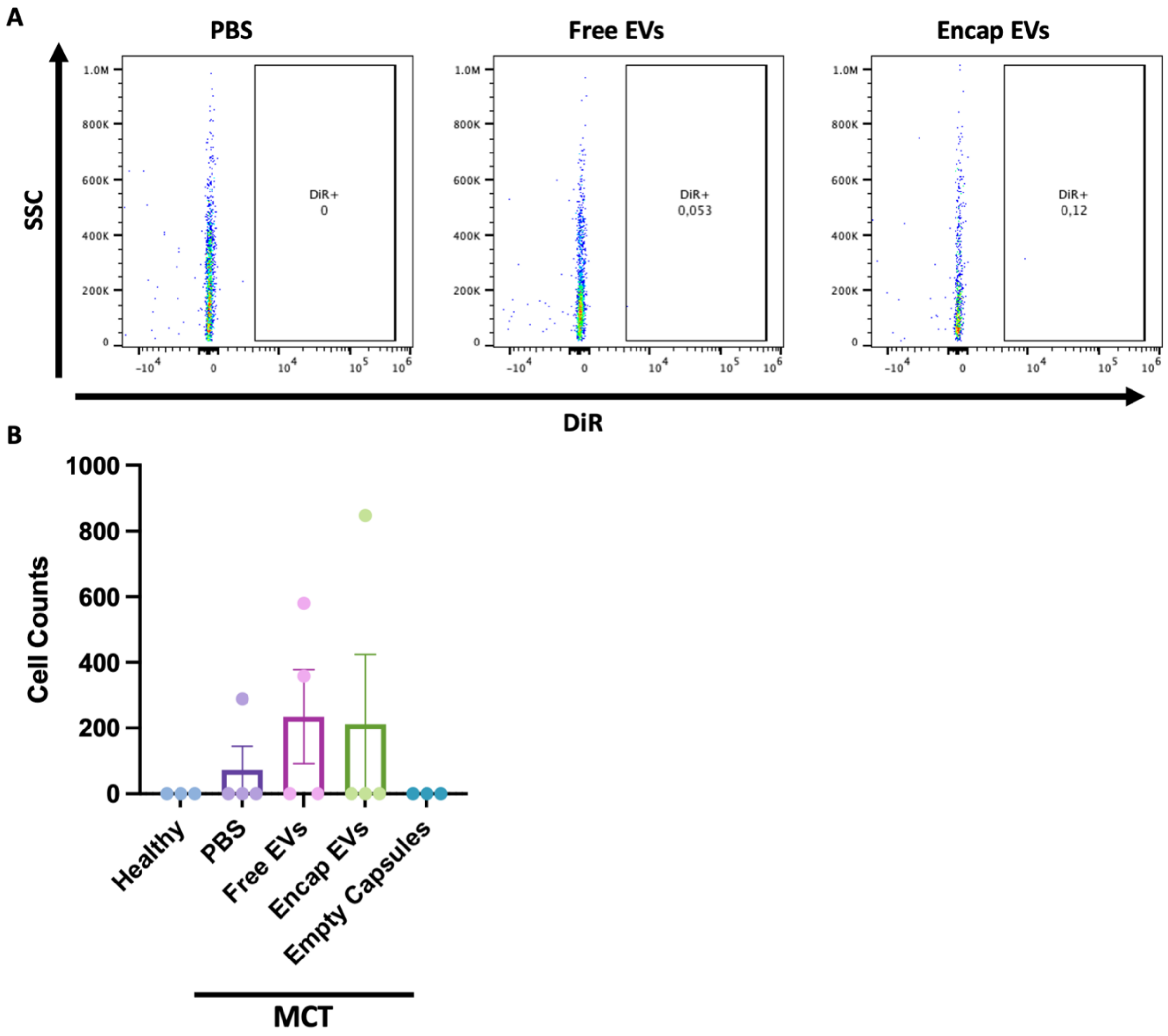

Supplemental Figure 4.9: DiR labelled EV uptake by CD45-CD31- cells.
(A) Representative flow plots showing minimal uptake of DiR+ EVs by CD45-CD31- cells, and (B) quantification showing no difference between any of the treatment groups. Data represents mean ± SEM, n = 3-4.

References

1. Simonneau, G. *et al.* Haemodynamic definitions and updated clinical classification of pulmonary hypertension. *Eur Respir J* **53**, (2019).
2. McGoon, M. D. *et al.* Pulmonary arterial hypertension: epidemiology and registries. *J Am Coll Cardiol* **62**, (2013).
3. Badlam, J. B. *et al.* United States Pulmonary Hypertension Scientific Registry: Baseline Characteristics. *Chest* **159**, 311–327 (2021).
4. Long, L. *et al.* Selective enhancement of endothelial BMPR-II with BMP9 reverses pulmonary arterial hypertension. *Nat Med* **21**, 777–785 (2015).
5. Wang, X.-J. *et al.* Germline *BMP9* mutation causes idiopathic pulmonary arterial hypertension. *European Respiratory Journal* **53**, 1801609 (2019).
6. Eyries, M. *et al.* Widening the landscape of heritable pulmonary hypertension mutations in paediatric and adult cases. *European Respiratory Journal* **53**, (2019).
7. Hong, K.-H. *et al.* Genetic Ablation of the *Bmpr2* Gene in Pulmonary Endothelium Is Sufficient to Predispose to Pulmonary Arterial Hypertension. *Circulation* **118**, 722–730 (2008).
8. Deng, Z. *et al.* Familial primary pulmonary hypertension (gene PPH1) is caused by mutations in the bone morphogenetic protein receptor-II gene. *Am J Hum Genet* **67**, 737–744 (2000).
9. Machado, R. D. *et al.* Mutations of the TGF-beta type II receptor BMPR2 in pulmonary arterial hypertension. *Hum Mutat* **27**, 121–132 (2006).
10. Humbert, M. *et al.* Pulmonary arterial hypertension in France: results from a national registry. *Am J Respir Crit Care Med* **173**, 1023–1030 (2006).
11. Larkin, E. K. *et al.* Longitudinal Analysis Casts Doubt on the Presence of Genetic Anticipation in Heritable Pulmonary Arterial Hypertension. *Am J Respir Crit Care Med* **186**, 892–896 (2012).
12. Evans, J. D. W. *et al.* BMPR2 mutations and survival in pulmonary arterial hypertension: An individual participant data meta-analysis. *Lancet Respir Med* **4**, 129–137 (2016).
13. Lavoie, J. R. *et al.* Proteomic Analysis Implicates Translationally Controlled Tumor Protein as a Novel Mediator of Occlusive Vascular Remodeling in Pulmonary Arterial Hypertension. *Circulation* **129**, 2125–2135 (2014).
14. Atkinson, C. *et al.* Primary Pulmonary Hypertension Is Associated With Reduced Pulmonary Vascular Expression of Type II Bone Morphogenetic Protein Receptor. *Circulation* **105**, 1672–1678 (2002).
15. Upton, P. D., Davies, R. J., Trembath, R. C. & Morrell, N. W. Bone Morphogenetic Protein (BMP) and Activin Type II Receptors Balance BMP9 Signals Mediated by Activin Receptor-like Kinase-1 in Human Pulmonary Artery Endothelial Cells. *Journal of Biological Chemistry* **284**, 15794–15804 (2009).
16. Tillet, E. *et al.* A heterodimer formed by bone morphogenetic protein 9 (BMP9) and BMP10 provides most BMP biological activity in plasma. *Journal of Biological Chemistry* **293**, 10963–10974 (2018).
17. Harrison, R. E. *et al.* Transforming Growth Factor-β Receptor Mutations and Pulmonary Arterial Hypertension in Childhood. *Circulation* **111**, 435–441 (2005).
18. Nasim, M. T. *et al.* Molecular genetic characterization of SMAD signaling molecules in pulmonary arterial hypertension. *Hum Mutat* **32**, 1385–1389 (2011).
19. Wang, L. *et al.* BMP9 and BMP10 Act Directly on Vascular Smooth Muscle Cells for Generation and Maintenance of the Contractile State. *Circulation* **143**, 1394–1410 (2021).
20. Nikolic, I. *et al.* Bone morphogenetic protein 9 is a mechanistic biomarker of portopulmonary hypertension. *Am J Respir Crit Care Med* **199**, 891–902 (2019).

21. Tu, L. *et al.* Selective BMP-9 Inhibition Partially Protects Against Experimental Pulmonary Hypertension. *Circ Res* **124**, 846–855 (2019).
22. Theilmann, A. L. *et al.* Endothelial BMPR2 Loss Drives a Proliferative Response to BMP (Bone Morphogenetic Protein) 9 via Prolonged Canonical Signaling. *Arterioscler Thromb Vasc Biol* **40**, 2605–2618 (2020).
23. Yung, L. M. *et al.* ACTRIIA-Fc rebalances activin/GDF versus BMP signaling in pulmonary hypertension. *Sci Transl Med* **12**, 5660 (2020).
24. Humbert, M. *et al.* Sotatercept for the Treatment of Pulmonary Arterial Hypertension. *New England Journal of Medicine* **384**, 1204–1215 (2021).
25. Gräf, S. *et al.* Identification of rare sequence variation underlying heritable pulmonary arterial hypertension. *Nature Communications 2018 9:1* **9**, 1–16 (2018).
26. Kerstjens-Frederikse, W. S. *et al.* TBX4 mutations (small patella syndrome) are associated with childhood-onset pulmonary arterial hypertension. *J Med Genet* **50**, 500–506 (2013).
27. Ma, L. *et al.* A Novel Channelopathy in Pulmonary Arterial Hypertension. *New England Journal of Medicine* **369**, 351–361 (2013).
28. Zhu, N. *et al.* Rare variant analysis of 4241 pulmonary arterial hypertension cases from an international consortium implicates FBLN2, PDGFD, and rare de novo variants in PAH. *Genome Med* **13**, 1–18 (2021).
29. Vassiliou, A. G. *et al.* Knockdown of bone morphogenetic protein type II receptor leads to decreased aquaporin 1 expression and function in human pulmonary microvascular endothelial cells. *Can J Physiol Pharmacol* **98**, 834–839 (2020).
30. Vassiliou, A. G. *et al.* Decreased bone morphogenetic protein type II receptor and BMP-related signalling molecules' expression in aquaporin 1-silenced human pulmonary microvascular endothelial cells. *Hellenic Journal of Cardiology* **62**, 84–86 (2021).
31. Budhiraja, R., Tuder, R. M. & Hassoun, P. M. Endothelial Dysfunction in Pulmonary Hypertension. *Circulation* vol. 109 159–165 Preprint at https://doi.org/10.1161/01.CIR.0000102381.57477.50 (2004).
32. Zelt, J. G. E. *et al.* Mortality trends in pulmonary arterial hypertension in canada: a temporal analysis of survival per ESC/ERS Guideline Era. *Eur Respir J* 2101552 (2021) doi:10.1183/13993003.01552-2021.
33. Hoeper, M. M. *et al.* Temporal trends in pulmonary arterial hypertension: Results from the COMPERA registry. *Eur Respir J* 2102024 (2021) doi:10.1183/13993003.02024-2021.
34. Kurakula, K. *et al.* Endothelial Dysfunction in Pulmonary Hypertension: Cause or Consequence? *Biomedicines* **9**, 57 (2021).
35. Jurasz, P., Courtman, D., Babaie, S. & Stewart, D. J. Role of apoptosis in pulmonary hypertension: From experimental models to clinical trials. *Pharmacol Ther* **126**, 1–8 (2010).
36. Taraseviciene-Stewart, L. *et al.* Inhibition of the VEGF receptor 2 combined with chronic hypoxia causes cell death-dependent pulmonary endothelial cell proliferation and severe pulmonary hypertension. *The FASEB Journal* **15**, 427–438 (2001).
37. Gomez-Arroyo, J. G. *et al.* The monocrotaline model of pulmonary hypertension in perspective. *Am J Physiol Lung Cell Mol Physiol* **302**, L363-9 (2012).
38. Ciuclan, L. *et al.* A Novel Murine Model of Severe Pulmonary Arterial Hypertension. *Am J Respir Crit Care Med* **184**, 1171–1182 (2011).
39. Tanaka, Y., Schuster, D. P., Davis, E. C., Patterson, G. A. & Botney, M. D. The role of vascular injury and hemodynamics in rat pulmonary artery remodeling. *Journal of Clinical Investigation* **98**, 434–442 (1996).
40. Okada, K. *et al.* Pulmonary hemodynamics modify the rat pulmonary artery response to injury. A neointimal model of pulmonary hypertension. *Am J Pathol* **151**, 1019 (1997).

41. Goldthorpe, H. *et al.* Occlusive lung arterial lesions in endothelial-targeted, fas-induced apoptosis transgenic mice. *Am J Respir Cell Mol Biol* **53**, 712–718 (2015).
42. Deng, Y. *et al.* Optimizing imaging of the rat pulmonary microvasculature by micro-computed tomography. *Pulm Circ* **9**, (2019).
43. Dutly, A. E. *et al.* Fluorescent microangiography (FMA): an improved tool to visualize the pulmonary microvasculature. *Laboratory Investigation* **86**, 409–416 (2006).
44. Abe, K. *et al.* Haemodynamic unloading reverses occlusive vascular lesions in severe pulmonary hypertension. *Cardiovasc Res* **111**, 16–25 (2016).
45. Dickinson, M. G., Bartelds, B., Borgdorff, M. A. J. & Berger, R. M. F. The role of disturbed blood flow in the development of pulmonary arterial hypertension: lessons from preclinical animal models. *American Journal of Physiology-Lung Cellular and Molecular Physiology* **305**, L1–L14 (2013).
46. HEATH, D. & EDWARDS, J. E. The Pathology of Hypertensive Pulmonary Vascular Disease. *Circulation* **18**, 533–547 (1958).
47. Engelfriet, P. M. *et al.* Pulmonary arterial hypertension in adults born with a heart septal defect: the Euro Heart Survey on adult congenital heart disease. *Heart* **93**, 682–687 (2007).
48. Van Der Feen, D. E. *et al.* Cellular senescence impairs the reversibility of pulmonary arterial hypertension. *Sci Transl Med* **12**, (2020).
49. Rai, P. R. *et al.* The Cancer Paradigm of Severe Pulmonary Arterial Hypertension. *Am J Respir Crit Care Med* **178**, 558–564 (2008).
50. Dvorak, H. F. Tumors: Wounds That Do Not Heal—Redux. *Cancer Immunol Res* **3**, 1–11 (2015).
51. Hanahan, D. & Weinberg, R. A. The Hallmarks of Cancer. *Cell* **100**, 57–70 (2000).
52. Cao, L., Li, W., Kim, S., Brodie, S. G. & Deng, C.-X. Senescence, aging, and malignant transformation mediated by p53 in mice lacking the Brca1 full-length isoform. *Genes Dev* **17**, 201–213 (2003).
53. Culley, M. K. & Chan, S. Y. Endothelial Senescence: A New Age in Pulmonary Hypertension. *Circ Res* **130**, 928–941 (2022).
54. Boucherat, O. *et al.* The cancer theory of pulmonary arterial hypertension. *Pulm Circ* **7**, 285–299 (2017).
55. Michelakis, E. D. *et al.* Dichloroacetate, a Metabolic Modulator, Prevents and Reverses Chronic Hypoxic Pulmonary Hypertension in Rats. *Circulation* **105**, 244–250 (2002).
56. Caruso, P. *et al.* Identification of MicroRNA-124 as a Major Regulator of Enhanced Endothelial Cell Glycolysis in Pulmonary Arterial Hypertension via PTBP1 (Polypyrimidine Tract Binding Protein) and Pyruvate Kinase M2. *Circulation* **136**, 2451–2467 (2017).
57. Diebold, I. *et al.* BMPR2 Preserves Mitochondrial Function and DNA during Reoxygenation to Promote Endothelial Cell Survival and Reverse Pulmonary Hypertension. *Cell Metab* **21**, 596–608 (2015).
58. Zhang, H. *et al.* Metabolic and Proliferative State of Vascular Adventitial Fibroblasts in Pulmonary Hypertension Is Regulated Through a MicroRNA-124/PTBP1 (Polypyrimidine Tract Binding Protein 1)/Pyruvate Kinase Muscle Axis. *Circulation* **136**, 2468–2485 (2017).
59. Hoeper, M. M. *et al.* Imatinib mesylate as add-on therapy for pulmonary arterial hypertension: Results of the randomized IMPRES study. *Circulation* **127**, 1128–1138 (2013).
60. Van Der Feen, D. E. *et al.* Multicenter preclinical validation of BET inhibition for the treatment of pulmonary arterial hypertension. *Am J Respir Crit Care Med* **200**, 910–920 (2019).
61. Meloche, J. *et al.* Role for DNA damage signaling in pulmonary arterial hypertension. *Circulation* **129**, 786–797 (2014).
62. Farber, H. W. *et al.* Five-Year Outcomes of Patients Enrolled in the REVEAL Registry. *Chest* **148**, 1043–1054 (2015).

63. Kozu, K. *et al.* Sex differences in hemodynamic responses and long-term survival to optimal medical therapy in patients with pulmonary arterial hypertension. *Heart Vessels* **33**, 939–947 (2018).
64. Chaudhary, K. R., Deng, Y., Yang, A., Cober, N. D. & Stewart, D. J. Penetrance of Severe Pulmonary Arterial Hypertension in Response to Vascular Endothelial Growth Factor Receptor 2 Blockade in a Genetically Prone Rat Model Is Reduced by Female Sex. *J Am Heart Assoc* **10**, (2021).
65. Tofovic, S. P., Zhang, X., Jackson, E. K., Dacic, S. & Petrusevska, G. 2-Methoxyestradiol mediates the protective effects of estradiol in monocrotaline-induced pulmonary hypertension. *Vascul Pharmacol* **45**, 358–367 (2006).
66. Frump, A. L. *et al.* Estradiol improves right ventricular function in rats with severe angioproliferative pulmonary hypertension: effects of endogenous and exogenous sex hormones. *Am J Physiol Lung Cell Mol Physiol* **308**, L873–L890 (2015).
67. Philip, J. L. *et al.* Exogenous Estrogen Preserves Distal Pulmonary Arterial Mechanics and Prevents Pulmonary Hypertension in Rats. *Am J Respir Crit Care Med* **201**, 371–374 (2020).
68. Ventetuolo, C. E. *et al.* Higher estradiol and lower dehydroepiandrosterone-sulfate levels are associated with pulmonary arterial hypertension in men. *Am J Respir Crit Care Med* **193**, 1168–1175 (2016).
69. Alzoubi, A. *et al.* Dehydroepiandrosterone restores right ventricular structure and function in rats with severe pulmonary arterial hypertension. *American Journal of Physiology-Heart and Circulatory Physiology* **304**, H1708–H1718 (2013).
70. Austin, E. D. *et al.* Alterations in oestrogen metabolism: implications for higher penetrance of familial pulmonary arterial hypertension in females. *European Respiratory Journal* **34**, 1093–1099 (2009).
71. White, K. *et al.* Activity of the Estrogen-Metabolizing Enzyme Cytochrome P450 1B1 Influences the Development of Pulmonary Arterial Hypertension. *Circulation* **126**, 1087–1098 (2012).
72. Dean, A. *et al.* Role of the Aryl Hydrocarbon Receptor in Sugen 5416–induced Experimental Pulmonary Hypertension. *Am J Respir Cell Mol Biol* **58**, 320–330 (2018).
73. Mair, K. M. *et al.* Sex-Dependent Influence of Endogenous Estrogen in Pulmonary Hypertension. *Am J Respir Crit Care Med* **190**, 456–467 (2014).
74. Kawut, S. M. *et al.* Anastrozole in pulmonary arterial hypertension: A randomized, double-blind, placebo-controlled trial. *Am J Respir Crit Care Med* **195**, 360–368 (2017).
75. Jiang, B. *et al.* Marked Strain-Specific Differences in the SU5416 Rat Model of Severe Pulmonary Arterial Hypertension. *Am J Respir Cell Mol Biol* **54**, 461–468 (2016).
76. Rabinovitch, M., Guignabert, C., Humbert, M. & Nicolls, M. R. Inflammation and Immunity in the Pathogenesis of Pulmonary Arterial Hypertension. *Circ Res* **115**, 165–175 (2014).
77. Chu, J. W., Kao, P. N., Faul, J. L. & Doyle, R. L. High Prevalence of Autoimmune Thyroid Disease in Pulmonary Arterial Hypertension. *Chest* **122**, 1668–1673 (2002).
78. Soon, E. *et al.* Elevated Levels of Inflammatory Cytokines Predict Survival in Idiopathic and Familial Pulmonary Arterial Hypertension. *Circulation* **122**, 920–927 (2010).
79. Rich, S. *et al.* Antinuclear antibodies in primary pulmonary hypertension. *J Am Coll Cardiol* **8**, 1307–1311 (1986).
80. Perros, F. *et al.* Pulmonary Lymphoid Neogenesis in Idiopathic Pulmonary Arterial Hypertension. *Am J Respir Crit Care Med* **185**, 311–321 (2012).
81. Zawia, A. *et al.* Altered Macrophage Polarization Induces Experimental Pulmonary Hypertension and Is Observed in Patients With Pulmonary Arterial Hypertension. *Arterioscler Thromb Vasc Biol* **41**, 430–445 (2021).

82. Frid, M. G. *et al.* Hypoxia-Induced Pulmonary Vascular Remodeling Requires Recruitment of Circulating Mesenchymal Precursors of a Monocyte/Macrophage Lineage. *Am J Pathol* **168**, 659–669 (2006).
83. Botney, M. D., Bahadori, L. & Gold, L. I. Vascular remodeling in primary pulmonary hypertension. Potential role for transforming growth factor-beta. *Am J Pathol* **144**, 286 (1994).
84. Zaiman, A. L. *et al.* Role of the TGF-β/Alk5 Signaling Pathway in Monocrotaline-induced Pulmonary Hypertension. *Am J Respir Crit Care Med* **177**, 896–905 (2008).
85. Chen, Y.-F. *et al.* Dominant negative mutation of the TGF-β receptor blocks hypoxia-induced pulmonary vascular remodeling. *J Appl Physiol* **100**, 564–571 (2006).
86. Long, L. *et al.* Altered Bone Morphogenetic Protein and Transforming Growth Factor-β Signaling in Rat Models of Pulmonary Hypertension. *Circulation* **119**, 566–576 (2009).
87. Yung, L.-M. *et al.* A Selective Transforming Growth Factor-β Ligand Trap Attenuates Pulmonary Hypertension. *Am J Respir Crit Care Med* **194**, 1140–1151 (2016).
88. Tian, W. *et al.* Phenotypically Silent Bone Morphogenetic Protein Receptor 2 Mutations Predispose Rats to Inflammation-Induced Pulmonary Arterial Hypertension by Enhancing the Risk for Neointimal Transformation. *Circulation* **140**, 1409–1425 (2019).
89. Ulrich, S., Nicolls, M. R., Taraseviciene, L., Speich, R. & Voelkel, N. Increased Regulatory and Decreased CD8+ Cytotoxic T Cells in the Blood of Patients with Idiopathic Pulmonary Arterial Hypertension. *Respiration* **75**, 272–280 (2008).
90. Hautefort, A. *et al.* T-Helper 17 Cell Polarization in Pulmonary Arterial Hypertension. *Chest* **147**, 1610–1620 (2015).
91. Cortez, V. S. *et al.* SMAD4 impedes the conversion of NK cells into ILC1-like cells by curtailing non-canonical TGF-β signaling. *Nat Immunol* **18**, 995–1003 (2017).
92. Cerdeira, A. S. *et al.* Conversion of Peripheral Blood NK Cells to a Decidual NK-like Phenotype by a Cocktail of Defined Factors. *The Journal of Immunology* **190**, 3939–3948 (2013).
93. Hanna, J. *et al.* Decidual NK cells regulate key developmental processes at the human fetal-maternal interface. *Nat Med* **12**, 1065–1074 (2006).
94. Bruno, A. *et al.* The Proangiogenic Phenotype of Natural Killer Cells in Patients with Non-Small Cell Lung Cancer. *Neoplasia* **15**, 133-IN7 (2013).
95. Krzywinska, E. *et al.* Loss of HIF-1α in natural killer cells inhibits tumour growth by stimulating non-productive angiogenesis. *Nature Communications 2017 8:1* **8**, 1–13 (2017).
96. Ormiston, M. L. *et al.* Impaired natural killer cell phenotype and function in idiopathic and heritable pulmonary arterial hypertension. *Circulation* **126**, 1099–1109 (2012).
97. Rätsep, M. T. *et al.* Spontaneous pulmonary hypertension in genetic mouse models of natural killer cell deficiency. *American Journal of Physiology-Lung Cellular and Molecular Physiology* **315**, L977–L990 (2018).
98. Ormiston, M. L., Deng, Y., Stewart, D. J. & Courtman, D. W. Innate immunity in the therapeutic actions of endothelial progenitor cells in pulmonary hypertension. *Am J Respir Cell Mol Biol* **43**, 546–554 (2010).
99. Ormiston, M. L. *et al.* A Lymphocyte-Dependent Mode of Action for Imatinib Mesylate in Experimental Pulmonary Hypertension. *Am J Pathol* **182**, 1541–1551 (2013).
100. Suen, C. M., Chaudhary, K. R., Deng, Y., Jiang, B. & Stewart, D. J. Fischer rats exhibit maladaptive structural and molecular right ventricular remodelling in severe pulmonary hypertension: a genetically prone model for right heart failure. *Cardiovasc Res* **115**, 788–799 (2019).
101. Gillich, A. *et al.* Capillary cell-type specialization in the alveolus. *Nature* **586**, 785–789 (2020).
102. Schupp, J. C. *et al.* Integrated Single-Cell Atlas of Endothelial Cells of the Human Lung. *Circulation* **144**, 286–302 (2021).

103. Schaum, N. *et al.* Single-cell transcriptomics of 20 mouse organs creates a Tabula Muris. *Nature* **562**, 367–372 (2018).
104. Hong, J. *et al.* Single-cell study of two rat models of pulmonary arterial hypertension reveals connections to human pathobiology and drug repositioning. *Am J Respir Crit Care Med* **203**, 1006–1022 (2021).
105. Abe, K. *et al.* Formation of Plexiform Lesions in Experimental Severe Pulmonary Arterial Hypertension. *Circulation* **121**, 2747–2754 (2010).
106. Vitali, S. H. *et al.* The Sugen 5416/Hypoxia Mouse Model of Pulmonary Hypertension Revisited: Long-Term Follow-Up. *Pulm Circ* **4**, 619–629 (2014).
107. Stenmark, K. R., Meyrick, B., Galie, N., Mooi, W. J. & McMurtry, I. F. Animal models of pulmonary arterial hypertension: The hope for etiological discovery and pharmacological cure. *Am J Physiol Lung Cell Mol Physiol* **297**, 1013–1032 (2009).
108. Boucherat, O., Agrawal, V., Lawrie, A. & Bonnet, S. The Latest in Animal Models of Pulmonary Hypertension and Right Ventricular Failure. *Circ Res* **130**, 1466–1486 (2022).
109. Morimatsu, Y. *et al.* Development and Characterization of an Animal Model of Severe Pulmonary Arterial Hypertension. *J Vasc Res* **49**, 33–42 (2012).
110. van Albada, M. E. *et al.* The role of increased pulmonary blood flow in pulmonary arterial hypertension. *European Respiratory Journal* **26**, 487–493 (2005).
111. Hoshikawa, Y. *et al.* Hypoxia induces different genes in the lungs of rats compared with mice. *Physiol Genomics* **12**, 209–219 (2003).
112. Weisel, F. C. *et al.* Impact of S-Adenosylmethionine Decarboxylase 1 on Pulmonary Vascular Remodeling. *Circulation* **129**, 1510–1523 (2014).
113. Dai, Z. & Zhao, Y.-Y. Discovery of a murine model of clinical PAH: Mission impossible? *Trends Cardiovasc Med* **27**, 229–236 (2017).
114. Dai, Z., Li, M., Wharton, J., Zhu, M. M. & Zhao, Y.-Y. Prolyl-4 Hydroxylase 2 (PHD2) Deficiency in Endothelial Cells and Hematopoietic Cells Induces Obliterative Vascular Remodeling and Severe Pulmonary Arterial Hypertension in Mice and Humans Through Hypoxia-Inducible Factor-2α. *Circulation* **133**, 2447–2458 (2016).
115. Steiner, M. K. *et al.* Interleukin-6 Overexpression Induces Pulmonary Hypertension. *Circ Res* **104**, 236–244 (2009).
116. Li, X. & Wang, C.-Y. From bulk, single-cell to spatial RNA sequencing. *Int J Oral Sci* **13**, 36 (2021).
117. Ogbeide, S., Giannese, F., Mincarelli, L. & Macaulay, I. C. Into the multiverse: advances in single-cell multiomic profiling. *Trends in Genetics* **38**, 831–843 (2022).
118. Sikkema, L. *et al.* An integrated cell atlas of the lung in health and disease. *Nature Medicine 2023 29:6* **29**, 1563–1577 (2023).
119. Kalucka, J. *et al.* Single-Cell Transcriptome Atlas of Murine Endothelial Cells. *Cell* **180**, 764-779.e20 (2020).
120. Godoy, R. S. *et al.* Single-cell transcriptomic atlas of lung microvascular regeneration after targeted endothelial cell ablation. *Elife* **12**, (2023).
121. Rodor, J. *et al.* Single-cell RNA-seq profiling of mouse endothelial cells in response to pulmonary arterial hypertension. *Cardiovasc Res* (2021) doi:10.1093/cvr/cvab296.
122. Crnkovic, S. *et al.* Single-cell transcriptomics reveals skewed cellular communication and phenotypic shift in pulmonary artery remodeling. *JCI Insight* **7**, (2022).
123. Yoder, M. C. *et al.* Redefining endothelial progenitor cells via clonal analysis and hematopoietic stem/progenitor cell principals. *Blood* **109**, 1–3 (2007).
124. Foster, W. S., Suen, C. M. & Stewart, D. J. Regenerative Cell and Tissue-based Therapies for Pulmonary Arterial Hypertension. *Canadian Journal of Cardiology* **30**, 1350–1360 (2014).

125. Alphonse, R. S. *et al.* The isolation and culture of endothelial colony-forming cells from human and rat lungs. *Nat Protoc* **10**, 1697–1708 (2015).
126. Yu, S. *et al.* Isolation and characterization of endothelial colony-forming cells from mononuclear cells of rat bone marrow. *Exp Cell Res* **370**, 116–126 (2018).
127. Zhao, Y. D. *et al.* Rescue of monocrotaline-induced pulmonary arterial hypertension using bone marrow-derived endothelial-like progenitor cells: Efficacy of combined cell and eNOS gene therapy in established disease. *Circ Res* **96**, 442–450 (2005).
128. Kang, K.-T., Lin, R.-Z., Kuppermann, D., Melero-Martin, J. M. & Bischoff, J. Endothelial colony forming cells and mesenchymal progenitor cells form blood vessels and increase blood flow in ischemic muscle. *Sci Rep* **7**, 770 (2017).
129. Ikutomi, M. *et al.* Diverse contribution of bone marrow-derived late-outgrowth endothelial progenitor cells to vascular repair under pulmonary arterial hypertension and arterial neointimal formation. *J Mol Cell Cardiol* **86**, 121–135 (2015).
130. Kolf, C. M., Cho, E. & Tuan, R. S. Mesenchymal stromal cells. Biology of adult mesenchymal stem cells: regulation of niche, self-renewal and differentiation. *Arthritis Res Ther* **9**, 204 (2007).
131. Dmitrieva, R. I. *et al.* Bone marrow- and subcutaneous adipose tissue-derived mesenchymal stem cells Differences and similarities © 2012 Landes Bioscience . Do not distribute . © 2012 Landes Bioscience . Do not distribute . *Cell Cycle* **11**, 377–383 (2012).
132. Strioga, M., Viswanathan, S., Darinskas, A., Slaby, O. & Michalek, J. Same or Not the Same? Comparison of Adipose Tissue-Derived Versus Bone Marrow-Derived Mesenchymal Stem and Stromal Cells. *Stem Cells Dev* **21**, 2724–2752 (2012).
133. Melchiorri, A. J., Nguyen, B.-N. B. & Fisher, J. P. Mesenchymal stem cells: roles and relationships in vascularization. *Tissue Eng Part B Rev* **20**, 218–28 (2014).
134. Jeong, H. *et al.* Mesenchymal Stem Cell Therapy for Ischemic Heart Disease: Systematic Review and Meta-analysis. *Int J Stem Cells* **11**, 1–12 (2018).
135. de Mendonça, L. *et al.* Mesenchymal stromal cell therapy reduces lung inflammation and vascular remodeling and improves hemodynamics in experimental pulmonary arterial hypertension. *Stem Cell Res Ther* **8**, 220 (2017).
136. Bian, S. *et al.* Extracellular vesicles derived from human bone marrow mesenchymal stem cells promote angiogenesis in a rat myocardial infarction model. *J Mol Med* **92**, 387–397 (2014).
137. Xin, H. *et al.* Systemic administration of exosomes released from mesenchymal stromal cells promote functional recovery and neurovascular plasticity after stroke in rats. *Journal of Cerebral Blood Flow and Metabolism* **33**, 1711–1715 (2013).
138. Hu, G. W. *et al.* Exosomes secreted by human-induced pluripotent stem cell-derived mesenchymal stem cells attenuate limb ischemia by promoting angiogenesis in mice. *Stem Cell Res Ther* **6**, (2015).
139. Aliotta, J. M. *et al.* Exosomes induce and reverse monocrotaline-induced pulmonary hypertension in mice. *Cardiovasc Res* **110**, 319–330 (2016).
140. Klinger, J. R. *et al.* Mesenchymal Stem Cell Extracellular Vesicles Reverse Sugen/Hypoxia Pulmonary Hypertension in Rats. *Am J Respir Cell Mol Biol* (2019) doi:10.1165/rcmb.2019-0154oc.
141. Todorova, D., Simoncini, S., Lacroix, R., Sabatier, F. & Dignat-George, F. Extracellular Vesicles in Angiogenesis. *Circ Res* **120**, 1658–1673 (2017).
142. Théry, C. *et al.* Minimal information for studies of extracellular vesicles 2018 (MISEV2018): a position statement of the International Society for Extracellular Vesicles and update of the MISEV2014 guidelines. *J Extracell Vesicles* **7**, 1535750 (2018).
143. Viñas, J. L. *et al.* Transfer of microRNA-486-5p from human endothelial colony forming cell–derived exosomes reduces ischemic kidney injury. *Kidney Int* **90**, 1238–1250 (2016).

144. Willis, G. R. *et al.* Mesenchymal stromal cell exosomes ameliorate experimental bronchopulmonary dysplasia and restore lung function through macrophage immunomodulation. *Am J Respir Crit Care Med* **197**, 104–116 (2018).
145. Wiklander, O. P. B. *et al.* Extracellular vesicle in vivo biodistribution is determined by cell source, route of administration and targeting. *J Extracell Vesicles* **4**, 26316 (2015).
146. Lai, C. P. *et al.* Dynamic biodistribution of extracellular vesicles in vivo using a multimodal imaging reporter. *ACS Nano* **8**, 483–494 (2014).
147. Gupta, D. *et al.* Quantification of extracellular vesicles in vitro and in vivo using sensitive bioluminescence imaging. *J Extracell Vesicles* **9**, (2020).
148. Wiklander, O. P. B. *et al.* Extracellular vesicle in vivo biodistribution is determined by cell source, route of administration and targeting. *J Extracell Vesicles* **4**, 1–13 (2015).
149. Wen, S. W. *et al.* The biodistribution and immune suppressive effects of breast cancer-derived exosomes. *Cancer Res* **76**, 6816–6827 (2016).
150. Royo, F., Cossío, U., Ruiz De Angulo, A., Llop, J. & Falcon-Perez, J. M. Modification of the glycosylation of extracellular vesicles alters their biodistribution in mice. *Nanoscale* **11**, 1531–1537 (2019).
151. Viñas, J. L. *et al.* Receptor-Ligand Interaction Mediates Targeting of Endothelial Colony Forming Cell-derived Exosomes to the Kidney after Ischemic Injury. *Sci Rep* **8**, 1–12 (2018).
152. Karoubi, G., Ormiston, M. L., Stewart, D. J. & Courtman, D. W. Single-cell hydrogel encapsulation for enhanced survival of human marrow stromal cells. *Biomaterials* **30**, 5445–5455 (2009).
153. Thomas, D., O'Brien, T. & Pandit, A. Toward Customized Extracellular Niche Engineering: Progress in Cell-Entrapment Technologies. *Advanced Materials* **30**, 1703948 (2018).
154. Uludag, H., De Vos, P. & Tresco, P. a. Technology of mammalian cell encapsulation. *Adv Drug Deliv Rev* **42**, 29–64 (2000).
155. Bonnans, C., Chou, J. & Werb, Z. Remodelling the extracellular matrix in development and disease. *Nat Rev Mol Cell Biol* **15**, 786–801 (2014).
156. Mak, W. C. *et al.* Controlled Delivery of Human Cells by Temperature Responsive Microcapsules. *J Funct Biomater* **6**, 439–453 (2015).
157. Mao, A. S. *et al.* Deterministic encapsulation of single cells in thin tunable microgels for niche modelling and therapeutic delivery. *Nat Mater* **1**, 1–10 (2016).
158. Edd, J. F. *et al.* Controlled encapsulation of single-cells into monodisperse picolitre drops † ‡. (2008) doi:10.1039/b805456h.
159. Köster, S. *et al.* Drop-based microfluidic devices for encapsulation of single cells. *Lab Chip* **8**, 1110–1115 (2008).
160. Mayfield, A. E. *et al.* The effect of encapsulation of cardiac stem cells within matrix-enriched hydrogel capsules on cell survival, post-ischemic cell retention and cardiac function. *Biomaterials* **35**, 133–142 (2014).
161. Kanda, P. *et al.* Deterministic Encapsulation of Human Cardiac Stem Cells in Variable Composition Nanoporous Gel Cocoons to Enhance Therapeutic Repair of Injured Myocardium. *ACS Nano* acsnano.7b08881 (2018) doi:10.1021/acsnano.7b08881.
162. Lv, K. *et al.* Incorporation of small extracellular vesicles in sodium alginate hydrogel as a novel therapeutic strategy for myocardial infarction. *Theranostics* **9**, 7403–7416 (2019).
163. Evans, C. E., Cober, N. D., Dai, Z., Stewart, D. J. & Zhao, Y.-Y. Endothelial Cells in the Pathogenesis of Pulmonary Arterial Hypertension. *European Respiratory Journal* 2003957 (2021) doi:10.1183/13993003.03957-2020.
164. Cober, N. D., VandenBroek, M. M., Ormiston, M. L. & Stewart, D. J. Evolving Concepts in Endothelial Pathobiology of Pulmonary Arterial Hypertension. *Hypertension* **79**, 1580–1590 (2022).

165. Teichert-Kuliszewska, K. *et al.* Bone morphogenetic protein receptor-2 signaling promotes pulmonary arterial endothelial cell survival: Implications for loss-of-function mutations in the pathogenesis of pulmonary hypertension. *Circ Res* **98**, 209–217 (2006).
166. Hurskainen, M. *et al.* Single cell transcriptomic analysis of murine lung development on hyperoxia-induced damage. *Nature Communications 2021 12:1* **12**, 1–19 (2021).
167. Asosingh, K. *et al.* Single-cell transcriptomic profile of human pulmonary artery endothelial cells in health and pulmonary arterial hypertension. *Scientific Reports 2021 11:1* **11**, 1–13 (2021).
168. McGinnis, C. S. *et al.* MULTI-seq: sample multiplexing for single-cell RNA sequencing using lipid-tagged indices. *Nat Methods* **16**, 619–626 (2019).
169. Chaudhary, K. R. *et al.* Efficacy of treprostinil in the SU5416-hypoxia model of severe pulmonary arterial hypertension: haemodynamic benefits are not associated with improvements in arterial remodelling. *Br J Pharmacol* **175**, 3976 (2018).
170. Hao, Y. *et al.* Integrated analysis of multimodal single-cell data. *Cell* **184**, 3573-3587.e29 (2021).
171. Germain, P.-L. *et al.* Doublet identification in single-cell sequencing data using scDblFinder. *F1000Research 2021 10:979* **10**, 979 (2021).
172. Tan, Y. & Cahan, P. SingleCellNet: A Computational Tool to Classify Single Cell RNA-Seq Data Across Platforms and Across Species. *Cell Syst* **9**, 207-213.e2 (2019).
173. Skinnider, M. A. *et al.* Cell type prioritization in single-cell data. *Nat Biotechnol* **39**, 30–34 (2021).
174. Crowell, H. L. *et al.* muscat detects subpopulation-specific state transitions from multi-sample multi-condition single-cell transcriptomics data. *Nat Commun* **11**, (2020).
175. Liberzon, A. *et al.* The Molecular Signatures Database Hallmark Gene Set Collection. *Cell Syst* **1**, 417–425 (2015).
176. Subramanian, A. *et al.* Gene set enrichment analysis: A knowledge-based approach for interpreting genome-wide expression profiles. *Proceedings of the National Academy of Sciences* **102**, 15545–15550 (2005).
177. Krämer, A., Green, J., Pollard, J. & Tugendreich, S. Causal analysis approaches in Ingenuity Pathway Analysis. *Bioinformatics* **30**, 523–530 (2014).
178. Badia-i-Mompel, P. *et al.* decoupleR: ensemble of computational methods to infer biological activities from omics data. *Bioinformatics Advances* **2**, (2022).
179. Garcia-Alonso, L., Holland, C. H., Ibrahim, M. M., Turei, D. & Saez-Rodriguez, J. Benchmark and integration of resources for the estimation of human transcription factor activities. *Genome Res* **29**, 1363–1375 (2019).
180. Bergen, V., Lange, M., Peidli, S., Wolf, F. A. & Theis, F. J. Generalizing RNA velocity to transient cell states through dynamical modeling. *Nature Biotechnology 2020 38:12* **38**, 1408–1414 (2020).
181. Lange, M. *et al.* CellRank for directed single-cell fate mapping. *Nature Methods 2022 19:2* **19**, 159–170 (2022).
182. Wakabayashi, T. & Naito, H. Cellular heterogeneity and stem cells of vascular endothelial cells in blood vessel formation and homeostasis: Insights from single-cell RNA sequencing. *Front Cell Dev Biol* **11**, (2023).
183. Fu, F. *et al.* Role of Transmembrane 4 L Six Family 1 in the Development and Progression of Cancer. *Front Mol Biosci* **7**, (2020).
184. Kim, Y.-K. *et al.* Absolute scaling of single-cell transcriptomes identifies pervasive hypertranscription in adult stem and progenitor cells. *Cell Rep* **42**, 111978 (2023).
185. Ferrer, E. *et al.* A Potential Role for Exosomal Translationally Controlled Tumor Protein Export in Vascular Remodeling in Pulmonary Arterial Hypertension. *Am J Respir Cell Mol Biol* **59**, 467–478 (2018).
186. Muhl, L. *et al.* Single-cell analysis uncovers fibroblast heterogeneity and criteria for fibroblast and mural cell identification and discrimination. *Nat Commun* **11**, 3953 (2020).

187. Qing, X. & Keith, I. M. Targeted blocking of gene expression for CGRP receptors elevates pulmonary artery pressure in hypoxic rats. *American Journal of Physiology-Lung Cellular and Molecular Physiology* **285**, L86–L96 (2003).
188. Cussac, L.-A. *et al.* TRPV4 channel mediates adventitial fibroblast activation and adventitial remodeling in pulmonary hypertension. *American Journal of Physiology-Lung Cellular and Molecular Physiology* **318**, L135–L146 (2020).
189. Xiao, Y., Gong, D. & Wang, W. Soluble Jagged1 Inhibits Pulmonary Hypertension by Attenuating Notch Signaling. *Arterioscler Thromb Vasc Biol* **33**, 2733–2739 (2013).
190. Solinc, J. *et al.* The Platelet-Derived Growth Factor Pathway in Pulmonary Arterial Hypertension: Still an Interesting Target? *Life* **12**, 658 (2022).
191. Kwapiszewska, G., Johansen, A. K. Z., Gomez-Arroyo, J. & Voelkel, N. F. Role of the Aryl Hydrocarbon Receptor/ARNT/Cytochrome P450 System in Pulmonary Vascular Diseases. *Circ Res* **125**, 356–366 (2019).
192. Stenmark, K. R., Frid, M. & Perros, F. Endothelial-to-Mesenchymal Transition. *Circulation* **133**, 1734–1737 (2016).
193. Yang, J. *et al.* Guidelines and definitions for research on epithelial–mesenchymal transition. *Nat Rev Mol Cell Biol* **21**, 341–352 (2020).
194. Kalna, V. *et al.* The Transcription Factor ERG Regulates Super-Enhancers Associated With an Endothelial-Specific Gene Expression Program. *Circ Res* **124**, 1337–1349 (2019).
195. Nagai, N. *et al.* Downregulation of ERG and FLI1 expression in endothelial cells triggers endothelial-to-mesenchymal transition. *PLoS Genet* **14**, e1007826 (2018).
196. Xia, B. *et al.* NR2F2 plays a major role in insulin-induced epithelial-mesenchymal transition in breast cancer cells. *BMC Cancer* **20**, 626 (2020).
197. Szulcek, R. *et al.* Delayed Microvascular Shear Adaptation in Pulmonary Arterial Hypertension. Role of Platelet Endothelial Cell Adhesion Molecule-1 Cleavage. *Am J Respir Crit Care Med* **193**, 1410–1420 (2016).
198. Deng, Y. *et al.* Vicious cycle of hemodynamic perturbation and endothelial injury in development and progression of pulmonary arterial hypertension. *bioRxiv* 2023.10.16.562339 (2023) doi:10.1101/2023.10.16.562339.
199. Masri, F. A. *et al.* Hyperproliferative apoptosis-resistant endothelial cells in idiopathic pulmonary arterial hypertension. *American Journal of Physiology-Lung Cellular and Molecular Physiology* **293**, L548–L554 (2007).
200. Yuan, K. *et al.* Mural Cell SDF1 Signaling Is Associated with the Pathogenesis of Pulmonary Arterial Hypertension. *Am J Respir Cell Mol Biol* **62**, 747–759 (2020).
201. Bordenave, J. *et al.* Lineage Tracing Reveals the Dynamic Contribution of Pericytes to the Blood Vessel Remodeling in Pulmonary Hypertension. *Arterioscler Thromb Vasc Biol* **40**, 766–782 (2020).
202. Yuan, K. *et al.* Lung Pericytes in Pulmonary Vascular Physiology and Pathophysiology. in *Comprehensive Physiology* 2227–2247 (Wiley, 2021). doi:10.1002/cphy.c200027.
203. Shen, Y. *et al.* Construction of CAR-T cells targeting TM4SF1 and its anti-tumor capacity in ovarian cancer. *Immunol Lett* **255**, 1–9 (2023).
204. Chen, G. *et al.* Targeting TM4SF1 exhibits therapeutic potential via inhibition of cancer stem cells. *Signal Transduct Target Ther* **7**, 350 (2022).
205. Lin, C.-I. *et al.* TM4SF1: a new vascular therapeutic target in cancer. *Angiogenesis* **17**, 897–907 (2014).
206. Le Hiress, M. *et al.* Proinflammatory Signature of the Dysfunctional Endothelium in Pulmonary Hypertension. Role of the Macrophage Migration Inhibitory Factor/CD74 Complex. *Am J Respir Crit Care Med* **192**, 983–997 (2015).

207. Gorelova, A., Berman, M. & Al Ghouleh, I. Endothelial-to-Mesenchymal Transition in Pulmonary Arterial Hypertension. *Antioxid Redox Signal* **34**, 891–914 (2021).
208. Szalai, B. *et al.* Signatures of cell death and proliferation in perturbation transcriptomics data—from confounding factor to effective prediction. *Nucleic Acids Res* **47**, 10010–10026 (2019).
209. Park, S. R. *et al.* Single-Cell Transcriptome Analysis of Colon Cancer Cell Response to 5-Fluorouracil-Induced DNA Damage. *Cell Rep* **32**, 108077 (2020).
210. Zhang, L.-Z., Huang, L.-Y., Huang, A.-L., Liu, J.-X. & Yang, F. CRIP1 promotes cell migration, invasion and epithelial-mesenchymal transition of cervical cancer by activating the Wnt/β-catenin signaling pathway. *Life Sci* **207**, 420–427 (2018).
211. Trounson, A. & Mcdonald, C. Cell Stem Cell Review Stem Cell Therapies in Clinical Trials: Progress and Challenges. *Stem Cell* **17**, 11–22 (2015).
212. Hofmann, M. *et al.* Monitoring of bone marrow cell homing into the infarcted human myocardium. *Circulation* **111**, 2198–2202 (2005).
213. Li, S. H. *et al.* Tracking cardiac engraftment and distribution of implanted bone marrow cells: Comparing intra-aortic, intravenous, and intramyocardial delivery. *Journal of Thoracic and Cardiovascular Surgery* **137**, 1225-1233.e1 (2009).
214. Schwarz, T. M. *et al.* Vascular Incorporation of Endothelial Colony-Forming Cells Is Essential for Functional Recovery of Murine Ischemic Tissue Following Cell Therapy. *Arterioscler Thromb Vasc Biol* **32**, (2012).
215. Timmermans, F. *et al.* Endothelial progenitor cells: identity defined? *J Cell Mol Med* **13**, 87–102 (2009).
216. Medina, R. J. *et al.* Endothelial Progenitors : A Consensus Statement on Nomenclature. *Stem Cells Transl Med* 1316–1320 (2017).
217. Chang, K. Y. *et al.* Mortality in Pulmonary Arterial Hypertension in the Modern Era: Early Insights From the Pulmonary Hypertension Association Registry. *J Am Heart Assoc* **11**, (2022).
218. Zelt, J. G. E., Chaudhary, K. R., Cadete, V. J., Mielniczuk, L. M. & Stewart, D. J. Medical Therapy for Heart Failure Associated With Pulmonary Hypertension. *Circ Res* **124**, 1551–1567 (2019).
219. Perrin, S. *et al.* New pharmacotherapy options for pulmonary arterial hypertension. *Expert Opin Pharmacother* **16**, 2113–2131 (2015).
220. Bhogal, S., Mukherjee, D., Banerjee, S., Tan, W. & Paul, T. K. Current Trends and Future Perspectives in the Treatment of Pulmonary Arterial Hypertension. *Curr Probl Cardiol* **43**, 191–216 (2018).
221. Huang, W.-C. *et al.* Therapeutic Benefits of Induced Pluripotent Stem Cells in Monocrotaline-Induced Pulmonary Arterial Hypertension. *PLoS One* **11**, 1–18 (2016).
222. Banno, K. & Yoder, M. C. Tissue regeneration using endothelial colony-forming cells: promising cells for vascular repair. *Pediatric Research 2018 83:1* **83**, 283–290 (2017).
223. Shapiro, A. M. J. *et al.* Insulin expression and C-peptide in type 1 diabetes subjects implanted with stem cell-derived pancreatic endoderm cells in an encapsulation device. *Cell Rep Med* **2**, (2021).
224. Mao, A. S. *et al.* Deterministic encapsulation of single cells in thin tunable microgels for niche modelling and therapeutic delivery. *Nat Mater* **16**, 236–243 (2017).
225. Kanda, P. *et al.* Deterministic paracrine repair of injured myocardium using microfluidic-based cocooning of heart explant-derived cells. *Biomaterials* **247**, (2020).
226. Tam, R. Y., Smith, L. J. & Shoichet, M. S. Engineering Cellular Microenvironments with Photo- and Enzymatically Responsive Hydrogels: Toward Biomimetic 3D Cell Culture Models. *Acc Chem Res* **50**, 703–713 (2017).
227. Colombo, M., Raposo, G. & Théry, C. Biogenesis, secretion, and intercellular interactions of exosomes and other extracellular vesicles. *Annu Rev Cell Dev Biol* **30**, 255–289 (2014).

228. Willis, G. R., Fernandez-Gonzalez, A., Reis, M., Mitsialis, S. A. & Kourembanas, S. Macrophage immunomodulation: The gatekeeper for mesenchymal stem cell derived-exosomes in pulmonary arterial hypertension? *Int J Mol Sci* **19**, (2018).
229. Cruz, F. F. & Rocco, P. R. M. Stem-cell extracellular vesicles and lung repair. *Stem Cell Investig* **4**, 78 (2017).
230. Wang, N. *et al.* Mesenchymal stem cells-derived extracellular vesicles, via miR-210, improve infarcted cardiac function by promotion of angiogenesis. *Biochim Biophys Acta Mol Basis Dis* **1863**, 2085–2092 (2017).
231. Wang, J. *et al.* Mesenchymal Stem Cell-Derived Extracellular Vesicles Alleviate Acute Lung Injury Via Transfer of miR-27a-3p. *Crit Care Med* **48**, E599–E610 (2020).
232. Porzionato, A. *et al.* Intratracheal administration of mesenchymal stem cell-derived extracellular vesicles reduces lung injuries in a chronic rat model of bronchopulmonary dysplasia. *American Journal of Physiology-Lung Cellular and Molecular Physiology* (2021) doi:10.1152/ajplung.00148.2020.
233. Tieu, A., Stewart, D. J. & Lalu, M. M. Mesenchymal Stem Cell-Derived Extracellular Vesicles: Good Things Come in Small Packages. *Critical Care Medicine* vol. 48 1095–1097 Preprint at https://doi.org/10.1097/CCM.0000000000004368 (2020).
234. Kou, M. *et al.* Mesenchymal stem cell-derived extracellular vesicles for immunomodulation and regeneration: a next generation therapeutic tool? *Cell Death & Disease 2022 13:7* **13**, 1–16 (2022).
235. Wilson, J. G. *et al.* Mesenchymal Stem (Stromal) Cells for Treatment of ARDS: A Phase 1 Clinical Trial. *Lancet Respir Med* **3**, 24 (2015).
236. Yuana, Y. *et al.* Handling and storage of human body fluids for analysis of extracellular vesicles. *J Extracell Vesicles* **4**, (2015).
237. Lázaro-Ibánez, E. *et al.* Selection of Fluorescent, Bioluminescent, and Radioactive Tracers to Accurately Reflect Extracellular Vesicle Biodistribution in Vivo. *ACS Nano* **15**, 3212–3227 (2021).
238. Xu, J. H., Liang, J. P., Zhu, C. J. & Lian, Y. J. Mesenchymal Stem Cell-Derived Extracellular Vesicles Therapy for Pulmonary Hypertension: A Comprehensive Review of Preclinical Studies. *J Interv Cardiol* **2022**, (2022).
239. Song, K., Huang, M., Shi, Q., Du, T. & Cao, Y. Cultivation and identification of rat bone marrow-derived mesenchymal stem cells. *Mol Med Rep* **10**, 755–760 (2014).
240. Souza-Moreira, L., Soares, V. C., Dias, S. da S. G. & Bozza, P. T. Adipose-derived Mesenchymal Stromal Cells Modulate Lipid Metabolism and Lipid Droplet Biogenesis via AKT/mTOR –PPARγ Signalling in Macrophages. *Sci Rep* **9**, (2019).
241. Benavente-Babace, A., Haase, K., Stewart, D. J. & Godin, M. Strategies for controlling egress of therapeutic cells from hydrogel microcapsules. *J Tissue Eng Regen Med* **13**, 612–624 (2019).
242. Godoy, R. S. *et al.* Newly Emergent Apelin Expressing Endothelial Stem-like Cells Orchestrate Lung Microvascular Repair. *bioRxiv* 2021.07.12.452061 (2021) doi:10.1101/2021.07.12.452061.
243. Li, Y. *et al.* A Simple Glutathione-Responsive Turn-On Theranostic Nanoparticle for Dual-Modal Imaging and Chemo-Photothermal Combination Therapy. *Nano Lett* **19**, 5806–5817 (2019).
244. Qi, J. *et al.* Towards more accurate bioimaging of drug nanocarriers: turning aggregation-caused quenching into a useful tool. *Adv Drug Deliv Rev* **143**, 206–225 (2019).
245. Mohan, A., Agarwal, S., Clauss, M., Britt, N. S. & Dhillon, N. K. Extracellular vesicles: Novel communicators in lung diseases. *Respiratory Research* vol. 21 1–21 Preprint at https://doi.org/10.1186/s12931-020-01423-y (2020).
246. Wiklander, O. P. B. *et al.* Extracellular vesicle in vivo biodistribution is determined by cell source, route of administration and targeting. *J Extracell Vesicles* **4**, 26316 (2015).

247. Kang, M., Jordan, V., Blenkiron, C. & Chamley, L. W. Biodistribution of extracellular vesicles following administration into animals: A systematic review. *Journal of Extracellular Vesicles* vol. 10 Preprint at https://doi.org/10.1002/jev2.12085 (2021).
248. Abello, J., Nguyen, T. D. T., Marasini, R., Aryal, S. & Weiss, M. L. Biodistribution of gadolinium- and near infrared-labeled human umbilical cord mesenchymal stromal cell-derived exosomes in tumor bearing mice. *Theranostics* **9**, 2325 (2019).
249. Wolf, M. *et al.* A functional corona around extracellular vesicles enhances angiogenesis, skin regeneration and immunomodulation. *J Extracell Vesicles* **11**, (2022).
250. Veiseh, O. *et al.* Size- and shape-dependent foreign body immune response to materials implanted in rodents and non-human primates. *Nat Mater* **14**, 643–651 (2015).
251. Vegas, A. J. *et al.* Combinatorial hydrogel library enables identification of materials that mitigate the foreign body response in primates. *Nat Biotechnol* **34**, 345–352 (2016).
252. S, L., R, B., G, C. & JW, S. Matrix mechanics and water permeation regulate extracellular vesicle transport. *Nat Nanotechnol* **15**, 217–223 (2020).
253. Tang, Q. *et al.* TM4SF1 promotes EMT and cancer stemness via the Wnt/β-catenin/SOX2 pathway in colorectal cancer. *Journal of Experimental & Clinical Cancer Research* **39**, 232 (2020).
254. Van Der Feen, D. E., Berger, R. M. F. & Bartelds, B. Converging paths of pulmonary arterial hypertension and cellular senescence. *American Journal of Respiratory Cell and Molecular Biology* vol. 61 11–20 Preprint at https://doi.org/10.1165/rcmb.2018-0329TR (2019).
255. De-Carvalho, D. P., Jacinto, A. & Saúde, L. The right time for senescence. *Elife* **10**, (2021).
256. Born, E. *et al.* Eliminating Senescent Cells Can Promote Pulmonary Hypertension Development and Progression. *Circulation* **147**, 650–666 (2023).
257. Sakai, S., Mu, C., Kawabata, K., Hashimoto, I. & Kawakami, K. Biocompatibility of subsieve-size capsules versus conventional-size microcapsules. *J Biomed Mater Res A* **78A**, 394–398 (2006).
258. Gupta, P., Alheib, O. & Shin, J.-W. Towards single cell encapsulation for precision biology and medicine. *Adv Drug Deliv Rev* 115010 (2023) doi:10.1016/j.addr.2023.115010.
259. Coronel, M. M. *et al.* Immunotherapy via PD-L1–presenting biomaterials leads to long-term islet graft survival. *Sci Adv* **6**, (2020).
260. Cober, N. D. *et al.* Single-cell microencapsulation improves lung retention of endothelial colony forming cells after intravascular delivery and unmasks therapeutic benefit in severe pulmonary arterial hypertension. doi:10.1101/2022.11.05.514522.
261. Schindelin, J. *et al.* Fiji: an open-source platform for biological-image analysis. *Nature Methods 2012 9:7* **9**, 676–682 (2012).